LBL-9022

VECTOR CURRENT SCATTERING IN TWO DIMENSIONAL QUANTUM CHROMODYNAMICS*

Neil L. Fleishon
(Ph.D. Thesis)

Lawrence Berkeley Laboratory
University of California
Berkeley, California 94720

April 10, 1979

NOTICE

This report was prepared as an account of work sponsored by the United States Government. Neither the United States nor the United States Department of Energy, nor any of their employees, nor any of their contractors, subcontractors, or their employees, makes any warranty, express or implied, or assumes any legal liability or responsibility for the accuracy, completeness or usefulness of any information, apparatus, product or process disclosed, or represents that its use would not infringe privately owned rights.

* This work was supported by the High Energy Physics Division of the U. S. Department of Energy under contract No. W-7405-ENG-48.

DISTRIBUTION OF THIS DOCUMENT IS UNLIMITED

TABLE OF CONTENTS

Dedication iii

Acknowledgments iv

I. Introduction 1

II. Elements of the Model 7

A. Two Dimensional Space-Time 7

B. Color SU(N) Gauge Theory 13

C. Free Field Short Distance Behavior of Currents 23

D. The N^{-1} Expansion 25

III. Hadronic Structure of The Model. 27

A. The Meson Wave Function 28

B. Properties of The Bound State Wave Function 38

C. Hadronic Scattering Amplitudes in The 't Hooft Model. 42

IV. Single Current Matrix Elements. 51

A. The Photon-Hadron Coupling. 51

B. The Inelastic Meson Form Factor 52

V. Two Current Matrix Elements 61

A. The Vacuum Polarization 61

B. Meson Decay to Photons. 63

C. The Inelastic Form Factor of The Photon 65

VI. The Compton Scattering Amplitude. 67

A. Calculation of the Amplitude. 67

B. Exclusive Limits 71

C. Inclusive Limits. 78

VII. Conclusion 92

Appendix A. 95

Simple Wave Function Identities due to Parity Invariance

Appendix B. 98

Current Scattering in the 't Hooft Model

Appendix C. 101

Divergence Properties of Current Amplitudes

References 107

Figure Captions. 112

Figures. 119

Table I. 131

DEDICATION

To Ellen and Mari,

For being there.

Thanks, with much love.

ACKNOWLEDGMENTS

It has been my pleasure, over the last four years, to have done my research work in the theory group of the Lawrence Berkeley Laboratory. I would like to thank everyone at the lab and at the University of California, Berkeley who has helped make this experience an enriching and rewarding one.

My special thanks to my research advisor, Mike Chanowitz, who invested much time, energy, and patience in me and my work. I am also indebted to R. Cahn, J. D. Jackson, E. Rabinovici, and M. Suzuki for for their help and encouragement.

Finally, I would like to express my gratitude to the Theory Division secretarial staff. I deeply appreciate the help of Luanne Neumann, who patiently typed this manuscript.

LBL-9022

VECTOR CURRENT SCATTERING IN TWO DIMENSIONAL QUANTUM CHROMODYNAMICS

Neil L. Fleishon
(Ph.D. Thesis)

Lawrence Berkeley Laboratory
University of California
Berkeley, California 94720

April 10, 1979

ABSTRACT

We consider the interaction of vector currents with hadrons in a two dimensional SU(N) color gauge theory coupled to fermions in leading order in an N^{-1} expansion. After giving a detailed review of the model, we consider various transition matrix elements of one and two vector currents between hadronic states. A pattern is established whereby the low mass currents interact via meson dominance and the highly virtual currents interact via bare quark-current couplings.

This pattern is especially evident in the hadronic contribution to inelastic Compton scattering, $M_{\mu\nu} = \int dx\ e^{iq\cdot x} < n|T^*(J_\mu(x)J_\nu(0))|m >$, which we investigate in various kinematic limits. It is shown that in the dual Regge region of soft processes the currents interact as purely hadronic systems. Modification of dimensional counting rules is indicated by a study of a large angle scattering analogue. In several hard inclusive non-light cone processes, parton model ideas are confirmed. The impulse approximation is valid in a Bjorken-Paschos-like limit with very virtual currents. A Drell-Yan type annihilation mechanism is found in photoproduction of massive lepton pairs, leading to identification of a parton wave function for the current.

I. INTRODUCTION

The experimental realities of hadronic physics lead to the consideration of a non-Abelian gauge theory of colored gluons interacting with fermionic quarks as a possible candidate for describing the dynamics of the strong interactions. The high energy dependence of electron-positron annihilation and the scaling behavior (with violations thereof) of deep inelastic leptoproduction shows that, as seen by large mass currents, the hadronic constituents are weakly coupled on a short distance scale. This is understood to be a consequence of the proven asymptotically free [1] structure of the theory. On the other hand, it is hoped that the long distance problems that arise in perturbation theory are indicative of a mechanism for quark confinement.

A dynamical system which has the properties of asymptotic freedom and quark confinement and, at the same time, gives an S-matrix which is analytic and unitary on the space of physical states is clearly special, being highly constrained. It is therefore of interest to ask whether the dominant phenomenological prejudices about hadronic interactions, which have developed to explain isolated aspects of the dynamics without much regard for the overall constraints, can be realized consistently in a realistic theory of hadrons.

These prejudices fall into two large areas - dual Regge ideas [2] about soft processes (no large final state transverse momentum) and parton model [3] ideas about hard processes. Regge models are

implicitly bound state models, and describe coherent, diffractive scattering. Currents are introduced by the ansatz of vector dominance, which assumes that the current interaction with the strongly interacting system is mediated by hadrons with the quantum numbers of the current. The parton model description is in terms of pointlike hadron constituents seen in processes with large momentum transfer. Current-hadron interactions are viewed as an incoherent sum of current-constituent scatterings in this kinematic region.

The standard strong interaction gauge theory is quantum chromodynamics, QCD, based on the group $SU(N)$, with $N = 3$, coupled to spin ½ quarks transforming as the fundamental representation. The insolubility of the theory due to infrared singularities prevents the extraction of the mass shell S-matrix elements via standard perturbation theory techniques. A likely form of attack, perturbing in N^{-1}, developed by 't Hooft [4] has not led to any significant clarification of the quantitative problem in four dimensions. In two dimensions, one space and one time, however, $(QCD)_2$ can be solved exactly to leading order in N^{-1} [5].

The spectrum of $(QCD)_2$ in this approximation consists of an infinite sequence of zero width color singlet bound states. There is no continuum corresponding to free quarks. Examination of hadronic amplitudes [6] indicates analyticity [7] and consistency with unitarity in the color singlet sector with no long range forces. Asymptotic freedom is trivial due to the fact that $(QCD)_2$ is superrenormalizable. The model is thus a "realistic" model of

strong interactions, in the sense that it is a consistent structure with the required properties. As such, it has often been used as a laboratory to investigate hadron dynamics with the hope that, in the process of understanding its working mechanisms, insights into the four dimensional problem might arise.

Extrapolation to four dimensions must however be regarded with caution due to the special unphysical features arising from the lack of transverse dimensions. The usual Regge ideas are inappropriate since there is no continuous independent variable associated with the t-channel and no spin. There are no dynamical degrees of freedom associated with the gluon field, so that "glueballs" cannot appear. On the other hand, there are experimental indications of strong transverse momentum damping in high energy hadronic interactions, giving rise to the speculation that two dimensional physics may be a useful first approximation to scattering in the real world.

Previous work in the 't Hooft model, $(QCD)_2$ to leading order in N^{-1}, for the most part substantiates theoretical ideas. Examination of current form factors and two current vacuum expectation values [6, 8] confirms light cone scaling ideas and shows how underlying quark dynamics is recovered from amplitudes which show only hadronic intermediate states. The hadronic production of massive lepton pairs which, though not light cone dominated, is amenable to a naive parton model impulse approximation treatment, shows parton scaling structure [9]. Soft hadronic amplitudes

show power law high energy behavior with the power determined by the properties of quanta exchanged in the crossed channel, direct and crossed channel factorization, and signature, indicative of the operation of some precursive dual Regge mechanisms [10,11]. There is, however, no indication of a pomeron in the model. Finally, a possible modification [8] of dimensional counting rules [12] by small dynamically determined powers is suggested.

The purpose of this paper is to examine the interaction of hadrons with vector currents in the 't Hooft model. We are, of course, motivated by the possibility of abstracting our results to photon-hadron interactions in four dimensions. Through the treatment of simple single current vacuum to meson and meson to meson matrix elements, the salient properties of the current interaction are established. The current is dominated by hadrons in the Regge limit and interacts with bare pointlike quanta in the hard scattering limit. This pattern carries over to the two current matrix elements and gives rise to a rich, unified, picture of the photon-hadron Compton scattering process which is our major concern [13].

We investigate inelastic Compton scattering in the 't Hooft model by considering the connected part of the matrix element of the time ordered product of two vector currents between mesonic states. After computing this amplitude, we examine it in various limits of interest. The incident virtual photon is taken spacelike and the outgoing virtual photon is taken timelike in our calculation. In general, we do not consider the zero mass "on shell" photon limit in

order to avoid possible unwanted effects strongly dependent on the two dimensionality of the theory.

Several authors have investigated various aspects of the Compton amplitude in this model. Einhorn [8] has discussed the imaginary part of the forward elastic amplitude with very spacelike photons in connection with inclusive leptoproduction. Brower, et al. have looked at the zero photon mass limit [10]. In this paper we examine the full inelastic Compton scattering amplitude for arbitrary photon masses.

We show that scattering in the forward high energy limit is closely related to meson-meson scattering. The scattering amplitude shows all the Regge properties attributed to hadronic scattering. In particular, we find no conclusive evidence for fixed poles arising in the inelastic Compton amplitude which are not present in the hadronic amplitude.

We examine a part of the Compton amplitude in the forward high energy limit as an ansatz for large angle scattering for comparison with the predictions of the dimensional counting picture. After modification of the counting rules due to the lack of photon degrees of freedom is accounted for, important modifications in the asymptotic power dependence and coefficient of the amplitude remain due to non-perturbative aspects of the model.

Several inclusive limits are investigated. We show that the parton "handbag" model is realized for inclusive Compton scattering at large energy and momentum transfer with very virtual photons. In

the process of photoproduction of massive lepton pairs we find that the amplitude scales in agreement with the parton model prediction [14] based on the Drell-Yan parton-antiparton annihilation mechanism. We show that the partonic structure of the photon probed in this process arises totally from couplings to negative parity mesons.

The remainder of this paper is organized as follows: In Section II, we qualitatively discuss important properties of the major elements of the 't Hooft model. In the course of this discussion we try to emphasize the similarities and differences between $(QCD)_2$ and $(QCD)_4$ so that there is some guide as to how seriously the abstraction of the behavior of the 't Hooft model to the four dimensional world should be taken. Section III contains a review of the solution of the 't Hooft model, establishing notation and presenting formulae which will be of use. We discuss single current matrix elements in Section IV, and two current matrix elements in Section V, with the exception of the Compton scattering amplitude, which we treat in Section VI. In this section we compute the amplitude and then examine it in various kinematic limits. Exclusive scattering limits with finite mass photons are treated in Section V.B while inclusive processes and comparison to parton model descriptions are discussed in Section V.C. We include a proof of some simple parity identities in Appendix A, discuss other currents in Appendix B, and show the conservation of vector currents in Appendix C.

II. ELEMENTS OF THE MODEL

The strong interaction dynamics we consider in this paper is an SU(N) gauge theory of vector gluons and fermonic quarks in one space and one time dimension. This theory, two dimensional quantum chromodynamics, $(QCD)_2$, was first considered by 't Hooft [5] in leading order in an expansion in N^{-1}.

The purpose of this section is to review the important elements of the 't Hooft model - the two dimensional space-time, SU(N) gauge theory, and the N^{-1} expansion. We shall be expecially interested in highlighting the properties of the dynamics which are highly dependent on the two dimensionality of the space-time and comparing them to the properties of the four dimensional theory, $(QCD)_4$. This will give some idea of the extent to which behavior of $(QCD)_2$ can be reasonable abstracted to $(QCD)_4$.

A. Two Dimensional Space-Time.

1. Poincare Group Structure

Minkowski space in two dimensions is described by a set of real points (t, x). The Poincare group is the set of real, linear, transformations under which the distance between two points remains invariant. The distance between $x_1 = (t_1, z_1)$ and $x_2 = (t_2, z_2)$ is $(x_1 - x_2)^2 = (t_1 - t_2)^2 - (z_1 - z_2)^2$ so that the metric tensor is

$$g = \begin{bmatrix} 1 & 0 \\ 0 & -1 \end{bmatrix} = g^{-1} = g^T \quad . \qquad \text{(II.A. 1)}$$

We first look at homogeneous (origin preserving) transformations of the Lorentz group. The invariant length requirement requires the Lorentz group to be the set of real two by two matrices, $M(\lambda)$, such that

$$M^T(\lambda) g\, M(\lambda) = g \ . \qquad \text{(II.A. 2)}$$

The proper Lorentz group, continuously connected to the identity, is a one parameter group whose unimodular elements, M_o, are of the form

$$M_o(\lambda) = \begin{bmatrix} \cosh\lambda & \sinh\lambda \\ \sinh\lambda & \cosh\lambda \end{bmatrix} = \exp(\lambda K) \qquad \text{(II.A. 3)}$$

where

$$K \equiv \sigma_1 = \begin{bmatrix} 0 & 1 \\ 1 & 0 \end{bmatrix} \ . \qquad \text{(II.A. 4)}$$

The group is abelian with law of composition

$$M_o(\lambda) M_o(\lambda') = M_o(\lambda + \lambda') \ . \qquad \text{(II.A. 5)}$$

Physically, we see that the angular momentum and transverse boost generators in four dimensions do not appear once transverse dimensions are eliminated. The only transformation remaining is a

boost along the z direction with velocity $\beta = \tanh \lambda$, as seen by the familiar form of eq. (II.A. 3).

Since K in eq. (II.A. 4) is a real symmetric matrix, it can be diagonalized by a similarity transformation. This diagonal representation is called the light cone representation and is achieved by rotating to the light cone [see fig. (II.A. 1)]

$$\begin{bmatrix} x^+ \\ x^- \end{bmatrix} = \frac{1}{\sqrt{2}} \begin{bmatrix} 1 & 1 \\ 1 & -1 \end{bmatrix} \begin{bmatrix} t \\ z \end{bmatrix} . \qquad \text{(II.A. 6)}$$

In this representation, the metric tensor of eq. (II.A.1) is

$$g' = \begin{bmatrix} 0 & 1 \\ 1 & 0 \end{bmatrix} \qquad \text{(II.A. 7)}$$

and the Lorentz transformations of eq. (II.A. 3) become

$$M_o'(\lambda) = \begin{bmatrix} \exp \lambda & 0 \\ 0 & \exp -\lambda \end{bmatrix} = \exp \lambda K' \qquad \text{(II.A. 8)}$$

where

$$K' = \sigma_3 = \begin{bmatrix} 1 & 0 \\ 0 & -1 \end{bmatrix} . \qquad \text{(II.A. 9)}$$

Light cone coordinates thus scale under Lorentz transformation. Under a parity transformation, $z \to -z$, we have $x_\pm \to x_\mp$. Two Lorentz invariants can be formed from two vectors x and y, a scalar

product $x \cdot y = x_+ y_- + x_- y_+$ and a pseudoscalar product $x \wedge y = \varepsilon^{\mu\nu} x_\mu y_\nu = x_+ y_- - x_- y_+$. A pseudoscalar function of two vectors, possible in two dimensions because of the $\varepsilon^{\mu\nu}$ tensor, cannot be made in four dimensions.

The full Poincare group is gotten by including translations in the space and time directions. The group thus consists of transformations $\overline{M}(\lambda, x)$ of the form

$$\overline{M}(\lambda, x) = T(x)\, M_o(\lambda) = \exp\,(x \cdot P)\, \exp\,(\lambda K) \qquad \text{(II.A.10)}$$

where $T(x)$ is a translation by amount x. The group has the law of composition

$$\overline{M}(\lambda, x)\, \overline{M}(\lambda', x') = \overline{M}(\lambda + \lambda', \lambda x' + x)\ . \qquad \text{(II.A.11)}$$

The generators P_μ and K form a Lie algebra given by

$$\left[P_\mu, P_\nu\right] = 0 \qquad \left[K, P^\mu\right] = \varepsilon^{\mu\nu} P_\nu\ . \qquad \text{(II.A.12)}$$

We see from eq. (II.A. 12) that the operator P^2 is the only one that commutes with all elements of the Lie algebra. Thus all representations are characterised by an invariant mass and the carriers of the representation satisfy the Klein-Gordon equation. This differs from the four-dimensional case where there is another invariant operator which labels the spin of the representation. Spin

is not realized in two dimensions.

2. Simple Representations Of The Two Dimensional Poincare Group

a. Scalar. The scalar representation is carried by a set of fields $\phi(x)$ which transform under the action of the group as

$$\phi(y) \xrightarrow{\lambda, x} \phi(y' = \overline{M}(\lambda, x)y) \ . \qquad \text{(II.A. 13)}$$

b. Spinor. The spinor representation is constructed in analogy to the four dimensional case. The Dirac γ matrices are realized on a two dimensional space with the algebra

$$\{\gamma^{\mu}, \gamma^{\nu}\} = 2g^{\mu\nu} \ . \qquad \text{(II.A. 14)}$$

The γ's transform as components of a vector under Lorentz transformation. This gives the elements of this representation of the group as

$$M(\lambda) = \exp\left(-\frac{\lambda}{2}\gamma_5\right) \qquad \text{(II.A. 15)}$$

where

$$\gamma_5 = \frac{1}{2}[\gamma^-, \gamma^+] \qquad \text{(II.A. 16)}$$

and $M(\lambda)$ acts on the γ's by conjugation. We thus see that under a Poincare transformation

$$\psi(y) \xrightarrow{\lambda,x} \exp\left(\frac{\lambda}{2}\gamma_5\right)\psi(y' = \overline{M}(\lambda,x)y) \ . \qquad \text{(II.A. 17)}$$

The spinor space is separated into two distinct subspaces by the projection operators $P^{(+)} = \frac{1}{2}\gamma^-\gamma^+ = \frac{1}{2}(1+\gamma_5)$ and $P^{(-)} = \frac{1}{2}\gamma^+\gamma^- = \frac{1}{2}(1-\gamma_5)$. In the represention where $\psi = \begin{bmatrix}\psi^{(+)}\\ \psi^{(-)}\end{bmatrix}$ such that $P^{(+)}\psi = \begin{bmatrix}\psi^{(+)}\\ 0\end{bmatrix}$ and $P^{(-)}\psi = \begin{bmatrix}0\\ \psi^{(-)}\end{bmatrix}$ the γ matrices have the form $\gamma^- = \sqrt{2}\begin{bmatrix}0 & 1\\ 0 & 0\end{bmatrix}$ and $\gamma^+ = \sqrt{2}\begin{bmatrix}0 & 0\\ 1 & 0\end{bmatrix}$. The fields $\psi^{(\pm)}$, analogous to light cone coordinates, scale under Lorentz transformations. The operators $P^{(\pm)}$ in four dimensions project spin helicities of massless fermions. In two dimensions however γ_5 is the boost operator [see eq. (II.A. 15)] and plays the role of $\sigma_{\mu\nu}$ in four dimensions. This is explicit by comparing $\sigma_{\mu\nu} = \frac{1}{2}[\gamma_\mu,\gamma_\nu]$ to γ_5 as defined in eq. (II.A. 16). We thus expect some connection between helicity properties in four dimensions and momentum boosts in two dimensions. This connection will be clarified when we discuss short distance behavior below.

c. Vector. The vector representation is the one realized on the points of Minkowski space and has already been discussed. A vector field, $A_\mu(x)$, is a pair of fields which transforms under a Poincare transformation as

$$A_\mu(y) \xrightarrow{\lambda,x} (M_o(\lambda)A(y' = \overline{M}(\lambda,x)y))_\mu \ . \qquad \text{(II.A. 18)}$$

3. Kinematics In Two Dimensions

Scattering in two dimensions is, of course, restricted to a line. Thus particles either scatter forward or backward. Since there are no angles, fewer invariants are needed to specify an given scattering event. For an J-body process with all external masses known, $J-3$ invariants describe the two dimensional process compared with $3J-10$ invariants in four dimensions.

We see that in the case $J = 4$, only one continuous invariant is needed to describe the two dimensional scattering. The usual partial wave representation of the amplitude is not possible and Regge theory methods of analytic continuation into cross channel variables are inapplicable.

B. Color SU(N) Gauge Theory.

We consider a theory of massive fermions coupled to color SU(N) gauge gluons with coupling g. The Lagrangian density describing the system is

$$\mathcal{L} = \frac{1}{4} \mathrm{Tr}(G_{\mu\nu} G^{\mu\nu}) + \bar{q}^a (i\not{D} - m_a I) q^a \qquad \text{(II.B. 1)}$$

where

$$G_{\mu\nu} = \partial_\mu A_\nu - \partial_\nu A_\mu + g\,[A_\mu, A_\nu] \qquad \text{(II.B. 2)}$$

$$D_\mu = \partial_\mu I + g\,\tilde{A}_\mu \quad . \qquad \text{(II.B. 3)}$$

In the above, A_μ is an $N \times N$ matrix of anti-hermitian gluon fields [15] transforming as the adjoint representation of the group $U(N)$ and q^a is a fundamental multiplet of spinor quark fields with measurable internal quantum numbers, e.g. flavor, indicated by the superscript "a". The $U(1)$ gluon component has been removed in the quark-gluon vertices so that $\tilde{A}_\mu = A_\mu - N^{-1}\mathrm{Tr}(A_\mu)I$. The $U(1)$ component is thus a free field. (This formulation is used because it results in Feynman rules with transparent N dependence, as discussed below).

This theory describes the interaction of color gluons with fermions. The choice of spinor rather than scalar particles is motivated by the experimental evidence that hadronic constituents are spin ½ particles. On the other hand, there is no essential difference between spinors and scalars in two dimensions since spin is absent and statistics a matter of convention [16]. Scalar $(QCD)_2$ has been investigated [17] and results similar to those of spinor $(QCD)_2$ obtained.

Color $SU(N)$ is a gauge theory, i.e. the Lagrangian density of eq. (II.B. 1) is invariant under a gauge transformation of the type

$$q(x) \rightarrow \exp(i\Theta)q(x)$$

$$A_\mu(x) \rightarrow \exp(i\Theta)A_\mu(x)\exp(-i\Theta) - \frac{i}{g}\partial_\mu\Theta \qquad \text{(II.B. 4)}$$

where Θ is an $N \times N$ traceless hermitian matrix valued function of space-time. We choose to quantize the theory with the axial gauge condition, $n \cdot A = 0$, for some vector n. This choice leads to two simplifications in the solution of the theory.

First, the linearity of the gauge constraint eliminates the need to introduce Fadeev-Popov ghosts [18] into the theory. These ghosts are fictitious wrong statistics scalar fields in the adjoint representation of the gauge group whose inclusion in internal loops of Feynman diagrams is necessary to maintain the unitarity and renormalizability of the theory. The interactions of the $N \times N$ matrix ghost field, $\eta(x)$, are described by a term in the Lagrangian of the form

$$\mathcal{L}_G = \mathrm{Tr}(\eta^\dagger(x) \frac{\partial F}{\partial \Theta} \eta(x)) \qquad \text{(II.B. 5)}$$

where F is the equation of gauge constraint and $\partial F/\partial\Theta$ describes the change of F under an infinitesimal gauge transformation. For the axial gauge case $F = n \cdot A$. Using eq. (II.B. 4), we find that $\partial F = i[\Theta, n \cdot A] - \frac{i}{g}(n \cdot \partial)\Theta = -\frac{i}{g}(n \cdot \partial)\Theta$ since the first term is zero in axial gauge. The ghosts, thus, do not couple to anything in theory, and can be factored out of the S-matrix. This elimination of ghosts is independent of the number of space-time dimensions.

The second axial gauge simplification is, by contrast, highly

dimension dependent. Since in two dimensions, one component of a two component vector field has been eliminated by choice of gauge, the commutator appearing in eq. (II.B. 2) is zero. As a result, all three and four point gluon vertices disappear from the theory. This elimination of vertices cannot occur in four dimensions.

The model is most easily solved when quantized on the null plane. Light-cone quantization [19] involves the specification of initial conditions, i.e. canonical equal "time" commutation relations, on the lightlike surface $x_- = 0$, with the dynamics generated by the hamiltionian operator conjugate to x_-, P_+. Thus the roles of the coordinates are: x_- = "time", x_+ = "space", p_+ = "energy", p_- = "momentum". The initial condition surface $x_- = 0$, can be obtained from the surface $x_o = 0$ by a boost of the form given in eq.(II.A. 3) in the limit that λ approaches infinity. This quantization is thus appropriate for the description of the dynamics of the "infinite momentum frame".

The infinite momentum frame has been used extensively in current algebra [20] to derive fixed Q^2 sum rules and in parton models [21] to motivate the use of impulse approximation physics. Field theories in the infinite momentum limit [22] show a simplified structure which is particularly amenable to a non-relativistic type of description [23] where graphs with particles moving backward in time are eliminated.

Applications of infinite momentum are typically plagued by questions of the existence and uniformity of the infinite momentum

limit. This question also appears in the light cone quantization scheme. The point is that since there is no finite continuous transformation which transforms the $x_0 = 0$ surface to the $x_- = 0$ surface, spacelike quantization and light cone quantization do not a priori describe the same physical theory [24]. An investigation by Bars and Green [25] shows the consistency of the spacelike quantized and light cone quantized 't Hooft model.

Operator quantization of $(QCD)_2$ [25, 26] cannot be done so as to consistently generate the Poincare algebra of eq. (II.A. 12) due to the existence of a background color electric field. A consistent covariant theory can only be formulated on a Hilbert space whose states are all color singlets. There is thus an intimate connection between the Poincare structure and gauge group structure in $(QCD)_2$. We restrict ourselves to a color singlet Hilbert space in this work.

We choose to work in the covariant, $A_- = 0$ gauge so that Lorentz invariance is retained. This choice however, destroys the explicit parity invariance of the theory. Quantizing in $A_- = 0$ gauge, an equation of constraint for A_+ can be derived from the Euler-Lagrange equations:

$$\partial_-^2 A_+(x) = - ig\bar{q}(x)\gamma_- \tau q(x) \cdot \tau = - igj_-(x) \qquad \text{(II.B. 6)}$$

where the $N \times N$ matrices τ form the fundamental representation of the Lie algebra of the gauge group. Since there is no operator conjugate to A_+, the field can be eliminated with

$$A_+(x) = -\, ig\partial_-^{-2} j_-(x) \,. \qquad \text{(II.B. 7)}$$

There are thus no dynamical gluon fields in $(QCD)_2$. All that remains is an instantaneous Coulomb potential $V(x)$ which satisfies

$$\partial_-^2 V(x_+, x_-) = \delta(x_+)\delta(x_-) \quad . \qquad \text{(II.B. 8)}$$

The elimination of two gluon degrees of freedom can be done in this way in four dimensions also. However the transverse gluons in four dimensions remain as dynamical variables. We thus lose the hope of finding in $(QCD)_2$ any $(QCD)_4$ effects whose origins lie in the existence of gluon degrees of freedom.

The general solution of eq. (II.B. 8) for the potential $V(x_+, x_-)$ is

$$V(x_+, x_-) = \frac{1}{2}\, |x_+|\delta(x_-) + B(x_-)x_+ + C\,(x_-) \,. \qquad \text{(II.B. 9)}$$

The first term is the linearly rising Coulomb potential in two dimensions. Thus, even at a classical level, quarks must be confined in neutral color configurations. Confinement in $(QCD)_4$ is presumably very complicated, arising non-perturbatively from the singular infrared behavior of the theory. We see, then, that $(QCD)_2$, by virtue of its trivial confinement mechanism, can offer no insight into the dynamics of confinement in four dimensions.

The second term in eq. (II. B. 9) gives rise to a background color electric field and can be ignored in the color singlet sector. The last term, $C(x_-)$, corresponds to no new physics. It reflects the fact that the light cone gauge, $A_- = 0$, is preserved by the class of gauge transformations, eq. (II.B. 4), where Θ has no x_+ dependence.

The fermion field equations of motion derived from the Lagrangian of eq. (II.B. 1) in the $A_- = 0$ gauge include another equation of constraint:

$$i\partial_- q^{(-)}(x) = \frac{m_a}{\sqrt{2}} q^{(+)}(x) \qquad \text{(II.B. 10)}$$

where the superscripts denote the $(1 \pm \gamma_5)$ projections discussed above. The $q^{(-)}$ field can thus be eliminated by writing

$$q^{(-)}(x) = \frac{im_a}{2\sqrt{2}} \int d^2y \delta(x_- - y_-)\, \varepsilon(x_+ - y_+) q^{(+)}(y) \,. \qquad \text{(II.B. 11)}$$

There are thus only two degrees of freedom, $q^{(+)}$ and $\bar{q}^{(+)}$, remaining. The theory is quantized by setting up the canonical equal x_- anticommutation relations and solved in a perturbation series in the coupling g. The usual Feynman rules result and are given in fig. (II.B. 1). Notice that the gluons, in the adjoint representation, have the color structure of a quark-antiquark state. It is sometimes convenient to represent the gluon propagator as two quark lines as in fig. (II.B. 1) to keep track of the color flow through the diagram.

The singular behavior of the gluon propagator at zero momentum introduces infrared divergences into the theory. These infinities must be regulated. The regularization question is, in turn, tied to the residual gauge invariance in the problem. This can be clearly seen by taking the Fourier transform of eq. (II.B. 9) for the potential. The residual gauge term $C(\underline{x})$ gives rise to a $\delta(\underline{k})$ term in momentum space. If $C(\underline{x})$ is set equal to zero, the gluon propagator is given by the Fourier transform of the Coulomb potential, $P\frac{1}{\underline{k}^2} = \frac{1}{2}\left[\frac{1}{(\underline{k}+i\varepsilon)^2} + \frac{1}{(\underline{k}-i\varepsilon)^2}\right]$. (The symbol P refers to principal value). The propagator can also be regularized by cutting the $\underline{k} = 0$ point out of momentum space and taking the gluon propagator to be $\Theta(\underline{k}^2 - \lambda^2)/\underline{k}^2$ for some small fixed λ. This is 't Hooft's λ cutoff method and corresponds to $C(\underline{x}) = \delta(\underline{x})/\pi\lambda$[27]. Gauge invariant quantities should then be finite in the limit $\lambda \to 0$.

The principal value prescription is useful since all diagrams are finite and the non-trivial cancellations due to gauge invariance can be clearly seen. The 't Hooft prescription is better suited to rapid calculation of graphs because of simplifications due to the $\lambda \to 0$ limit. We will use this method of regularization in our discussion.

Having regularized the infrared divergences of the theory, we now look at the ultraviolet region. Using the familiar [28] power counting arguments, the superficial degree of a divergence, D,

of a Feynman diagram with n vertices, F external fermion lines, and B external boson lines is

$$D = 2 - \frac{1}{2} F - n \ . \qquad \text{(II.B12)}$$

The only superficially divergent diagram is thus the one loop correction to the gluon propagator $(n = 2,\ F = 0,\ D = 0)$ which is however finite due to the gauge invariance of the theory. The conclusion is that there are no ultraviolet divergences in the coupling constant perturbation theory of $(QCD)_2$. Mass and coupling constant renormalization is finite. This softening of the theory occurs because there is a dimension associated with the quark-gluon vertex;the coupling constant g has dimensions of mass. This is why n appears in eq.(II.B.12). Such theories are called superrenormalizable, as opposed to renormalizable theories like $(QCD)_4$ where the coupling constant is dimensionless and the degree of divergence of a diagram does not depend on the number of vertices.

Theories with dimensionful parameters are trivially asymptotically free [1]. This means that, at short distances, $(QCD)_2$ looks like a free field theory. This assertion can be formally shown using renormalization group techniques. The independence of the Green's functions of the theory on the renormalization point μ leads to the identification of a dimensionless running coupling

coupling constant, $\bar{\lambda}(Q^2)$, which gives the strength of the coupling when the scale of all momenta is set by Q^2. The Q^2 evolution of $\bar{\lambda}$ is given by

$$\frac{d\bar{\lambda}}{dt} = \beta(\bar{\lambda}) \qquad \text{(II.B.13)}$$

where $t = \log Q^2$ and $\beta(\lambda)$ is the differential change in the coupling due to a logarithmic change in the renormalization point μ. Since the coupling constant g has dimensions of mass in $(QCD)_2$, take a dimensionless parameter $\lambda = g(\mu)/\mu$, where $g(\mu)$ is typically calculated as a perturbation series of the form $g(\mu) = g(1 + ag^2/\mu^2 + \cdots)$. Then

$$\beta(\lambda) = \mu\frac{\partial\lambda}{\partial\mu} = -\lambda + O(\lambda^3) \ . \qquad \text{(II.B.14)}$$

If λ is small enough so that only the leading term may be retained, eq.(II.B.13) gives $\bar{g}^2(Q^2) = \mu^2\bar{\lambda}^2(Q^2) = g_o^2\, Q_o^2/Q^2$ where $g_o = \bar{g}(Q_o^2)$ for some value of Q_o. The running coupling constant scales exactly as a power and free field theory diagrams $(g = 0)$ dominate as $Q^2 \to \infty$.

This behavior is modified in $(QCD)_4$ where the coupling constant is dimensionless. The first, linear, term in eq. (II.B.14) does not appear. The asymptotic freedom of the theory is then determined by the sign of the cubic second term. Even if the sign is negative and asymptotic freedom results the form of the β function

induces logarithmic, interaction dependent, corrections to scaling not present in two dimensions.

C. Free Field Short Distance Behavior Of Currents

The short distance behavior of the product of two operators is given by the operator product expansion [29]

$$\lim_{q \to \infty} - i \int dx\, e^{iq\cdot x} \langle A| T(O_1(x) O_2(0)) |B\rangle = \sum_n d_n(q) \langle A| O_n(0) |B\rangle \qquad \text{(II.C. 1)}$$

where the $\{O_n\}$ are the local operators of the theory and the limit on q is such that the dominant region of integration comes from $x_\mu \sim 0$. The leading behavior of the coefficients $d_n(q)$ as $q \to \infty$ is determined by simple dimensional analysis from eq. (II.C. 1). If $D(O_n)$ is the mass dimension of the operator O_n, $d_n(q) = a_n(q) q^{P_n} + \cdots$ as $q \to \infty$ where $P_n = -2 + D(O_1) + D(O_2) - D(O_n)$ and $a_n(q)$ is a dimensionless function of $\log q$. Clearly the dominant terms in the short distance expansion will come from the operators of smallest dimension. In view of the asymptotic freedom of $(QCD)_2$ discussed above, the a_n can be calculated from free field theory.

There are four simple, gauge invariant, hermitian, fermionic currents, $J^{(C)}(x) = :\bar{q}(x)\gamma^{(C)} q(x):$, $(C = S, PS, V)$, where $\gamma^S = I$ (scalar), $\gamma^{PS} = i\gamma_5$ (pseudoscalar), $\gamma^V = \gamma^\mu$ (vector). Short distance products of these currents can be expanded to give

$$- i \int d^2x\, e^{iq\cdot x} \langle A| T(J^{(C)}(x) J^{(C)}(0)) |B\rangle = d_o^{(C)}(q) \langle A| B\rangle + \sum_{\{D\}} d_{1,D}^{(C)}(q) \langle A| J^{(D)}(0) |B\rangle \cdots . \qquad \text{(II.C 2)}$$

These are the dominant terms since the identity operator, $D(I)=0$, and the current operator, $D(J) = 1$, are the lowest dimension operators in the theory [30]. The free field values of the expansion coefficients can be obtained from simple Wick expansion. The coefficents $d_o^{(C)}(q)$, for example, are found to be $d_o^{(S)} = d_o^{(PS)} = N(2\pi)^{-1}\log(-q)^2$, $d_o^{(V)} = (q_{\mu\nu} - \frac{q_\mu q_\nu}{q^2})N(\pi)^{-1}$. The imaginary part of $d_o^{(C)}$ is related by the optical theorem to the cross section for the decay of the current $J^{(C)}$ into a quark-antiquark pair. Thus, since $d_o^{(V)}$ is real, the leading short distance behavior does not contribute to the process $e^+e^- \to X$ in two dimensions and the canonical scaling behavior does not occur. This is the simplest example of the general pattern of anomolous scaling behavior in two dimensions.

This origin of this behavior can be seen be examining the free field Dirac equation which, written in terms of the $(1 \pm \gamma_5)$ projections $\psi^{(+)}$ and $\psi^{(-)}$, is:

$$i\partial_{(\pm)}\psi^{(\pm)} = \frac{m}{\sqrt{2}}\psi^{(\mp)} \quad . \qquad \text{(II.C. 3)}$$

In the short distance limit, when the fermion mass is small compared to relevant mass scales, $\psi^{(+)}$ $(\psi^{(-)})$ becomes an eigenstate of $p_+(p_-)$ with zero eigenvalue. The field $\psi^{(+)}(\psi^{(-)})$ thus creates and destroys right (left) moving quanta only. The fermion currents, written in terms of $\psi^{(\pm)}$ are,

$$J^{(S)} = \psi^{(+)\dagger}\psi^{(-)} + \psi^{(-)\dagger}\psi^{(+)}$$

$$J^{(PS)} = i(\psi^{(+)\dagger}\psi^{(-)} - \psi^{(-)\dagger}\psi^{(+)}) \qquad \text{(II.C.4)}$$

$$J^{+} = \psi^{(+)\dagger}\psi^{(+)} \qquad J^{-} = \psi^{(-)\dagger}\psi^{(-)} \ .$$

The vector currents, as shown by eq. (II.C. 4), can only produce a quark-antiquark pair where both quanta are moving in the same direction. Since such a pair cannot be produced from vacuum due to momentum conservation, there is no contribution to $J^{(V)} \to q\bar{q}$ in leading order (fermion mass equal to zero).

We define the momentum helicity of a right (left) moving fermion or a left (right) moving antifermion as positive (negative). The discussion above shows that the leading short distance behavior is non-canonical in any process where momentum helicity is not conserved at a vector current vertex or is conserved at a scalar or pseudoscalar current vertex. The momentum helicity behavior in two dimensions is exactly analogous to spin helicity behavior in four dimensions, because, in both cases, the helicity states are projected out by $\frac{1}{2}(1 \pm \gamma_5)$.

D. The N^{-1} Expansion

't Hooft [4] has shown that the set of Feynman diagrams of a U(N) [31] color gauge theory with color singlet sources contributing to a given order in N^{-1} in an expansion of the theory as $N \to \infty$

with g^2N fixed is determined by purely topological properties. This is true in any number of space-time dimensions.

The Feynman rules of the theory can be written in an N independent way and all the quanta represented by color flow lines (as done, for example, in fig. (II.B. 1)). A diagram is then a two dimemsional surface with ℓ color loops, f fermion loops, and h handles. The N dependence arises from the color loops while the g dependence at the vertices is fixed by the structure of the theory. These can be related by Euler's theorem to show that a diagram $\Gamma(\ell,f, h) \sim (N^{-1})^{2h+f-2}$. The leading diagrams are planar ($h = 0$) with no internal fermion loops ($f = 1$). Figure (II.D. 1) shows a simple example of how the N-dependence on internal fermion loops comes about. Each internal loop results in a factor g^2 at the quark-gluon vertices without making any new color loops. Figure (II. D. 2) shows a simple example of how the N-dependence on handles comes about. Handles result in the twisted connection of color loops which are separate on the planar level.

Several important properties [32] of the mesonic amplitudes in leading order in N^{-1} can be abstracted from the planarity of the graphs:

(1). Mesons, color singlet quark-antiquark bound states, are absolutely stable to leading order. This is due to the color normalization of each external state in an amplitude. The probability for a meson to decay to two mesons is thus down by a factor of N^{-1}

from the probability for stable particle propagation.

(2). Similar color normalization arguments can be used to show that, in an inclusive process, the unseen state consists of only one meson. Generally, the implementation of unitarity through application of the optical theorem involves next to leading orders in N^{-1}, since the unitarity constraint is non-linear.

(3). The mesonic ampitudes are meromorphic functions of the Lorentz invariants. No multi-particle threshold cuts can be created on the planar level because a planar diagram cannot be cut through more than one quark-antiquark pair. This is illustrated by the example of fig. (II.D. 3) which shows a quark diagram which contributes to the buildup of a two particle intermediate state in the meson-meson scattering amplitude. This however cannot contribute to leading order in N^{-1} due to the internal fermion loop. The theory in leading order in N^{-1} is thus a tree diagram theory of mesons with simple Born exchange amplitudes.

III. HADRONIC STRUCTURE OF THE MODEL

The treatment of quantum chromodynamics in two dimensions to leading order in N^{-1} renders the 't Hooft model simple enough so that it can be solved exactly for mesonic amplitudes. These amplitudes are expressed as integrals over mesonic wave functions which are derived non-perturbatively by Bethe-Salpeter [33] techniques.

In this section we formulate the bound state problem and review [5, 6] its solution in $(QCD)_2$. We thus arrive at an equation

for the bound state wave function and discuss its properties. The entire theory is then reformulated as a graph theory of mesons, with the three and four point functions used as examples.

A. The Meson Wave Function.

The color singlet quark-antiquark bound state wave function is obtained from the residues of the poles of the color singlet quark antiquark four point vacuum amplitude, $D_{\alpha\beta;\gamma\delta}$, given by

$$(2\pi)^2\delta(p + p' - q - q')iD_{\alpha\beta;\,\gamma\delta}(p,p';q,q') = \int d^2x_1 d^2x_2 d^2y_1 d^2y_2$$

$$\exp(ip \cdot x_1 + ip' \cdot x_2 - iq \cdot y_1 - iq' \cdot y_2) \cdot$$

$$\cdot \langle 0|T(\mathrm{Tr}(\bar{\psi}_\alpha(x_1)\psi_\beta(x_2))\mathrm{Tr}(\bar{\psi}_\gamma(y_1)\psi_\delta(y_2)))|0\rangle \qquad \text{(IIIA.1)}$$

and shown in fig. (III. A.1). (The Greek letters are Dirac indices and the traces are in color space.) This is seen by examining the behavior of the amplitude due to a one particle intermediate state when the $\bar{\psi}\psi$ clusters are separated by a large distance in space-time. Defining the total momentum $P = p + p' = q + q'$ and the center of mass coordinates $x_1 = X + \frac{x}{2}$, $x_2 = X - \frac{x}{2}$, $y_1 = Y + \frac{y}{2}$, $y_2 = Y - \frac{y}{2}$, $\Delta = \frac{X - Y}{2}$ and using translation invariance to translate the system by $\frac{X + Y}{2}$, we have

$$iD_{\alpha\beta;\gamma\delta}(P;p,\ q) = \int d^2\Delta \int d^2x \int d^2y\ \exp(i\Delta \cdot P)\exp i\frac{x}{2} \cdot (2p-P)\exp -i\frac{y}{2} \cdot (2q-P) \cdot$$
$$\langle 0|T\left(\mathrm{Tr}(\bar{\psi}_\alpha(\tfrac{\Delta+x}{2})\psi_\beta(\tfrac{\Delta-x}{2}))\mathrm{Tr}(\bar{\psi}_\gamma(\tfrac{-\Delta+y}{2})\psi_\delta(\tfrac{-\Delta-y}{2}))\right)|0\rangle. \text{(III.A2)}$$

If $Tr(\bar{\psi}\,\psi)$ is the source of a single particle bound state of mass M_n and momentum k, $|\,k;\,M_n\rangle$, which is confined to a finite region of space time, there is a contribution, $D^o(P;p,q)$ to $D(P;p,q)$ coming from the region $\Delta > \Delta^o$, for some Δ^o large compared to the size of the bound state, which is given by

$$iD^o(P;p,q) = \int_{\Delta^o}^{\infty} d\Delta_o \int_{-\infty}^{\infty} d\underset{\sim}{\Delta} \int dx \int dy \int \frac{d^2k}{2k_o(2\pi)}\,\delta(k_o - \sqrt{\underset{\sim}{k}^2 + M_n^2}\,)$$

$$\exp(i\Delta\cdot(P-k))\,\exp(i\,\frac{x}{2}\cdot(2p-P))\,\exp(-\,i\,\frac{y}{2}\cdot(2q-P))$$

$$\langle 0|\,T(Tr(\bar{\psi}_\alpha(\tfrac{x}{2})\psi_\beta(-\,\tfrac{x}{2})))|k;\;M_n\rangle\langle k;\,M_n|T(Tr(\bar{\psi}_\gamma(\tfrac{y}{2})\psi_\delta(-\,\tfrac{y}{2})))|0\rangle \quad \text{(III.A.3)}$$

where we have used the restriction on Δ^o to split up the time ordered product, inserted a sum over single particle intermediate states, and used translation invariance. The Δ and k integrations can be done to give

$$D^o(P;p,q) = -\,\frac{1}{2P^o}\,\frac{\Phi^{(n)}_{\alpha\beta}(P,p)\chi^{(n)}_{\gamma\delta}(P,q)}{(P^o - \sqrt{P^2 + M_n^2} + i\varepsilon)}\,\exp\,i\Delta^o(P^o - \sqrt{P^2 + M^2}\,) \quad \text{(III.A.4)}$$

where the wave function $\Phi^{(n)}_{\alpha\beta}(P,p)$ is

$$\Phi^{(n)}_{\alpha\beta}(P,p) = \int d^2x\,\exp(-\,i\,\frac{x}{2}\cdot(2p-P))\langle P,M_n|\,T(Tr(\bar{\psi}_\alpha(\tfrac{x}{2})\psi_\beta(-\,\tfrac{x}{2})))|\,0\rangle$$

(III.A. 5)

and $\chi^{(n)}$ is the time reversed hermitian conjugate to $\Phi^{(n)}$. Equation (III.A. 4) shows that $\Phi^{(n)}$ can be obtained from the residue of the pole in the lower half P^o plane of $D(P;p,q)$. This is schematically indicated in fig. (III.A. 1).

The amplitude $D(P;p,q)$ in the 't Hooft model is given by a sum of planar diagrams like fig. (III.A. 2). These diagrams are characterized by uncrossed ladder exchange of gluons between renormalized fermion propagators. Thus, in order to solve the bound state problem, we must dress the quarks and then sum the infinite series of ladder exchange diagrams. There are no vacuum polarization or vertex corrections in the planar, two dimensional, theory.

1. Renormalizing the Quark Propagator.

The proper self energy vertex, $i\Sigma(p)$, is related to the full propagator $iS(p)$ by the sum shown in fig. (III.A. 3). The geometric series gives

$$i\Sigma(p) = (iS(p))^{-1} - (iS_o(p))^{-1} \qquad \text{(III.A. 6)}$$

where $S_o(p)$ is the bare propagator given in fig. (II.B. 1). The planarity of gluon further relates $S(p)$ to $\Sigma(p)$ as shown in fig. (III.A. 4) giving

$$i\Sigma(p) = ig^2 N \int \frac{d^2k\gamma_- iS(k)\gamma_-}{(2\pi)^2(p_- - k_-)^2} \quad . \qquad \text{(III.A. 7)}$$

The Dirac structure of eq. (III.A. 7) shows that $i\Sigma(p) = i\gamma_-\sigma(p)$.

Combining eqs. (III.A. 6) and (III.A. 7) , we get

$$\sigma(p) = ig^2N\int\frac{d^2k}{(2\pi)^2(p_- - k_-)^2}\;\frac{1}{(k_+ - \sigma(k) - \frac{m^2}{2k_-} + i\varepsilon k_-)} \quad \text{(III.A.8)}$$

which shows that $\sigma(p)$ is only a function of p_-. The k_+ integration is logarithmically divergent but can be done symmetrically to give

$$\sigma(p) = \frac{g^2N}{4\pi}\int\frac{dk_-}{(p_- - k_-)^2}\;\text{sgn}\,k_- = \frac{g^2N}{4\pi}\int\frac{dk_-}{k_-^2}\,\text{sgn}(p_- - k_-). \quad \text{(III.A.9)}$$

The integral over k_- is infrared singular. To regularize the integral we cut a hole around the origin from $-\lambda$ to λ by replacing eq.(III.A. 9)with

$$\sigma(p) = \frac{g^2N}{4\pi}\int\frac{dk_-}{k_-^2}\,\theta(k_-^2 - \lambda^2)\;\text{sgn}(p_- - k_-) = \frac{g^2N}{2\pi}\left[\frac{\text{sgn}(p_-)}{\lambda} - \frac{1}{p_-}\right]. \quad \text{(III.A.10)}$$

The full propagator is found from $\sigma(p)$ by eq. (III.A.6). It is given by

$$iS(p) = i\,\frac{\left(\gamma_+p_- + \gamma_-\left(p_+ - \frac{g^2N}{2\pi}\left[\frac{\text{sgn}(p_-)}{\lambda} - \frac{1}{p_-}\right]\right) + m\right)}{\left(p^2 - \frac{g^2N|p_-|}{\pi\lambda} + \tilde{m}^2 + i\varepsilon\right)} \quad \text{(III.A.11)}$$

where $\tilde{m}^2 = m^2 - g^2N/\pi$.

The λ cutoff dependence of the propagator is expected because $S(p) = \int d^2x \exp(ip \cdot x) \langle 0|T(\bar{\psi}(x)\psi(0)|0\rangle$ is not a gauge invariant matrix element. The mechanism for quark confinement, i.e. the disappearance of quark mass singularities in the physical S-matrix, is clear in this formulation. These singularities are shielded by the λ^{-1} term in the limit $\lambda \to 0$. As $\lambda \to 0$, the propagator is linearly proportional to λ if a γ_- stands to either side to eliminate the λ dependence of the numerator.

2. The Bound State Wave Equation.

Armed with the dressed propagator, the wave function can be found by summing all gluon ladder exchange diagrams. This can be done by writing an integral, Bethe-Salpeter, equation for the wave function $\Phi_n^{a\bar{b}}(P,p)$ describing the nth bound state of quark a with momentum p and antiquark $\bar{b}$ with momentum $P - p$. (The explicit Dirac indices of eq. (III.A. 5) have been dropped)

$$\Phi_n^{a\bar{b}}(P,p) = ig^2 N(iS(p))\gamma_- \int \frac{d^2k}{(2\pi)^2} \frac{\Phi_n^{a\bar{b}}(P,k)}{(p_- - k_-)^2} \gamma_-(iS(P - p)). \quad \text{(III.A.12)}$$

This equation is represented diagramatically in Figure (III.A.5).

The equation can be simplified due to the Dirac structure and to the instantaneous potential which depends only on minus momentum components. Defining the function $\phi_n^{a\bar{b}}$ by

$$\phi_n^{a\bar{b}}(P;p_-)\gamma_- = \int \gamma_- \Phi_n^{a\bar{b}}(P,p)\gamma_- dp_+ \quad \text{(III.A.13)}$$

gives

$$\phi_n^{a\bar{b}}(P,p_-) = -\frac{i g^2 N}{(2\pi)^2}\int dp_+\left(p_+ - \frac{\tilde{m}_a^2}{2p_-} - \left(\frac{g^2 N}{2\pi\lambda} - i\varepsilon\right)\operatorname{sgn} p_-\right)^{-1}$$

$$\left(P_+ - p_+ - \frac{\tilde{m}_b^2}{2(P_- - p_-)} - \left(\frac{g^2 N}{2\pi\lambda} - i\varepsilon\right)\operatorname{sgn}(P_- - p_-)\right)^{-1}\cdot\int dk_- \frac{\phi_n^{ab}(P,k_-)}{(p_- - k_-)^2}. \tag{III.A.14}$$

The p_+ integration can now be done as a contour integal. The only non-zero contribution comes when the poles are on opposite sides of the real axis. Taking P_- positive for a real particle, this imposes the condition that $P_- > p_- > 0$. Performing the integration gives

$$\left(P_+ - \frac{\tilde{m}_a^2}{2p_-} - \frac{\tilde{m}_b^2}{2(P_- - p_-)} - \frac{g^2 N}{\pi\lambda}\right)\phi_n^{a\bar{b}}(P,p_-) = -\frac{g^2 N}{2\pi}\,\theta(p_-)\theta(P_- - p_-)\cdot$$

$$\cdot\int\frac{dk_-}{k_-^2}\,\phi_n^{a\bar{b}}(P,p_- - k_-)\ . \tag{III.A.15}$$

The integral on the right hand side of equation (III.A.15) needs infrared regularization by the λ cutoff prescription. The λ dependence generated by the cutoff exactly cancels the λ dependence of the left hand side. Multiplying through by $2P_-$ and defining the variable $x = p_-/P_-$ in eq. (III.A.15) gives the 't Hooft

equation [5] for the meson bound state of mass M_n.

$$M_n^2 \phi_n^{a\bar{b}}(x) = \left(\frac{\tilde{m}_a^2}{x} + \frac{\tilde{m}_b^2}{(1-x)}\right)\phi_n^{a\bar{b}}(x) - g^2 \frac{N}{\pi} \mathcal{P}\int_0^1 dy \frac{\phi_n^{a\bar{b}}(y)}{(y-x)^2} = (H_o + V)\phi_n^{a\bar{b}}(x) \quad x\varepsilon[0, 1]$$

(III.A.16)

$$\phi_n^{a\bar{b}}(x) = 0 \qquad x\notin[0, 1]$$

where H_o is the free particle Hamiltonian (P_+) and V is the Coulomb potential. The Lorentz **invariant** variable function, x, is the fraction of the total meson momentum carried by the quark in an infinite momentum frame where the meson is moving to the right. This description is not parity invariant due to the choice of gauge.

The disappearance of the λ dependence in the 't Hooft equation indicates that the wave function is well defined with respect to infrared ambiguities and is gauge invariant. The gauge invariance of the wave function can be shown formally [8]. $\phi_n(x)$ can be expressed in terms of the function $\Phi_n(x)$ of eq. (III.A.5) through eq. (III.A.13) as

$$\phi_n(x) = \int dp_+ (\Phi^n_{\alpha\beta}\gamma_{-\beta\alpha}) = \int dp_+ \int d^2\xi \exp \frac{-i}{2}(\xi_+ P_-(2x-1) + \xi_-(2p_+ - P_+)) \cdot$$

$$\langle n| T(\psi^{(+)\dagger}(\tfrac{\xi}{2})\psi^{(+)}(-\tfrac{\xi}{2}))|0\rangle = 4\pi \int d\xi_+ \exp - i\xi_+ P_-(2x-1) \cdot$$

$$\cdot \langle n| T(\psi^{(+)\dagger}(\xi_+, 0)\psi^{(+)}(-\xi_+, 0))|0\rangle \,. \qquad \text{(III.A17)}$$

Due to the p_+ integration, only fields on the zero time ($\xi_- = 0$) surface contribute to the wave function. We compare this to the explicitly gauge invariant wave function $\Lambda(\xi)$ given by

$$\Lambda(\xi) = \langle n | T\left(\bar{\psi}(-\xi)\exp\left(i \int_{-\xi}^{\xi} A_\mu dx^\mu\right)\psi(\xi)\right) | 0 \rangle \qquad \text{(IIIA.18)}$$

which shows that a general quark-antiquark state involves an infinite number of gluons. Restricting ξ to the equal time surface in the gauge $A_- = 0$ eliminates the line integral operator and shows gauge invariance of the matrix element in eq. (III.A.17). Thus, the choice of the $A_- = 0$ gauge together with the choice of an infinite momentum frame with $x_- = 0$ equal time surface yield a simple gauge invariant quark-antiquark operator.

Investigations [34] into the existence of states of greater than two quarks by summing planar diagrams in $(QCD)_2$ show that a λ independent wave equation of the form of eq.(III.A16), with H_o equal to the total free particle energy and V equal to the sum of pairwise Coulomb exchanges, can be obtained provided the state is a color singlet. It is only for the meson state, however, that the planar diagram summation represents the leading order in an N^{-1} expansion.

3. The Color Singlet Quark-Antiquark Scattering Amplitude [6].

The remaining element needed in expressing the 't Hooft model in mesonic terms is the color singlet quark-antiquark scattering amplitude, $iT^{a\bar{b}}_{\alpha\beta;\gamma\delta}(P',p,p')$, which satisfies the ladder exchange integral equation depicted in fig. (III.A. 6),

$$iT^{a\bar{b}}_{\alpha\beta;\gamma\delta}(P',p,p') = \frac{ig^2}{(p_- - p'_-)^2}(\gamma_-)_{\alpha\gamma}(\gamma_-)_{\beta\delta} + \frac{g^2N}{(2\pi)^2}\int\frac{d^2k}{(p_- - k_-)^2}T^{a\bar{b}}_{\rho\sigma;\gamma\delta}(P,k,p')$$

$$\cdot(\gamma_- S(P-k))_{\beta\sigma}(\gamma_- S(k))_{\alpha\rho} \quad . \qquad \text{(III.A.19)}$$

$T_{\alpha\beta;\gamma\delta}(P;\ p,p')$ is related to $D_{\alpha\beta;\gamma\delta}(P:\ p,p')$ of eq. (III.A. 1) by truncating the external quark and antiquark lines. Its Dirac structure is $T_{\alpha\beta;\gamma\delta}(P;\ p,p') = (\gamma_-)_{\alpha\gamma}(\gamma_-)_{\beta\delta}T(P;p,p')$. The Dirac algebra gives

$$iT^{a\bar{b}}(P';\ p,p') = \frac{ig^2}{(p_- - p'_-)^2} - \frac{ig^2N}{(2\pi)^2}\int\frac{d^2k}{(p-k)^2}S^a_E(k)\left[iT^{a\bar{b}}(P,k,p')\right]S^{\bar{b}}_E(P-k)$$

(III.A.20)

where $S_E(p)$ is defined by $S_E(p)\gamma_- = \gamma_- S(p)\gamma_-$. To separate the integrals we take $\tau^{a\bar{b}}(P;p_-,p'_-) = \int dp_+ S_E(p)T^{a\bar{b}}(P;p,p')S_E(P-p)$. Following the same steps as for the wave equation, we find that $\tau(P;p_-,\ p'_-)$ satisfies an inhomogeneous 't Hooft equation:

(III.A.21)

$$(P^2 - \frac{\tilde{m}_a^2}{x} - \frac{\tilde{m}_b^2}{1-x})\tau^{a\bar{b}}(P;x,x') + \frac{g^2N}{\pi}\fint dy\ \frac{\tau^{a\bar{b}}(P;y,x')}{(y-x)^2} = \frac{-4i\pi g^2}{(x_- - x'_-)^2 P_-}$$

where $x = p_-/P_-$ and $x' = p'_-/P_-$. Solving by standard techniques gives

$$\tau^{a\bar{b}}(P;\, x,x') = -\frac{4i\pi g^2}{P_-} \sum_n \frac{\phi_n^{a\bar{b}}(x')}{P^2 - M_n^2} \int dy\, \frac{\phi_n^{a\bar{b}}(y)}{(y-x)^2}\,. \qquad \text{(III.A.22)}$$

Inserting this solution back into eq. (III.A.20), we find

$$iT^{a\bar{b}}(P,x,x') = \frac{ig^2}{P_-^2(x-x')^2} + \sum_n \Gamma_n^{a\bar{b}}(x)\, \frac{i}{P^2 - M_n^2}\, \Gamma_n^{a\bar{b}}(x') \qquad \text{(III.A.23)}$$

where $\Gamma_n^{a\bar{b}}(x)$ is the normalized meson vertex

$$\Gamma_n^{a\bar{b}}(x) = i\sqrt{\frac{\pi}{N}}\left[\frac{g^2N}{\pi}\right]\frac{1}{P}\int_0^1 dy\, \frac{\phi_n(y)}{(y-x)^2} = i\sqrt{\frac{\pi}{N}}\left[\frac{g^2N}{\pi}\right]$$

$$\left[\frac{2\phi_n(x)\theta(x)\theta(1-x)}{\lambda} + \frac{1}{P}\mathcal{P}\int dy\, \frac{\phi_n^{a\bar{b}}(y)}{(y-x)^2}\right] \qquad \text{(III.A.24)}$$

according to the λ cutoff regularization. This solution is displayed in fig. (III.A.6).

The meson vertex $\Gamma_n(x)$ is essentially the wave function $\phi_n^{a\bar{b}}(x)$ with external propagators cut off. It gives the amplitude for decay of a meson to a quark-antiquark pair. The correct color normalization appears in the explicit $N^{-\frac{1}{2}}$ factor. The λ

dependence shows the gauge variance of the vertex. The vertex grows as λ^{-1} as $\lambda \to 0$ for $0 < x < 1$. This λ^{-1} behavior cancels the λ behavior of the fermion propagator to give λ independent amplitudes for gauge invariant quantities as $\lambda \to 0$. The graphical structure of the bound state vertex expressed by eq. (III.A. 24) is shown in fig. (III.A. 7).

B. Properties of the Bound State Wave Function.

The 't Hooft Hamiltonian operator is hermitian on the space of functions $f(x)$, $x\varepsilon[0,1]$ such that $f(0) = f(1) = 0$. On this space it has been proven [51] that the spectrum of the operator is discrete and non-degenerate. The solutions, $\phi_n(x)$, to the 't Hooft equation are conventionally taken to be real and positive near $x = 0$. This implies

$$\phi_n^{a\bar{b}}(x) = (-1)^{n+1}\phi_n^{b\bar{a}}(1 - x) \ . \qquad \text{(III.B. 1)}$$

They form a complete, orthonormal set

$$\sum_n \phi_n^{a\bar{b}}(x)\phi_n^{a\bar{b}}(y) = \delta(x - y)$$

$$\int_0^1 dx\ \phi_n^{a\bar{b}}(x)\phi_m^{a\bar{b}}(x) = \delta_{nm} \ . \qquad \text{(III.B. 2)}$$

The meson Green's function, $G(x,y;\, q^2)$, can be written in terms of the wave functions as

$$G^{a\bar{b}}(x,y\,;\, q^2) = \sum_k \frac{\phi_k(x)\phi_k(y)}{q^2 - M_k^2 + i\varepsilon} \qquad \text{(III.B.3)}$$

and

$$G^{a\bar{b}}(x;\, q^2) = \int dy\; G^{a\bar{b}}(x,y;\, q^2). \qquad \text{(III.B.4)}$$

The edge point boundary conditions arise because the infinities in H_o at the points $x = 0, 1$ must be cancelled exactly by terms in the potential. This requires the <u>edge point behavior</u> of the wave function to be

$$\phi_n^{a\bar{b}}(x) = \begin{cases} C_n^{a\bar{b}}\; x^{\beta_a} & x \to 0 \\ (-1)^{n+1} C_n^{b\bar{a}}\; (1-x)^{\beta_b} & x \to 1 \end{cases} \qquad \text{(III.B.5)}$$

where $C_n^{a\bar{b}}$ and $C_n^{b\bar{a}}$ are positive constants and β is the solution, $0 < \beta < 1$, of

$$\pi\beta \cot \pi\beta = 1 - \left[\frac{\pi}{g^2 N}\right] m^2 . \qquad \text{(III.B.6)}$$

The wave function can be analytically extended [7] into the complex x plane with cuts running to infinity from $x = 0, 1$ along the negative and positive real axes. The branch point singularities give rise to the non-integer power behavior of eq. (III.B. 5).

The <u>large mass</u> wave functions, $M_n^2 >> m^2$, have the approximate form

$$\phi_n^{a\bar{b}}(x) = \sqrt{2} \quad \sin\,[\,(n+1)\pi x], \quad n >> 1 \qquad \text{(III.B. 7)}$$

except at the edge points where eq. (III.B. 5) describes the behavior. The mass of this state can be found from the 't Hooft equation to be

$$M_n^2 = \left[\frac{g^2 N}{\pi}\right] \pi^2 n \,, \qquad n >> 1 \,. \qquad \text{(III.B. 8)}$$

The large masses thus lie on straight line "Regge trajectories" of slope $\alpha' = g^2 N\pi$. More elaborate W.K.B. techniques have be used [7, 35] to find the first corrections to eqs. (III.B. 7) and (III.B. 8). An x dependent phase in the argument of the sin in eq. (III.B. 7) and further terms in eq. (III.B. 8) which grow like log n appear. Numerical calculations show that the W.K.B. form is reached very quickly. The edge point, large mass wave functions are universal <u>scaling functions</u> [8]. From the 't Hooft equation, it is easily seen that

$$\lim_{n \to \infty} \phi_n^{a\bar{b}}(g^2 N\xi/\pi M_n^2) = \phi^a(\xi)$$

$$\lim_{n \to \infty} (-1)^{n+1} \phi_n^{a\bar{b}}(1 - g^2 N\xi/\pi M_n^2) = \phi^b(\xi) \,. \qquad \text{(III.B. 9)}$$

The scaling functions depend only on quark properties and satisfy [36]

$$\int d\xi \phi^a(\xi) = \pi \left[\frac{\pi}{g^2 N}\right]^{\frac{1}{2}} m_a \quad . \qquad \text{(III.B.10)}$$

The Green's function also scales for large q^2

$$\lim_{q^2 \to \pm\infty} q^2 G^{a\bar{b}}(\pm g^2 N\xi/\pi q^2;\ q^2) = h^a_{\pm}(\xi) \qquad \text{(III.B.11)}$$

The wave functions satisfy several relations which arise from the underlying <u>parity</u> invariance of the theory. Since the spectrum is non-degenerate, every bound state has a definite intrinsic parity. The parity relations [6] involve integrals over wave functions which, as seen from eq. (III.A. 17), probe the origin of configuration space, which is invariant under a parity transformation.

$$m_a \int dx \frac{\phi_n^{a\bar{b}}(x)}{x} = (-1)^{n+1} \int dx \frac{\phi_n^{a\bar{b}}(x)}{(1-x)} \qquad \text{(III.B.12)}$$

$$M_n^2 \int dx\ \phi_n(x) = m_a^2 \int dx \frac{\phi_n^{a\bar{b}}(x)}{x} + m_b^2 \int dx \frac{\phi_n^{a\bar{b}}(x)}{1-x} \qquad \text{(III.B.13)}$$

Equation (III.B. 13) can be shown directly from simple manipulation of the 't Hooft equation. We give a proof of these relations by using parity invariance in the Bethe Salpeter formalism developed above in Appendix A.

C. Hadronic Scattering Amplitudes in the 't Hooft Model.

Knowledge of the meson vertex (eq. III.A. 24) and the quark-antiquark T-matrix (eq. III.A. 23) allows the calculation of any meson amplitude. In this section, we develop a step-by-step procedure to compute any amplitude involving γ_- vertices (this includes bound state vertices), using the meson three and four point functions as examples. This allows all of the matrix algebra to be done trivially so that it need never appear. A set of graphs arises from bare quark graphs which includes only mesonic elements - wave functions and propagators - folded into Coulomb potentials.

These rules, coupled with the assumption of electromagnetic gauge invariance, allow the calculation of all amplitudes discussed in this paper. Modifications due to γ_+, I, γ_5 vertices are considered in Appendix B and the divergencelessness of the vector current amplitudes shown in Appendix C.

For the remainder of this paper we define units of mass such that $g^2N/\pi \equiv 1$. These factors can always be restored by simple dimensional analysis.

Consider an amplitude with n vertices.

Step 1.: Connect the vertices in all cyclically inequivalent ways with clockwise directed quark lines to form $(n - 1)!$ rings. Insert a meson vertex function as shown in fig. (III.A. 7) at every meson vertex. Keep only those rings whose internal flavor flow is consistent with external particle flavor assignments. (see fig. (III.C. 1)).

Step 2. To every remaining ring diagram, draw another diagram inserting the T-matrix, as shown in fig. (III.A. 6) in all possible non-overlapping ways in the color singlet quark-antiquark channels, except across bound state vertices. (See fig. (III.C. 2))

In this step, we have performed the sum over all planar diagrams to get the leading order in N^{-1} contribution to the amplitude. The T-matrix does not appear across bound state vertices because it is already included in the wave function.

Step 3. Eliminate all gluons exchanged across bound state vertices. A remaining diagram has ℓ loops, f quark lines, B bound state vertices and G gluons. Compute the integer $m = f - \ell - B - G$ for each diagram. If $m > 0$ the diagram may be eliminated. (See fig. (III.C. 3)

In this step, we are looking at the leading λ behavior of a diagram as $\lambda \to 0$. Elimination of the gluon across the vertex is the graphical equivalent of eliminating the non-leading piece in eq. (III.A. 24) as $\lambda \to 0$ and simplifies counting. The leading λ behavior of the diagram is λ^m; each fermion propagator gives a factor of λ (eq. III.A. 11), each loop integration effectively eliminates a fermion propagator as in the derivation of the 't Hooft equation, each wave function contributes λ^{-1} from the first term in eq. (III.A. 24), and the infrared singular part of every gluon propagator contributes λ^{-1}. Simple topology shows that this constraint eliminates all graphs with two or more bare current vertices.

Step 4. The remaining diagrams represent integrals over loop momenta. The integrals over the plus momentum components can be trivially done by contour integration. This splits each loop of f fermion lines into a set of $(f - 1)$ time orderings, with the direction of a quark line determined by its minus momentum component, positive momentum flowing to the right.

To every diagram, construct a set of time ordered diagrams by deforming the graph in all possible ways consistent with minus momentum conservation at the external vertices. This deformation is done by considering all orderings of the vertices. See fig. (III.C. 4).

Step 5: In the time ordered diagrams, if there is a bound state vertex where the quark and antiquark are not both pointing in the same direction as the vertex, insert a gluon to achieve this configuration. See fig. (III.C. 5).

This step reinserts the non-leading piece of the vertex which was dropped in Step 3.

Step 6: Consider all time ordered diagrams which do not contain any meson propagators. Recompute m as in Step 3, with the difference that G is the number of gluons in the diagrams which do not change the directions of the quark lines at its vertices. If $m > 0$, drop the diagram. See fig. (III.C. 5).

This step counts the λ dependence of the time ordered diagrams by determining whether the singular part of the gluon propagator can contribute. This λ^{-1} term can only contribute if

the minus component of momentum flowing through the gluon is zero.

The planarity of the diagram insures that $m \geqslant -1$. There are thus two cases:

Case 1: $m = 0$.

(i) Scale the minus momentum of each quark line by dividing by some external minus momentum component so that each quark line is characterized by a Lorentz invariant momentum fraction variable. The allowed ranges of the invariant integration variables are determined by the time orderings of the diagram.

(ii) To every loop with $f_{r(\ell)}$ right (left) directed quark lines, $f = f_r + f_\ell$, assign a factor $(-1)^{f_r}(i)^{f+1}\binom{f-2}{f_\ell - 1}\frac{N}{2\pi}\int$, where the limits on the integration are determined by the time ordering. This factor arises from keeping track of the contour integration over plus momentum components.

(iii) To every quark-gluon vertex assign a factor g.

(iv) To every gluon carrying momentum fraction w which does not change the directions of quark lines at its vertices assign a factor $2i\delta(w)$.

(V) To every other gluon carrying momentum fraction w assign a factor i/w^2.

(vi) To every bound state vertex with momentum fraction z, with quark a carrying momentum fraction w and antiquark to carrying momentum fraction $z - w$ assign a factor $-2g\phi^{a\bar{b}}(\frac{w}{z})$.

(vii) Change loop integration variables so that all integrals go from zero to one. This is the conventional standard form for displaying the amplitude.

(viii) Insert factors of scale momentum as needed to satisfy Lorentz index requirements.

Case II: $m = -1$.

This case only arises in connection with the n meson $\rightarrow$ n meson function where the incident and outgoing mesons alternate around the ring. These diagrams thus occur as part of the four, six, eight, etc. point amplitudes. The $\mathcal{A}^{ut}$ diagram of fig. (III.C. 1) is an example.

These diagrams all go as λ^{-1} but, as demanded by gauge invariance, the sum of them cancels out to this order. The next to leading λ^{0} order must be recovered by taking into account the next to leading pieces of the meson vertex, gluon propagator and fermion propagator. The total meson vertex correction is easily seen to vanish as a result of the vanishing of the λ^{-1} contribution.

(i) To every $m = -1$ diagram with G gluons which do not change direction of the quark lines at its vertices compute using the $m = 0$ rules with the exception that one of the G gluons carrying momentum fraction w be assigned a factor i/w^2. Do this for each of the G gluons, generating G terms.

This takes into account the non-leading gluon exchange correction, giving rise to terms with gluon denominators which can be zero in the loop integration region. These infrared singularities are cancelled by the fermion propagator corrections by the following prescription:

Take the $m = -1$ diagram with n vertices and insert a gluon across one of the vertices. Do this for each vertex, one at a time, to create n diagrams. Compute these diagrams using the $m = 0$ rules, except that a factor of i/w^2 is assigned to the inserted gluon carrying momentum fraction w. One of these diagrams, with the gluons inserted across the ith state, will have the same gluon denominator as one of the diagrams computed above when all terms are written in the standard form. Add this term to the amplitude. It should eliminate the infrared singularity. In addition add an off mass shell term by inserting a factor $(M_i^2 - p_i^2)\delta$ (gluon denominator) into the integrand of the term just added.

Step 7: Now consider diagrams with meson propagators. They connect subprocesses whose amplitudes are calculated by the rules above. Connect the subprocess amplitudes by meson propagators $\sum_k i/p^2 - M_k^2 + i\varepsilon$ where p^2 is the invariant mass of the meson channel. The bound state summations are to be done before any integration.

We have thus given a set of rules which generates explicitly infrared finite, gauge invariant, amplitudes. The separation and elimination of individual graphs contributing to an amplitude is a

gauge variant procedure. The amplitudes are not explicitly parity invariant, as seen from their dependence on minus momentum components. This stems from the lack of parity invariance in the choice of gauge. The equality of amplitudes calculated in parity reversed frames leads to highly non-trivial parity relations. These identities can hopefully be shown directly by clever manipulation of the properties of bound state wave functions. While no such proofs of these identities exist, numerical calculations are consistent with their validity [9].

The rules of this section are stated as if for a general n vertex amplitude. We believe these rules to be applicable in general but have not checked them beyond the four vertex amplitudes computed in this paper. In particular the prescription for handling $m = -1$ diagrams might need modification. Using these rules we find the mesonic three point vertex to be given by

$$i\mathcal{T}_{n;km}\left(p_n, x = \frac{p_{k-}}{p_{n-}}\right) = 2igx(1-x)\int_0^1 dwdy\ \phi_k^{a\bar{b}}(w)\phi_m^{b\bar{c}}(y) \cdot \left[\frac{\phi_n^{a\bar{c}}(xw) - \phi_n^{a\bar{c}}(y(1-x)+x)}{(y(1-x)+x(1-w))^2}\right] . \tag{III.C.1}$$

The notation and diagrammatic representation of this formula is given in fig. (III.C. 6). Each contribution involves exchange of a gluon, reflected by the denominator of eq. (III.C. 1).

The four point meson-meson scattering amplitude can also be computed

$$i\mathcal{A}^{(s,t)}_{jk;mn}(p_j;x_k,x_m,x_n) = -4i\frac{\pi}{N}x_k x_n \int dwdy \frac{\phi_j(1-x_n(1-w))\phi_k(y)\phi_m\left(\frac{x_k}{x_m}y\right)\phi_n(w)}{(x_m + wx_n - x_k y)^2}$$

$$-\sum_\ell \mathcal{T}_{\ell;kj}\left(\frac{x_k}{1+x_k}\right)\frac{i}{s-M_\ell^2+i\varepsilon}\mathcal{T}_{\ell;mn}\left(\frac{x_m}{1+x_k}\right) - \sum_\ell \mathcal{T}_{j;\ell n}(1-x_n)\frac{i}{t-M_\ell^2+i\varepsilon}\mathcal{T}_{m;k\ell}\left(\frac{x_k}{x_m}\right).$$

$$i\mathcal{A}^{(u,s)}_{jk;mn} = i\mathcal{A}^{(s,t)}_{jk;mn}\ (m \to n;\ t \to u)$$

$$i\mathcal{A}^{(u,t)}_{jk;mn} = 4i\frac{\pi}{N}x_k \int_0^1 dw\phi_k(w)\int_0^1 dy \left\{ x_m\phi_m(y)\phi_n\left(\frac{x_k w}{x_n}\right)\left[\frac{\phi_j(x_m y)-\phi_j(x_m-x_k(1-w))}{(x_m(1-y)-x_k(1-w))^2}\right]\right.$$

$$+ x_n\phi_n(y)\phi_m\left(1-\frac{x_k}{x_m}(1-w)\right)\left[\frac{\phi_j(1-x_n(1-y)) - \phi_j(x_m-x_k(1-w))}{(yx_n - wx_k)^2}\right]$$

$$\left. + \left[\frac{p_m^2-M_m^2}{x_m} + \frac{p_n^2-M_n^2}{x_n}\right]\phi_j(x_m - x_k(1-w))\phi_m\left(1-\frac{x_k}{x_m}(1-w)\right)\phi_n\left(\frac{x_k}{x_n}w\right)\right\}$$

$$-\sum_\ell \mathcal{T}_{j;\ell n}(1-x_n)\left[\frac{i}{t-M_\ell^2+i\varepsilon}\right]\mathcal{T}_{m;\ell k}\left(\frac{1-x_n}{x_m}\right) - \sum_\ell \mathcal{T}_{j;m\ell}(x_m)\frac{i}{u-M_\ell^2+i\varepsilon}\mathcal{T}_{n;k\ell}\left(\frac{x_k}{x_n}\right).$$

(III.C.2)

The notation and diagrammatic representation of this formula is given in fig. (III.C. 7). As indicated, the amplitude can be written in terms

of three point functions and contact terms in each channel. We have made the usual separation into graphs arising from the (st), (us), and (ut) duality sectors. (See fig. (III.C. 1(b))). The expressions given here are valid for the kinematic region which will be of interest; the $1 > x_m, x_n > x_k$.

In any process, the external flavor content may allow contributions from diagrams with quarks circulating in opposite directions (see fig. (III.C. 1)). Denoting the amplitude calculated from a given graph by Z and that of the arrow reversed graph by $\bar{Z}$, the relation between Z and $\bar{Z}$, apart from changing flavor labels, is

$$Z\left[\phi(x)\right] = \bar{Z}\left[\phi(1-x)\right] . \qquad \text{(III.C. 3)}$$

IV. SINGLE CURRENT MATRIX ELEMENTS

We proceed now to the main objective of this paper, the investigation of the behavior of photon-hadron interactions in the 't Hooft model. The photon, of course, does not exist as a dynamic degree of freedom in two dimensions. Its source field, the flavor conserving, Lorentz vector, local bilinear in quark fields, $J_\mu^{em}(x) = \sum_a e_a :\bar{q}^a(x)\gamma_\mu q^a(x):$, is a non-trivial operator whose behavior can be studied in the 't Hooft model as a photon analogue.

It has been argued [37] that, due to the momentum helicity conserving structure of the fermionic theory discussed above, the electromagnetic analogue is better realized by Lorentz scalar rather than vector currents. We describe how our results can be applied to the scalar case in Appendix B.

A. The Photon-Hadron Coupling $\gamma^*(q) \to n$.

The direct coupling of the electromagnetic current to a meson n, $\mathcal{J}_\mu^n(q) = \langle n(q)| J_\mu | 0\rangle$, can be calculated from the diagram of fig. (IV.A. 1) for the minus current component. Using current conservation we find

$$\mathcal{J}_\mu^n(q) = \varepsilon_{\mu\nu}\, q^\nu \left\{ e_a \left[\frac{N}{\pi}\right]^{\frac{1}{2}} \int_0^1 dx \phi_n^{a\bar{a}}(x) \right\} \qquad \text{(IV.A. 1)}$$

The existence of the $\varepsilon_{\mu\nu}$ tensor in two dimensions allows a gauge invariant coupling between a "scalar" meson and the electromagnetic current. The current coupling in four dimensions to a vector meson

is proportional to the polarization vector of the meson.

Parity invariance gives a constraint on the intrinsic parity of the meson. If we denote the intrinsic parity of the meson n by $(-1)^n$ and $q'_\lambda = q^\lambda$, the parity relation

$$\mathcal{J}^{\,n}_{\mu}(q) = (-1)^n \mathcal{J}^{\mu,n}(q') \qquad \text{(IV.A. 2)}$$

implies that n is odd and the meson has negative intrinsic parity. This follows just from parity invariance and the form of the gauge invariant coupling. We can directly check that this is the case by taking $x \leftrightarrow 1 - x$ in the integrand of eq.(IV.A. 1) and using eq. (III.B. 1) to show that the photon couples to an odd parity meson.

B. The Inelastic Meson Form Factor: $n(p) \to \gamma^*(q) \to m(p+q)$.

The computation of the amplitude for electromagnetically induced transition from a meson state n to state m, $\mathcal{F}^{nm}_{\mu} = \langle m(p+q)|J_\mu|n(p)\rangle$, depends on the details of the scattering. We take the transition to be an excitation, i.e. $M_m^2 > M_n^2$. There is only one divergenceless first rank tensor function of two momenta in two dimensions and the form factor can be written

$$\mathcal{F}^{nm}_{\mu}(p,q) = \varepsilon_{\mu\nu}\, q^\nu \mathcal{F}^{nm}(q^2) \ . \qquad \text{(IV.B. 1)}$$

We consider first the case where the incident photon is timelike. The amplitude can be computed from the diagrams of fig.

(IV.B. 1), and is given by

$$\mathcal{F}^{nm}(z = q_-/p_{m-}) = 2e_a \frac{(1-z)}{z} \int_0^1 dy\, \phi_n^{a\bar{b}}(y) \Big\{ \phi_m^{a\bar{b}}(y(1-z) + z)$$

$$+ z^2 \int dw G^{a\bar{a}}(w;q^2) \left[\frac{\phi_n^{a\bar{b}}(zw) - \phi_m^{a\bar{b}}(y(1-z) + z)}{(y(1-z) + z(1-w))^2} \right] \Big\}$$

$$+ (-1)^{n+m}(a \leftrightarrow \bar{b}) \qquad \text{(IV.B. 2)}$$

where the Lorentz invariant z is restricted by kinematics to $0 < z < 1 - M_n^2/M_m^2$. The scaling variable z can be written in terms of external masses as the solution of the momentum conservation condition

$$\frac{M_n^2}{1-z} + \frac{q^2}{z} = M_m^2, \quad 0 < z < 1 - M_n^2/M_m^2 \qquad \text{(IV.B. 3)}$$

The two solutions to this quadratic, z_1 and $z_2 = q^2/M_m^2 z_1$, correspond to parity reversed kinematics. Parity invariance demands that

$$\mathcal{F}^{nm}(z_1) = (-1)^{n+m+1}\mathcal{F}^{nm}(z_2 = q^2/M_m^2 z_1), \qquad q^2 > 0 \qquad \text{(IV.B. 4)}$$

When the incident current is spacelike, the two parity reversed reference frames give rise to amplitudes which have

explicitly different functional forms. The frames are distinguished by the sign of q_-, the minus component of the current momentum. We denote Frame I (II) by the frame in which q_- is negative (positive). The effect of a negative q_- in the time-ordered diagrams of fig. (IV.B. 1) is to flip the direction of the current, so that in Frame I the amplitude is calculated as if the current is outgoing and timelike. This effectively interchanges the initial and final meson states in the amplitude, giving

$$\mathscr{F}^{nm}_{I}(x = -q_-/p_{n-}) = -\mathscr{F}^{mn}(x) \qquad \text{(IV.B.5)}$$

where $\mathscr{F}^{nm}_{I}$ denotes the Frame I amplitude and the scaling variable x is kinematically restricted to $1 > x > 0$ and satisfies

$$M_n^2 - \frac{q^2}{x} = \frac{M_m^2}{1-x} \ , \qquad 1 > x > 0 \ . \qquad \text{(IV.B.6)}$$

The Frame II diagrams are the same as the timelike diagrams, giving rise to the same functional form for the Frame II amplitude $\mathscr{F}^{nm}_{II}$.

$$\mathscr{F}^{nm}_{II}(z = q_-/p_{m-}) = \mathscr{F}^{nm}(z) \ . \qquad \text{(IV.B.7)}$$

The variable z satisfies eq.(IV.B.3) but is now restricted to $1 > z > 1 - M_n^2/M_m^2$. There is only one solution to the quadratic of eq. (IV.B.3) in this region. Parity invariance implies

$$\mathscr{F}^{mn}(x = -q_-/p_{n-}) = (-1)^{n+m}\mathscr{F}^{nm}(z = -q^2(1-x)/M_m^2 x), \quad q^2 < 0. \tag{IV.B. 8}$$

The two terms in the curly brackets of eq. (IV.B.2) have a simple physical interpretation which we have indicated in fig.(IV.B.1). The first represents the coupling of the bare current to the mesons while the second represents the coupling of the hadronic current content to the mesons through the three point function. This separation is gauge invariant.

The parity relations of eqs. (IV.B. 4) and (IV.B. 8) are highly nontrivial. We cannot show them by direct maniputation but can use these equalities to bring out some interesting properties of the form factor not evident in either expression alone.

Having derived the form factors, we can look at the imaginary part of the forward Compton scattering amplitude. In the leading order in N^{-1} tree diagram theory this is proportional to the form factor squared, where the mass of the final state is equal to the photon-hadron center of mass energy, $\sqrt{s}$. We take this energy to be large and look at $\lim_{M_m \to \infty} \mathscr{F}^{nm}$ first for finite $q^2 < 0$ and then for $q^2 \to -\infty$. For simplicity we discuss the case where $e_b = 0$.

(1) Finite $q^2 < 0$.

We are here considering forward Compton scattering of almost real photons, a process which would be described by Regge theory ideas

in four dimensions. In the large M_m^2 limit, eqs. (IV.B. 3) and (IV.B. 4) show that the scaling variables are pushed to the edge points: $z = 1 - M_n^2/M_m^2$ and $x = -q^2/M_m^2$. Evaluating both sides of eq. (IV.B. 8) in this limit we get

$$2e_a(M_m^2)^{-\beta_a} C_n^{a\bar{b}} I^a(q^2) = 2e_a(M_m^2)^{-\beta_a}(-q^2) f^a(q^2) I_n^{a\bar{b}} \qquad \text{(IV.B. 9)}$$

where

$$I^a(q^2) = (-q^2)^{\beta_a} \int_0^\infty d\eta \phi^a(-q^2\eta) \left\{ \left[(1+\eta)^{\beta_a} - \eta^{\beta_a} \right] + \right.$$

$$\left. + \int_0^1 dy G^{a\bar{a}}(y;q^2) \left[\frac{y^{\beta_a} - (\eta+1)^{\beta_a}}{(1-y+\eta)^2} \right] \right\} \qquad \text{(IV.B.10)}$$

$$I_n^{a\bar{b}} = -(M_n^2)^{\beta_a} \int_0^1 dw \phi_n^{b\bar{a}}(w) \int_0^\infty d\eta \eta^{\beta_a} \left[\frac{\phi^b(M_n^2(1+\eta)) - \phi^b(M_n^2 w)}{(1-w+\eta)^2} \right] \qquad \text{(IV.B.11)}$$

and $f^a(q^2)$ is defined as

$$\lim_{x \to 0} G^{a\bar{a}}(x;q^2) = f^a(q^2) x^\beta \qquad \text{(IV.B.12)}$$

which implies that

$$f^a(q^2) = \sum_k \left[\int_0^1 \frac{dy \phi_k(y)}{q^2 - M_k^2} \right] C_k^{a\bar{a}} \quad . \qquad \text{(IV.B.13)}$$

The equality of eq. (IV.B. 9) shows that the ratio

$$\frac{C_n^{a\bar{b}}}{I_n^{a\bar{b}}} = r^a(q^2) \qquad \text{(IV.B. 14)}$$

independent of n and $\bar{b}$. As a result we can evaluate $r^a(q^2)$ in the $n \to \infty$ limit. This gives

$$r^a(q^2) = \frac{v^a \sin\pi\beta_a}{\pi} \qquad \text{(IV.B. 15)}$$

We thus find that

$$\lim_{M_m^2 \to \infty} \mathcal{F}^{nm}(q^2)' = 2e_a (M_m^2)^{-\beta_a} C_n^{a\bar{b}} \left[- q^2 f^a(q^2)\right] \left[\frac{\pi}{v^a \sin\pi\beta_a}\right]$$

$$= 2e_a s^{-\beta_a} \mathcal{V}_n^{a\bar{b}} \mathcal{V}_\gamma^a(q^2) \qquad \text{(IV.B. 16)}$$

where

$$\mathcal{V}_n^{a\bar{b}} = C_n^{a\bar{b}} \left[\frac{\pi}{v^a \sin\pi\beta_a}\right]^{\frac{1}{2}} \qquad \text{(IV.B. 17)}$$

$$\mathcal{V}_\gamma^a = \sum_k \left[\frac{\int_0^1 dy\,\phi_k(y)}{(M_k^2/q^2 - 1)}\right] C_k^{a\bar{a}} \left[\frac{\pi}{v^a \sin\pi\beta_a}\right]^{\frac{1}{2}}. \qquad \text{(IV.B. 18)}$$

With the form factor in the form of eq. (IV.B. 16), a Reggeized form for the imaginary part of the Compton amplitude can be

constructed and investigated. The analysis is identical to that of the meson-meson scattering amplitude done by Brower, et al. [10].

The function $\mathcal{V}_\gamma(q^2)$ given in eq. (IV.B. 18) shows how the photon couples to the strongly interacting system, analogous to $\mathcal{V}_n^{a\bar{b}}$, which describes the meson coupling. (More precisely $\mathcal{V}_\gamma^2(\mathcal{V}_n^2)$ is essentially the photon-photon-(meson-meson-) Reggeon vertex.) Comparing eqs. (IV.B. 17) and (IV.B. 18), we see that the photon interacts as if it were a certain weighted sum of mesons with photon quantum numbers. The photon is totally meson dominated. The mechanism responsible for this simple description is the mechanism which causes the term proportional to $f^a(q^2)$ to dominate in the Frame II amplitude (see eq.(IV.B. 9)). This dominant contribution comes from the region of phase space where the exchanged gluon in the three point function has vanishing minus momentum, giving rise to large factors coming from gluon denominators. This soft gluon exchange region dominates because the scaling variables are pushed to their edge points.

Looking at the diagrams of fig. (IV.B. 1), we note that the presence of the first bare coupling diagram is not reflected in the final pole dominated form of the form factor in the limit considered. This feature is more general, as can be seen by writing the form factor via dispersion relation from the crossed $\gamma^* \to n+m$ amplitude [8]. The first diagram of fig. (IV.B. 1) does not appear at all

in this current decay. The form factor can thus be written generally in unsubtracted form as

$$\mathcal{F}^{nm}(q^2) = e_a \sum_k \frac{\left[\int_0^1 dy\phi_k(y)\right]\chi_{knm}}{q^2 - M_k^2 + i\varepsilon} \quad . \qquad \text{(IV.B. 19)}$$

(2) Large $q^2 \to -\infty$ [8].

Deep inelastic leptoproduction in the Bjorken [3] limit probes the light cone structure of the theory which, via asymptotic freedom, reflects underlying bare quark dynamics. In this limit, we take $|q^2|$, $M_m^2 \to \infty$ in fixed ratio, $-q^2/M_m^2 = x_{BJ}/1 - x_{BJ}$, with x_{BJ} being the usual parton model scaling variable which is fixed between zero and one. The simplest description of this process in the 't Hooft model is in Frame I where x approaches x_{BJ} in the Bjorken limit. In this limit the bare coupling diagram completely dominates and a scaling amplitude results:

$$\lim_{BJ} \mathcal{F}^{nm}(x) = 2\pi e_a \frac{(1-x)}{x} \frac{m_a}{M_m^2} \phi_n(x) \qquad \text{(IV.B. 20)}$$

We have used eq. (III.B. 10) in deriving this result. The anomolous scaling behavior of eq. (IV.B. 20) due to the presence of the quark mass factor results from the momentum helicity non-conservation at the current vertex. The fermion's direction is changed by the photon, as can most easily be seen in the Breit frame.

The second term in the form factor is suppressed by the large denominator of the Green's function. This suppression cannot be overcome by soft gluon exchange because the scaling variable x is not at its edge point.

This example using the form factor thus shows the transition from a meson dominated description to a bare coupling description as the mass scale of the current increases.

V. TWO CURRENT MATRIX ELEMENTS

A. The Vacuum Polarization.

The minus-minus component of the vacuum expectation value of two currents, $\P_{\mu\nu} = \int d^2x\, e^{iq\cdot x} \langle 0|T^*(J_\mu(x)J_\nu(0))|0\rangle$, has the simple pole dominated structure indicated in fig. (V.A. 1). The amplitude is logarithmically ultraviolet divergent and must be regulated by a subtraction at $q^2 = 0$. This leads to the gauge invariant expression

$$\P_{\mu\nu}(q^2) = \sum_k \mathcal{J}^k_\mu \frac{i}{q^2 - M_k^2 + i\varepsilon} \mathcal{J}^k_\nu = \left\{-g_{\mu\nu}q^2 + q_\mu q_\nu\right\} ie_a^2 \frac{N}{\pi} \sum_k \frac{\left[\int_0^1 dx\phi_k(x)\right]^2}{q^2 - M_k^2 + i\varepsilon} . \tag{V.A.1}$$

The asymptotic freedom of $(QCD)_2$ guarantees that, as $q^2 \to -\infty$, this agrees with the result of calculating the lowest order quark diagram. Using the completeness relation of eq. (III.B. 2), we get

$$\lim_{q^2 \to -\infty} \P_{\mu\nu}(q^2) = \left\{-q_{\mu\nu} + \frac{q_\mu q_\nu}{q^2}\right\} ie_a^2 \frac{N}{\pi} \tag{V.A.2}$$

which agrees with $d_0^{(V)}$ computed from free quark field theory in Sec. (II.C). Furthermore, using eq. (III.B.13), [6,8] it is easy to show that the next order in q^2 corrections to $\P_{\mu\nu}$ are determined by bare quark masses. We thus see how non-trivial wave function identities conspire to make the hadronic theory reflect the underlying quark physics at short distance.

The physical region of interest of $\P_{\mu\nu}$ is the limit as $q^2 \to +\infty$ which is probed in the inclusive annihilation of the vector current into mesons. This is not a smooth limit due to the delta function discontinuity every time q^2 passes over a resonance. The delta function reflects the zero width of the bound states, which is a consequence of retaining only the leading order in the N^{-1} expansion. Some smoothing procedure like resonance averaging is needed in dealing with inclusive final states to take into account non-leading N^{-1} effects. Here, we simply interpolate between large mass states using $M_k^2 \to k\pi^2$. Thus, for inclusive annihilation of the current, we find

$$\lim_{q^2 \to \infty} \mathrm{Im}(i\P_{\mu\nu}) = \left\{g_{\mu\nu}q^2 - q_\mu q_\nu\right\} e_a^2 N \sum_k \delta(q^2 - M_k^2)\left[\int_0^1 dx\phi_k(x)\right]^2$$

$$= \left\{g_{\mu\nu}q^2 - q_\mu q_\nu\right\} \frac{e_a^2 N}{2\pi^2} \int_\Lambda^\infty dk\delta(q^2/\pi^2 - k)\left[\int_0^1 dx\phi_k(x)\right]^2$$

$$= \left\{g_{\mu\nu}q^2 - q_\mu q_\nu\right\} \frac{e_a^2 N}{2\pi^2} \left[\int_0^1 dx\phi_k(x)\right]^2_{k=q^2/\pi^2}$$

$$= \left\{g_{\mu\nu} - \frac{q_\mu q_\nu}{q^2}\right\} 2e_a^2 N \left[\frac{m_a^2}{q^2}\right] \qquad \text{(V.A.3)}$$

where eq. (III.B.10) has been used in the last line. There is an extra factor of ½ in the second line to give the correct density of states counting since only odd parity states are included. Again, the anomolous scaling behavior of the annihilation amplitude due to helicity nonconservation appears through the explicit dependence on the bare quark mass.

The appearance of the bare quark mass factor and the correct normalization of the annihilation cross section is insured by eq. (III.B.10). This equation is a prototypical example of a relation between summation over final states and constituent parton parameters. Relations of this type must exist in order to make the smooth transition from the bound state hadronic description to the short distance parton description of the theory.

B. Meson Decay To Photons: $n(p) \to \gamma^*(q_1) + \gamma^*(q_2)$.

We have derived the amplitude,

$\mathcal{K}^n_{\mu\nu} = \int d^2x\, e^{iq_1\cdot x} < 0|J_\mu(x)J_\nu(0)|n(p)>$, for the decay of a meson n to two vector currents with positive outgoing minus momentum components. There is only one independent, second-rank, divergenceless, Lorentz tensor in two dimensions (as opposed to two such tensors in four dimensions). The decay amplitude can be written generally as (see fig. (V.B.1) for notation)

$$\mathcal{K}^n_{\mu\nu} = i\left\{- g_{\mu\nu}q_1\cdot q_2 + q_{1\nu}q_{2\mu}\right\}\mathcal{K}^n(x_1 = q_{1-}/p_{n-}, x_2 = q_{2-}/p_{n-}; q_1^2, q_2^2) \tag{V.B.1}$$

where the variables x_1 and x_2 run between zero and one and satisfy

$$M_n^2 = \frac{q_1^2}{x_1} + \frac{q_2^2}{x_2}, \quad x_1 + x_2 = 1 . \qquad \text{(V.B.2)}$$

In the 't Hooft model

$$\mathcal{K}^n(x_1x_2;q_1^2q_2^2) = 2e_a^2\sqrt{\frac{N}{\pi}}\ \frac{(1+(-1)^n)}{x_1x_2} \int_0^1 dy\ x_2^2 G(y;q_2^2)$$

$$\cdot \left\{\phi_n(yx_2) - \frac{x_1^2}{2} \int_0^1 dz\ G(z;q_1^2)\left[\frac{\phi_n(x_1z)+\phi_n(x_2y)}{((1-y)x_2 + (1-z)x_1)^2}\right]\right\} + (q_1 \leftrightarrow q_2). \qquad \text{(V.B.3)}$$

The decay process can be thought of as the Bose symmetrized emission of one of the currents from the meson via the inelastic form factor followed by the decay of the resulting meson into the other current via the direct current-meson coupling. The interference of diagrams with quarks circulating in opposite directions with respect to each other gives rise to an overall factor in the amplitude which allows only even parity mesons to decay into two photons. This is required by parity and Bose symmetry. Parity demands

$$\mathcal{K}^n(q_1,q_2) = (-1)^n\mathcal{K}^n(q_1',q_2') \qquad \text{(V.B.4)}$$

where $q'_\lambda = q^\lambda$. In the center of mass of the decaying meson, however, we have $q'_1 = q_2$ and $q'_2 = q_1$. The Bose symmetry of the amplitude under $q_1 \leftrightarrow q_2$ insures that n must be even.

C. The Inelastic Form Factor Of The Photon: $\gamma^*(q_1) + \gamma^*(q_2) \to m(q_1 + q_2)$.

We consider here the amplitude, $\mathcal{N}^n_{\mu\nu} = \int d^2x\, e^{-iq_1\cdot x}$ $\langle m(q_1+q_2)|T^*(J_\mu(x)J_\nu(0)|0\rangle$, for a spacelike photon, $q_1^2 < 0$, and a timelike photon, $q_2^2 > 0$, to annihilate to form a final state meson m. Since $q_1^2 < 0$, there are two inequivalent parity reversed frames. In Frame II, with q_{1-} positive the amplitude is explicitly related by crossing to $\mathcal{K}_{\mu\nu}$ of eq. (V.B.3)

$$\left[\mathcal{N}^m_{\mu\nu}(x_1 = q_{1-}/p_{n-}, x_2 = q_{2-}/p_{n-}; q_1, q_2)\right]_{II} =$$

$$\mathcal{K}^m_{\mu\nu}(x_1 = q_{1-}/p_{n-}, x_2 = q_{2-}/p_{n-}; q_1 q_2) \ . \qquad \text{(V.C.1)}$$

The Frame I amplitude is given by the diagram of fig. (V.C.1), which shows that the process takes place via the inelastic form factor of a meson dominating the timelike photon channel,

$$\left[\mathcal{N}^m_{\mu\nu}(z = -q_{1-}/q_{2-}; q_1, q_2)\right]_I = -i\left\{-g_{\mu\nu}q_1\cdot q_2 + q_{1\nu}q_{2\mu}\right\}2e_s^2\sqrt{\frac{N}{\pi}}\,\frac{(1+(-1)^m)(1-z)}{z}$$

$$\int_0^1 dy\,\phi_m(y)\left\{G(y(1-z)+z;q_2^2) + z^2\int dw\, G(w,q_1^2)\right.$$

$$\left.\cdot\left[\frac{G(zw;q_2^2) - G(y(1-z)+z;q_2^2)}{(y(1-z)+z(1-w))^2}\right]\right\} \ . \qquad \text{(V.C.2)}$$

With this expression, we can investigate the parton model aspects of deep inelastic leptoproduction from a photon in analogy to our discussion of Sec. (IV.B.). In the Bjorken limit, $-q_1^2/M_m^2 = x_{BJ}/1-x_{BJ}$ with $M_m^2 \to \infty$, the incident spacelike current probes the quark distribution of the finite mass timelike photon. This process thus measures the photon wave function. Taking the Bjorken limit, $z \to x_{BJ}$, the amplitude of eq.(V.C.2) becomes

$$\lim_{BJ} \mathcal{N}_{\mu\nu}(z) = -i\left\{-g_{\mu\nu}q_1 \cdot q_2 + q_{1\nu}q_{2\mu}\right\} 2\pi e_a \frac{(1-z)}{z}\frac{m_a}{M_m^2}\left[2e_a\sqrt{\frac{N}{\pi}}\,G(z,q_2^2)\right] \tag{V.C.3}$$

with only the bare coupling part of the form factor contributing. Comparing with eq.(IV.B.20) for the Bjorken limit of the meson form factor, we can define a photon wave function $\phi_\gamma(x)$ in analogy with $\phi_n(x)$ where

$$\phi_\gamma(x) \sim e_a\sqrt{\frac{N}{\pi}}\,G(x;q_2^2)$$

$$\sim e_a\sqrt{\frac{N}{\pi}}\sum_k\left[\int_0^1 \frac{dy\,\phi_k(y)}{q_2^2 - M_k^2}\right]\phi_k(x) \tag{V.C.4}$$

The $N^{\frac{1}{2}}$ appears explicitly because J_μ is not a normalized color singlet operator while the charge reflects the photon-quark-antiquark coupling. Again, as in Sec. (IV.B), we have arrived at a totally meson dominated description of a finite mass vector current. The photon wave function is a linear combination of meson wave functions, the same linear combination as in eq.(IV.B.18).

VI. THE COMPTON SCATTERING AMPLITUDE

A. Calculation Of The Amplitude

We now turn to the calculation of the scattering process $\gamma^*(q) + n(p_n) \to \gamma^*(q') + m(p_m)$ in the 't Hooft model by considering the Lorentz tensor $M^{nm}_{\mu\nu}(q,q';p_n,p_m) = \int d^2x e^{-iq\cdot x} \langle n|T^*(J_\mu(x)J_\nu(0))|m\rangle$. The states $|n\rangle$ and $|m\rangle$ are mesonic bound states of quark "a" and antiquark "$\bar{b}$". In order to facilitate comparison with experiments involving virtual Compton scattering we take the momentum of the incident current spacelike, $q^2 < 0$, and that of the final state current timelike $q'^2 > 0$. The spacelike incident current distinguishes the two parity reversed frames. The incident current minus momentum component, q_-, is negative(positive)in Frame I (II). The amplitudes computed in these frames are related by parity

$$\left[M^{nm}_{\mu\nu}(q_i)\right]_{I} = (-1)^{n+m} \left[M^{\mu\nu,nm}(q_i)\right]_{II} \qquad \text{(VI.A.1)}$$

where the Roman numeral subscript denotes the frame in which the tensor is calculated. In this section, the Compton scattering amplitude is derived in both frames. We do this because each amplitude has properties which are useful for demonstrating different aspects of the physical picture. In addition, comparison of the two expressions related by eq.(VI.A.1) brings out non-trivial features which are not evident in the amplitudes separately.

The amplitude, which is a crossing Bose symmetric $(M_{\mu\nu}(-q,q') = M_{\nu\mu}(q',-q))$, divergenceless $(q^\mu M_{\mu\nu} = q'^\nu M_{\mu\nu} = 0)$,

second rank tensor, can be written in terms of a single structure function as

$$M^{nm}_{\mu\nu}(q,q';p_n,p_m) = (-g_{\mu\nu}q\cdot q' + q'_\mu q_\nu)\mathcal{M}^{nm}(q,q';p_n,p_m) \qquad \text{(VI.A.2)}$$

where $\mathcal{M}^{nm}$ is symmetric under the interchange $q \leftrightarrow -q'$ and is Lorentz scalar or pseudoscalar depending on the parities of the external mesons.

The computation in Frame I is considerably simplified by the fact that the incident current has negative minus momentum component. Since construction of the amplitude is only sensitive to "time" orderings of minus components, the incident current is automatically crossed and treated symmetrically with respect to the outgoing current. We are thus calculating, in effect, the one-to-three process $n(p_n) \to \gamma^*(-q) + \gamma^*(q') + m(p_m)$. The minus-minus component of the Compton amplitude is given in the model by the diagrams of fig.(VI.A.1), which are characterized by simple Born exchange in each of the s,t, and u channels. The structure function is given by

$$\left[\mathcal{M}^{nm}(p_n,x_1 = -q_-/p_{n-},x_2 = q'_-/p_{n-})\right]_I =$$

$$\cdot \sum_k \Big\{ \mathcal{F}^{nk}(p_n,x_1)\,\frac{i}{s - M_k^2 + i\varepsilon}\,\mathcal{F}^{km}(p_n + q, x_2/1 - x_1)$$

$$+ \mathcal{F}^{nk}(p_n,x_2)\,\frac{i}{u - M_k^2 + i\varepsilon}\,\mathcal{F}^{km}(p_n - q', x_1/1 - x_2)$$

$$+ \mathcal{T}_{n;km}(p_n,x)\,\frac{i}{t - M_k + i\varepsilon}\,\mathcal{H}^{k,a}(q' - q, x_1/x, x_2/x)$$

EQ.(VI.A.3) Cont. on P.69

$$+ \mathcal{T}_{n,mk}(p_n, 1 - x) \frac{i}{t - M_k^2 + i\varepsilon} \mathcal{K}^{k,\bar{b}}(q'-q, x_1/x, x_2/x) \Big\}$$

(VI.A.3)

where $s, t,$ and u are the usual Mandelstam variables and $x = x_1 + x_2$. The terms in curly brackets correspond one-to-one with the diagrams of fig.(VI.A.1). In this form, it is immediately seen that unitarity is satisfied in each channel to leading order in N^{-1}.

The structure of the amplitude is more complicated in Frame II. It is very useful, however, in that it is closely related to the meson-meson scattering amplitude. We have tried to indicate this relation in fig.(VI.A.2). Since the current is flavor conserving, each of the duality sectors of the amplitude contributes weighted by the charges of the appropriate quarks. This is indicated by the first graph of fig. (VI.A.2), which shows that the "meson dominated" hadronic two-to-two function is a term in the Compton amplitude. Contained in this term however there is a piece arising from the off mass shell part of eq.(III.C.2) which has no counterpart in hadronic scattering. The inverse propagator in this term cancels the outgoing photon channel meson propagator, resulting in a contribution which looks like the bare coupling of the outgoing current to the contact term of the (ut) duality sector. The remaining terms in the amplitude, shown in fig. (VI.A.2) have at least one bare current vertex. The Frame II scattering amplitude is given by

$$\left[\mathcal{M}^{nm}\left(q, z = \frac{p_{n-}}{q_-}, z' = \frac{q'_-}{q_-}\right)\right]_{II} = \frac{-iN}{\pi} \sum_{k,\ell} \int du dv\ \phi_k(u)\phi_\ell(v)$$

$$\cdot \frac{i}{q^2 - M_k^2 + i\varepsilon} \cdot \frac{i}{q'^2 - M_\ell^2 + i\varepsilon}$$

$$\cdot \Big(e_a^2 \left[\bar{\mathcal{A}}^{(st)}_{kn;m\ell}(q;z,1+z-z',z') + \mathcal{A}^{(ut)}_{kn;m\ell}(q;z,1+z-z',z')\right]$$

$$+ e_{\bar{b}}^2 \left[\mathcal{A}^{(st)}_{kn,m\ell}(q;z,1+z-z',z') + \bar{\mathcal{A}}^{(ut)}_{kn;m\ell}(q;z,1+z-z',z')\right]$$

$$+ e_a e_{\bar{b}} \left[\mathcal{A}^{(us)}_{kn;m\ell}(q;z,1+z-z',z') + \bar{\mathcal{A}}^{(us)}_{kn;m\ell}(q;z,1+z-z',z')\right]\Big)$$

$$+ 2z \int_0^1 dv \phi_n^{a\bar{b}}(v) \sum_k \left(e_a \phi_k^{a\bar{b}}\left(\frac{1+vz}{1+z}\right) + e_{\bar{b}} \phi_k^{a\bar{b}}\left(\frac{zv}{1+z}\right)\right) \frac{i}{s - M_k^2 + i\varepsilon}$$

$$\cdot \mathcal{J}^{km}\left(p + q, \frac{z'}{1+z}\right) + 2i\sqrt{\frac{N}{\pi}}\ \frac{(1+z-z')}{z'} \int dv dy$$

$$\cdot \sum_{k,\ell} \phi_k(v) \frac{i}{q^2 - M_k^2 + i\varepsilon} \left(e_a \mathcal{J}_{\ell;kn}\left(p_n + q, \frac{1}{1+z}\right) - e_{\bar{b}} \mathcal{J}_{\ell;nk}\left(p_n + q, \frac{z}{1+z}\right)\right)$$

$$\cdot \frac{i}{s - M_\ell^2 + i\varepsilon} \phi_m^{a\bar{b}}(y)\left(e_a \phi_\ell^{a\bar{b}}\left(\frac{y(1+z-z')+z'}{}\right) + e_{\bar{b}} \phi_\ell^{a\bar{b}}\left(\frac{(1+z-z')(1-y)}{1+z}\right)\right)$$

$$+ 2\sqrt{\frac{N}{\pi}}\ \frac{(1-z')}{z'} \int dy \sum_k (1 + (-1)^k)$$

$$\cdot \Big(e_a^2 G^{a\bar{a}}\ (y(1-z') + z'; q^2) \phi_k^{a\bar{a}}(y) \frac{i}{t - M_k^2 + i\varepsilon} \mathcal{J}_{m;kn}\left(p_m, \frac{1-z'}{1+z-z'}\right)$$

$$- (-1)^{m+n}(a \leftrightarrow \bar{b})\Big). \qquad \text{(VI.A.4)}$$

This expression is valid in the kinematic region where $1 > z' > z$.

The Compton amplitudes given in eqs.(VI.A.3) and (VI.A.4) are functions of Lorentz invariant "scaling" variables. In Frame I, x_1 and x_2 give the momenta of the crossed initial photon and final photon respectively as fractions of the incident meson momentum, while z and z' in Frame II give the momenta of the incident meson and final photon respectively as fractions of the incident photon momentum, where all momenta are measured in a left moving infinite momentum frame. These variables are related by $x_1 = - q^2 z/M_n^2$, $x_2 = q'^2 z/M_n^2 z'$.

In this section we have derived two expressions for the Compton scattering amplitude, related by eq.(VI.A.1), which are exact to leading order in N^{-1} in $(QCD)_2$. We now proceed to investigate the behavior of these amplitudes in various kinematic and current mass limits for inclusive and exclusive scattering processes. A summary of limits considered is given in Table I.

B. Exclusive Limits.

We now study the behavior of the Compton scattering amplitude in the limit that the center of mass energy gets large while all external masses are held fixed and finite. The scattering can either occur in the forward or backward direction in this two dimensional model. This is our analogue of high energy, inelastic, exclusive scattering of real or slightly virtual photons from hadrons.

(1). Forward Scattering-Regge Limit.

A simple picture of Compton scattering in the Regge limit

arises in Frame II. The incident current is in the positive direction in the center of mass with $q_- = \sqrt{\frac{s}{2}}\left(1 - \frac{M_n^2}{s} + 0\left(\frac{1}{s^2}\right)\right)$. The initial meson state n, moving in the opposite direction has vanishing minus component of momentum so that $z \approx \frac{M_n^2}{s}$.

The outgoing current is scattered such that $z' \cong 1 - \frac{(M_m^2 - M_n^2)}{s}$.

Thus, if $M_m^2 > M_n^2$, the kinematic region is the one to which eq. (VI.A.4) applies. We take this condition on the masses to be the case. Examining the amplitude in this limit, we find that the leading behavior comes entirely from the first graph of fig. (VI.A.2). The leading behavior of the Compton scattering is given by the part of the amplitude corresponding to the meson dominated equivalent hadronic scattering amplitude. This can be seen in a fairly straightforward way by noting that leading behavior with scaling variables at their edge points always arises from regions of phase space where as many gluons with minus momentum fractions of order s^{-1} can be exchanged as possible, giving large contributions from gluon denominators. These soft gluons are exchanged in graphs of which the three point hadronic function is a subgraph (see fig. (III.C.6)). Thus, roughly speaking, the more three point subprocesses there are in a graph, the more important that graph is in this high energy limit. It can easily be seen that all the graphs with two three point subprocesses are contained in the meson dominated hadronic amplitude. This is because a bare current vertex eliminates a three point subprocess.

The leading behavior of the Compton amplitude is thus gotten directly from that of the hadronic two-to-two scattering amplitude with the substitution $\phi^{a\bar{a}}(x) \to e_a G^{a\bar{a}}(x;q_i^2)$ in the $i^{\underline{th}}$ current channel. The Green's function in the current channels is given by $G^{a\bar{a}}(x;q^2) = \int dy \sum_k \phi_k^{a\bar{a}}(y)\, \phi_k^{a\bar{a}}(x)/q^2-M_k^2$. It can be shown using eq.(III.B.7) that the contribution from high mass mesons to this sum is negligible, so that $G^{a\bar{a}}(x;q^2) \approx \sum_k^{\Lambda} c_k(q^2)\phi_k^{a\bar{a}}(x)$ for some finite Λ. Thus the Compton amplitude is essentially a weighted sum of a finite number of hadronic two-to-two scattering functions with all external mesons of finite mass. Having established this correspondence, we have shown that the Compton amplitude has all the Regge properties of the equivalent hadronic process. We will therefore discuss some of these properties without proof, referring the reader to ref. 10 for details.

The leading terms of the amplitude in this forward limit arise from the (st) and (ut) duality sectors. The amplitude is power behaved, with power determined by the masses of the quarks in the t-channel. In the dominant, soft gluon exchange region the exchanged quarks are constrained to have vanishing minus momentum fraction of the incident hard photon. Feynman's mechanism [3] of the buildup of Regge behavior by wee parton exchange is concretely realized in the 't Hooft model. The power is given by $\alpha_{ij}(0) = -\beta_i - \beta_j$ where i and j denote the exchanged quarks. In the Compton scattering case $i = j = a$ or b. The amplitude

factorizes in the t-channel and is consistent with obeying an unsubtracted dispersion relation. $J = -1$ fixed pole terms are present.

Although we have shown a close correspondence between photon-hadron and hadron-hadron scattering in the 't Hooft model, we can say little about the analytic structure of the amplitudes. The dependence of eq.(VI.A.3) and (VI.A.4) on minus momentum components obscures the properties of these expressions as analytic functions of invariants. Thus, though we have been describing current channels as "meson dominated," this does not imply agreement with meson dominance models which make specific statements about the analytic behavior of the amplitude with respect to the photon mass variables. Comparison with the amplitude calculated in Frame I serves to clarify some of these issues.

The dimensionless variables x_1 and x_2 in Frame I both go to zero in the Regge limit, with $x_1 = -\frac{q^2}{s}\left[1 + \frac{(M_n^2 + q^2)}{s}\right]$ and $x_2 = \frac{q'^2}{s}\left[1 + \frac{(M_n^2 + q^2)}{s}\right]$. The terms with two bare current vertices dominate in the limit. The terms from the (st) and (ut) diagrams cancel to the two leading orders, resulting in Regge leading behavior. This cancellation points out a major difference between photon scattering and the equivalent general hadronic process. Since the electromagnetic current is flavor conserving, the (ut) and (st) amplitudes cannot separately be treated as analytic functions because they cannot be physically distinguished. Only the sum of the two

has any physical meaning, and it is only the sum that has the same leading behavior as in the parity reversed frame.

A non-leading contribution arising from the cancellation of these diagrams is a term which shows $J = -1$ fixed pole behavior. This fixed pole was discussed by Brower et al. [10] in the zero mass photon limit where it becomes the leading term. It only contributes to elastic scattering and, thus, cannot be seen in the Frame II analysis where the elastic boundary is outside the applicable kinematic limit. The existence of fixed poles in the four dimensional Compton scattering amplitude has been considered [38]. These are non-hadronic in origin, since fixed poles in hadronic amplitudes in four dimensions are forbidden by unitarity and hermitian analyticity. Fixed poles with polynomial residues in the Compton amplitude can be motivated by continuation of operator product expansion techniques to the Regge region [39]. In two dimensions fixed poles can appear in both hadronic and Compton amplitudes. We can conclude from the Frame II analysis, where terms involving bare current vertices are proportional to $s^{-(1+\beta)}$ in the limit, that in <u>inelastic</u> Compton scattering in the 't Hooft model in the forward high energy region the photon acts as a purely hadronic system. In particular, the only fixed pole contributions to the inelastic amplitude are those directly related to the fixed poles of the meson-meson scattering amplitude.

Futher analysis in Frame I shows that the leading order Regge behaved terms arise from diagrams with bare current vertices and from diagrams with meson dominated vertices, as opposed to the situation in Frame II. The frame dependence points out the fact that this separation of vertices may not have a general analytic meaning.

(2). Large Angle Scattering Limit.

The exclusive scattering of photons and hadrons at fixed angle in the center of mass at high energy can be studied in the model by adopting an ansatz of Brower, et al. [10] in order to make contact with the dimensional counting rules. We consider the limiting power behavior of that analytic dual sector of the amplitude where the variables associated with the meson poles are getting large as an analogue to large angle scattering power behavior. Thus, in the forward limit considered above, the (us) part of the amplitude is appropriate. Note that, in accordance with this prescription, this is the only limit in which contact with large angle scattering can be reached. If we tried to study the possibly more physical limit of backward scattering, we would be led to consider the (st) dual sector which is, however, not analytic by itself as discussed above.

The behavior of the (us) sector of the Compton amplitude in the Regge limit in Frame II approaches that of the (us) sector of the two-to-two hadronic scattering function. Thus, from the study of the hadronic amplitude [10] we find that $M^{(us)} \sim s^{-2-\beta_a-\beta_b}$.

In the standard dimensional counting picture, the fact that the Compton amplitude has the same power behavior as the equivalent hadronic amplitude would indicate that all current vertices are meson dominated, since contributions from bare photon couplings, if present, are enhanced with respect to the meson dominated ones. This enhancement, however, is due to the couplings to transverse photons only, and does not appear in longitudinal current couplings. Thus, in our two dimensional model where all currents are longitudinal, we expect the observed power law behavior equivalence between the hadronic and Compton amplitudes.

Although this equivalence can be motivated in the dimensional counting picture, calculation of the integral power falloff by computing contributions from lowest order irreducible quark diagrams like fig.(VI.B.1) in superrenormalizable $(QCD)_2$ where all quarks have finite fractions of hadron momentum gives an s^{-3} prediction for the "large angle" behavior of the amplitude since there are three propagators far from mass shell. Disagreement with the $s^{-2+\beta}$ 't Hooft model behavior stems from the fact that in a superrenormalizable theory it costs a factor of s^{-1} to redistribute the momentum in the bound state via one gluon exchange as in fig.(VI.B.1) so that the quarks in the final state hadron all have finite momentum fraction. In the 't Hooft model this redistribution doesn't cost anything (except for nonperturbative factors $s^{-\beta}$) due to the fact that the gluon interaction is instantaneous and that there are no transverse degrees of freedom. This results in a softening of the

Bethe-Salpeter wave function kernel so that the 't Hooft wave function falls off more slowly as one of the constituent quark masses goes far off shell with the other quark mass fixed than would be assumed in the counting rule picture based on a superrenormalizable field theory [40].

Aside from differences which seem to be specific to the dimensionality of the theory, modifications of counting rule ideas are indicated in the model [41]. The coefficient of the power of s in the amplitude cannot be interpreted exclusively in terms of short distance physics. Terms involving exchanged mesons built up non-perturbatively from gluon exchange contribute. In addition, the integral power predictions of the counting rules are modified by the β's, powers dependent on masses of constituent quarks. These powers arise from infrared singularities in the wave function and are closely related to the Regge intercepts in the model.

C. Inclusive Limits.

We turn now to the study of the inclusive Compton process $\gamma^*(q) + n(p_k) \to \gamma^*(q') + X$ where X represents the unobserved final hadronic state. The parton model makes definite predictions concerning the structure of the cross section in several inclusive limits. Inclusive production of large mass lepton pairs via photoproduction and deep inelastic leptoproduction, two non-light cone processes, are investigated in this section for the purpose of checking the validity of parton predictions in the 't Hooft model. We will show that the amplitude for these processes scales in the 't Hooft model

and that the scaling functions are interpretable in terms of free scattering of constituent quarks.

Recall that, as discussed in Sec.(V.A.), the inclusive amplitude is computed by taking $|X>$ to be a one large mass particle state $|m>$, and smoothed by taking M_m equal to the invariant mass of the inclusive channel. This interpolation is performed with the proviso that terms in the squared amplitude proportional to $(-1)^m$ arising from parity oscillations of the final state meson are dropped.

(1). Bjorken-Paschos Compton Limit With Very Virtual Photons.

We first examine a limit of the Compton amplitude where the photon masses and momentum transfers to the hadron system are all large. This limiting case would be applicable, for example, to the deep inelastic electroproduction of massive lepton pairs. Intuitively we expect that the large photon masses will suppress the hadronic content of the photon so that the current couples to the parton via the bare electromagnetic pointlike interaction. Further, the large momentum transfer suggests the validity of impulse approximation ideas. In this view, the two currents must interact with the same quark so as to avoid large energy in intermediate states. We are thus led to a model of the scattering process in this limit in terms of free parton "handbag" scattering amplitudes incoherently summed and folded into parton momentum distribution functions.

A description of inclusive Compton scattering at large momentum transfer with real photons in terms of a parton "handbag diagram" model has been proposed by Bjorken and Paschos [42]. We

cannot examine this limit directly since, in two dimensions, the Mandelstam variables cannot all be made large simultaneously as long as the photon masses stay finite. This problem was encountered in the large angle exclusive scattering limit discussed above, where the power behavior of the (μs) sector was analyzed as a large angle power behavior analogue. Here, however, we are interested in the structure of the coefficient of the power. There is no reason to associate this coefficient with the (us) sector coefficent, which, in this case, consists of "crossed handbag" coherence terms which are assumed to be non-leading in the parton model.

The very virtual photon limit is achieved kimenatically by taking $q^2, q'^2, s, t, \nu = p_n \cdot (q - q')/M_n$ large with their ratios fixed. In our two dimensional case this limit can be realized by taking $q^2 = \frac{-x_1}{1 - x_1} s$, $q'^2 = \frac{x_2 s}{1 - x_1} \left[1 - \frac{2M_n \nu(1 - x_1)}{s}\right]$.

The fixed dimensionless variables x_i describe the momentum transfer across the current vertices: $x_1 = -q^2/2p_n \cdot q$, $x_2 = q'^2/2p_n \cdot q'$, $x = x_1 + x_2 \equiv x_{BJ} = -t/2M_n\nu$. They are limited by $x_2 < x < 1$ where $0 < x_2 < 1$. The Frame II scaling variables are given by $z = M_n^2(1 - x_1)/s$ and $z' = 1 - \frac{2M_n \nu}{s}(1 - x_1)$.

The naive parton model prediction is, as discussed above, gotten by summing the handbag diagrams shown in fig.(VI.C.1). The quark propagators in these diagrams which are attached to the wave function vertices are dressed while those between the current

vertices are bare. This prescription is gauge invariant for the class of gauges where $A_- = 0$. The amplitude computed in this parton model is

$$|M|^2 = |M_{\mu\nu}M^{\mu\nu}| = \left[\frac{2\pi}{M_n\nu}\right]^2 \left[1 + \frac{s(1-x_2)}{u(1-x_1)}\right]^2 \frac{1}{x_1x_2}$$

$$\cdot \left(e_a^4 m_a^2 |\phi_n^{a\bar{b}}(x)|^2 + e_{\bar{b}}^4 m_b^2 |\phi_n^{a\bar{b}}(1-x)|^2\right). \quad \text{(VI.C.1)}$$

The handbag model thus predicts a scaling cross section, where the scattering function $\nu^2|M|^2$ is, apart from kinematic factors, related to the deep inelastic leptoproduction structure function by making the replacement $e^2 \to e^4$. We now show that this parton description successfully gives the limiting behavior of the exact Compton amplitude in the 't Hooft model.

Frame I is, in this gauge, the natural frame in which to see simple parton behavior, as is evident in the close relation of the scaling variables in this frame to the usual parton variables. The behavior of the amplitude in this frame can be found simply by counting meson propagators, each of which contribute a factor of s^{-1}. The soft gluon mechanism, used to get leading Regge behavior, no longer operates due to the fact that x_1 and x_2 are not constrained to their edge points. This, in turn, is due to the large current masses. Thus, as the currents get highly virtual, they are no longer describable in purely hadronic terms. In fact, the leading

diagrams in this limit, those with the fewest meson propagators, are precisely those with bare current couplings to quarks. The other source of s dependence in the amplitude arises from the phase space pinch due to the large mass final state. Roughly speaking, this suppresses all terms in the amplitude equally. The leading contribution to the amplitude in this limit thus comes from the bare current-quark coupling terms in the s and u channel meson exchange diagrams of fig.(VI.A.1). Included in these diagrams are graphs where the currents interact with the same quark as well as those where they interact with different quarks. These latter "crossed" graphs cannot contribute in the handbag model. The impulse approximation is recovered, however, by looking at the amplitude in Frame II.

The limit in Frame II involves scaling variables at their edge points so that the behavior of the amplitude is less obvious. A little computation shows that the (us) sector of the amplitude is non-leading in the limit. These terms, proportional to $e_a e_{\bar{b}}$, are suppressed relative to the leading $e_a e_{\bar{b}}$ terms in Frame I. Parity conservation via eq.(VI.A.1) implies, therefore, cancellation of the leading Frame I terms. This cancellation implies that the quantity

$$\left| \int d\eta \phi^a(\eta) \left\{ \phi_n^{a\bar{b}}(x_1) \left[\frac{(1-x_1)}{s} h_+^a\left(\frac{\eta}{1-x_1}\right) + \frac{(1-x_2)}{u} \right] \right.\right.$$

$$\left.\left. + \phi_n^{a\bar{b}}(x_2) \left[\frac{(1-x_1)}{s} + \frac{(1-x_2)}{(-u)} h_-^a\left(\frac{\eta}{1-x_1}\left(1 - \frac{2M_N \nu(1-x_1)}{s}\right)\right)\right]\right\}\right|$$

is symmetric under the interchange $a \leftrightarrow b$. We have not been able to directly prove this symmetry property.

The remaining terms in Frame I are proportional to e_a^2 and $e_{\bar{b}}^2$, and arise from diagrams with bare quark current couplings. The limiting form of the amplitude is

$$\lim \left[\mathcal{M}^{nm}\right]_I = 4\,\frac{(1-x)}{x_1 x_2}\left[\frac{(1-x_1)}{s} + \frac{(1-x_2)}{u}\right]$$

$$\int_0^1 dw\,\phi_m^{a\bar{b}}(w)\left[e_a^2\phi_n^{a\bar{b}}(w(1-x)+x) + e_{\bar{b}}^2\phi_n^{a\bar{b}}(w(1-x))\right]. \tag{VI.C.2}$$

This is a somewhat intermediate form of the final result which we give to show that in this limit the two currents interact as if they were a single spacelike current carrying a fraction x of the minus component of the hadron momentum and interacting with the quarks via the bare vertex with an effective coupling constant

$$e_a^{eff} = -2e_a^2\,\frac{x}{x_1 x_2}\left[\frac{(1-x_1)}{s} + \frac{(1-x_2)}{u}\right]. \tag{VI.C.3}$$

With this coupling the invariant amplitude $\mathcal{M}^{nm}$ equals the part of the invariant form factor $\mathcal{F}^{nm}$ for the single current interaction which arises from the first, bare coupling, term in eq.(IV.B.5). The Bjorken-Paschos intuitive picture of the two currents giving a single large impulse to the hadronic system is realized

in the 't Hooft model. This instantaneous interaction of the two currents at a single vertex in an infinite momentum frame has been proposed by Brodsky and Roy [43] as a necessary condition for the application of parton model ideas to two photon processes.

Equation (VI.C.1) can be obtained by taking the large final state mass limit of eq.(VI.C.2), using eq.(III.B.10), squaring and using the elimination of cross terms due to $(-1)^m$ parity oscillations. Agreement with the parton handbag model is thus confirmed.

We conclude by pointing out that, in Frame I in the $A_- = 0$ gauge, the lowest order quark diagrams of the "handbag" model are expected to describe the behavior of the Compton amplitude in the light cone limit on the basis of asymptotic freedom arguments. The kinematic region which probes the light cone contribution to the Compton amplitude is discussed by Iliopoulos and Paschos (I-P) [44]. It is reached by a two step limiting procedure where first q^2, q'^2 and s are taken large in fixed ratio with t and ν fixed, after which t and ν are taken large with $x = -t/2M_n\nu$ fixed. This differs from the limit we have considered above where the ratio ν/s is held finite throughout. This one step limit does not a priori probe the light cone due to the possible presence of large final state mass oscillations in the matrix element $\langle X|T^*(J_\mu(x)J_\nu(0))|n\rangle$ which could invalidate the usual stationary phase analysis of leading momentum space contributions.

In the I-P limit, the second factor in the handbag amplitude of eq.(VI.C.1), is of order $(\nu/s)^2$ due to kinematics in two dimensions. This factor results from the Bose symmetrization of the amplitude. The function $\nu^2|M^2|$ thus approaches zero as $(\nu/s)^2$ in the light cone limit. We have found that in the I-P limit in the 't Hooft model $\nu^2|M^2|$ goes to zero in agreement with the handbag prediction.

(2). Photoproduction of Large Mass Lepton Pairs.

The inclusive photoproduction of lepton pairs, in the limit that the mass of the pair gets large in fixed ratio to the energy in the center of mass, has been studied [14] in the context of a field theoretic parton model in four dimensions with an ad hoc transverse momentum cutoff. Due to the large lepton pair mass, the cross section can be computed by considering the photon as a collection of on-shell partons, one of which annihilates with its antiparticle in the incident hadron at a bare electromagnetic vertex to form a highly virtual photon in the final state. The total cross section is given by the incoherent sum of $q\bar{q} \to \ell\bar{\ell}$ cross sections weighted by the parton momentum distribution functions of the photon and hadron. This parton model is shown in fig.(VI.C.2).

This photoproduction process is very similar to the Drell-Yan process, and application of the parton model is on the same theoretical footing in both cases. The major difference between the two is the presence, in photoproduction, of diagrams where the bare incident photon couples directly to quarks. In the parton model analysis, the bare coupling time ordered diagrams which

contribute in the infinite momentum frame look exactly like fig. (VI.C.2), allowing the bare coupling contributions to be included in the photon structure function.

The parton model prediction in the Drell-Yan scattering process is borneout in the 't Hooft model [9]. It is thus reasonable to hope that the same is true for photoproduction scaling. We will show that this is the case, although in any frame in this gauge the final state production mechanism appears non-partonic.

In this limit we take s and q'^2 large and in fixed ratio such that $\tau = q'^2/s$, while keeping the masses of the incident current and hadron finite. The hadronic contribution to the scattering process is given, in general, by

$$H^{\mu\nu}(p_n,q,q') = \sum_{\substack{\text{"pol}\\ \text{spin"}}} \int d^2y\, e^{-iq'\cdot y} < n(p_n)\gamma(q)|J^{\mu}(y)J^{\nu}(0)|n(p_n)\gamma(q) > . \tag{VI.C.4}$$

Computing this tensor via the parton model of fig.(VI.C.2) in two dimensions gives

$$H^{\mu\nu}_{\text{PARTON}} = \left\{ -g^{\mu\nu} + \frac{q'^{\mu}q'^{\nu}}{q'^2} \right\} \sum_a \frac{16\pi^2 e_a^2 m_a^2}{y_1 y_2 s} |\phi^a_{\gamma}(y_2)|^2 |\phi^{\bar{a}}_n(y_1)|^2 \tag{VI.C.5}$$

where the sum is over all flavors of quarks and antiquarks. The $\phi^a_i(x)$ are the usual wave functions describing the probability that, in an infinite momentum frame, parton "a" has momentum

fraction x of the total momentum of the ith particle. The wave functions are measured in deep inelastic leptoproduction. The scaling variables are given by $y_1 = \sqrt{2}\, q'_-/\sqrt{s}$ and $y_2 = \sqrt{2}\, q'_+/\sqrt{s}$ in the hadron-photon center of mass frame in which the photon is moving in the positive direction (Frame I). They are restricted by $\tau \leq y_i \leq 1$ and satisfy $\tau = y_1 y_2$. In terms of these variables we have $t = y_1(y_2 - 1)s$, $u = y_2(y_1 - 1)s$, $M_x^2 = (1 - y_2)(1 - y_1)s$ in the large s limit.

The important feature of eq.(VI.C.5) is that it is a sum of terms each of which is a product of a function of y_1 and a function of y_2. We now verify this scaling form in Frame I and Frame II separately in the 't Hooft model. By relating the expressions in each frame via parity, we extract simple expressions for the meson and photon wave function. This method is similar to the Drell-Yan analysis of ref. 9.

In Frame I the limit is achieved by taking $x_1 = -q^2/s$, $x_1 = y_1$. The leading diagrams are those with bare current coupling at both vertices. As in the Regge limit these terms cancel in leading order. The cancellation in next order is, however, not complete and a contribution arises from the (ut) duality sector diagram. In this order there is also a contribution from the (ut) diagram where the incident current is meson dominated and the outgoing current is bare. These leading diagrams are shown in fig.(VI.C. 3(a)). There are no other contributions. In particular, the large mass of the

final current suppresses the contribution from meson dominated final current vertices. The crossed terms, proportional to $e_a e_{\bar{b}}$, are also non-leading. In the limit we then have

$$\left[\Pi^{\mu\nu}\right]_I = \left\{-g^{\mu\nu} + \frac{q'^{\mu}q'^{\nu}}{q'^2}\right\} \left\{\frac{(4e_a^2)^2}{y_1 y_2 s} \left|\phi_n^{a\bar{b}}(y_1)\right|^2 \left[\frac{1}{\sqrt{-q^2}(1-y_2)} \int_0^\infty d\eta \phi^a(\eta)\right.\right.$$

$$\cdot \left[\left(h_-^a\left(y_2\left(\frac{\eta}{1-y_2} - q^2\right)\right) - h_-^a\left(\frac{y_2\eta}{1-y_2}\right)\right)\right.$$

$$\left.\left. + (-q^2)^2 \int_0^1 dv\, G(v,q^2) \left[\frac{h_-^a(q^2 y_2 v) - h_-^a\left(y_2\left(\frac{\eta}{1-y_2} - q^2\right)\right)}{\left(\frac{\eta}{1-y_2} - q^2(1-v)\right)^2}\right]\right]\right]^2$$

$$\left. + (a \leftrightarrow \bar{b})\right\} . \qquad \text{(VI.C.6)}$$

This expression clearly gives the parton model scaling form of eq. (VI.C.5). The meson probability amplitude is given by the meson wave function squared, consistent with what is found in leptoproduction scaling. The photon wave function is given by expression in square brackets.

The interpretation of this scattering in terms of parton annihilation arises naturally from the dominance of the (ut) sector diagrams in the limit. This is the only sector which contains those quark diagrams where the final current arises via the annihilation of a current quark and a meson quark. All other diagrams lead to an

interpretation of final current production due to quark bremmstrahlung. The formation of the final states in this frame is, however, distinctly non-partonic, as can be seen by comparing figs. (VI.C.2) and (VI.C.3(a)). The final states in the model are inextricably bound up with the incident current vertex, so that the final state production mechanism is reflected in the photon wave function.

We can get a better idea of the form of the photon wave function by computing in Frame II. Here, $z' = y_2$ and $z = M_n^2/s$ in the limit. In this frame the roles of the initial state particles are reversed, so that the amplitude is given by a simple expression for the current vertex and a complicated expression for the meson vertex. The dominant terms all arise from the (ut) sector. The contributions come from the off-mass shell term in the contact diagram and from t-channel meson exchange diagrams where the incident current is meson dominated which the outgoing current is bare, the last diagram in fig.(VI.A.2). These contributions are represented in fig.(VI.C.4). The limiting amplitude is given by

$$\left[H^{\mu\nu}\right]_{II} = \left\{g^{\mu\nu} - \frac{q'^{\mu}q'^{\nu}}{q'^2}\right\} \left\{\frac{(4e_a^2)^2 q^2}{y_1 y_2 s} \; M_n^4 |G(y_2,q^2)|^2 \right.$$

$$\left[y_1 \int_0^1 dw \phi_n(w) \left[\phi^b(M_n^2(1-y_1)(1-w)) \right.\right.$$

$$\left.\left.\left. + \int dv du \; g_-(vM_n^2, uM_n^2) \left[\frac{\phi^b(M_n^2(1-y_1)(1-\frac{v}{y_1})) - \phi^b(M_n^2(1-y_1)(1-w))}{(y_1 w - v)^2}\right]\right]\right]^2$$

$$\left. + (a \leftrightarrow \bar{b})\right\} . \quad \text{(VI.C.7)}$$

The remarks below eq.(VI.C.6) apply also in this frame with the roles of the incident meson and current interchanged. The final state production mechanism is not partonic, as seen by comparing figs.(VI.C.2) and (VI.C.3(b)), though the dominance of the (ut) sector again allows a quark-antiquark annihilation interpretation. The photon wave function normalized to unity which arises from the Frame II analysis is given by:

$$\phi_\gamma^a(x;q^2) = \frac{G^{a\bar{a}}(x;q^2)}{\sqrt{\int_0^1 dx(G^{a\bar{a}}(x;q^2))^2}}. \qquad \text{(VI.C.8)}$$

in agreement with the leptoproduction result of eq.(V.C.4). The partonic structure of the photon, in this model, arises from its couplings to mesons.

Relating eqs. (VI.C.6) and (VI.C.7) through eq.(VI.A.1) gives a simple expression for the amplitude which has the parton model form

$$H^{\mu\nu} = \left\{-g^{\mu\nu} + \frac{q'^\mu q'^\nu}{q'^2}\right\}\left(\frac{16(e_a^2)^2}{y_1 y_2 s} C_v^a |\phi_n^a(y_1)|^2 |\phi_\gamma^{\bar{a}}(y_2)|^2 + (a \to \bar{b})\right) , \qquad \text{(VI.C.9)}$$

where C_v does not have any y_i dependence. We have not tried to see if $C_v^a = m_a^2 C_v'$ as demanded by eq. (VI.C.5). In the course of relating the amplitudes in each frame, highly non-trivial equalitites are generated between scaling functions and wave functions. We have not tried to verify these identities but have checked consistency in power behavior at the edge points. These equalities are more

complicated examples of relations between final state summations and parton description than eq.(III.B.10) which we have used above.

VII. CONCLUSION

We have investigated the behavior of current scattering in the 't Hooft model, $(QCD)_2$ to leading order in N^{-1}. We have reviewed the formulation of the model in order to show how an asymptotically free theory with a realistic particle spectrum of color singlet hadronic states can be obtained from a Lagrangian containing only quark and gluon fields. Even in this simple theory, (compared to four dimensional version) highly nontrivial mechanisms operate. Detailed properties of the large mass wave functions give rise to the identity of eq.(III.B.10), which gives parton scaling behavior by summing over final state hadrons. We have shown that very complicated identities imposed by the underlying parity invariance of the theory simplify and clarify the structure of the scattering amplitudes. Alternatively, these identities can be considered as the consequence of the underlying color gauge invariance of the theory, since it is the choice of gauge that introduces the explicit lack of parity invariance. The possibility of similar mechanisms operating in four dimensions must be examined in light of the differences which we have discussed between $(QCD)_2$ and $(QCD)_4$ due to the difference in the number of space-time dimensions.

The most important aspect of the results presented from a phenomenological viewpoint is that there are no real suprises. Generally used ideas - vector meson dominance in soft processes and parton point coupling dynamics in hard processes - are found to accurately describe vector current scattering behavior

in the 't Hooft model. In this model we have found that "real" photon states are effectively linear combinations of hadronic bound states, a description which becomes inapplicable as the photon is taken far off mass shell. We have shown how highly non-trivial properties of hadronic wave functions allow parton model interpretation in various deep inelastic inclusive limits.

The most interesting departure from phenomenological lore is the ubiquitous modification of dimension counting rules by small factors dependent on exchanged quarks. These factors are related to confinement singularities [45] and may thus be present in more realistic confining theories. This has been stressed by Brower [46] in the more general context of the relation between large angle scattering power behavior and Regge intercepts.

Many aspects of scattering behavior in the 't Hooft model are almost certainly dependent on the absence of transverse dimensions. The lack of real vector meson degrees of freedom, for example, probably gives rise to qualitative behavior specific to two dimensions. The failure of the pomeron to arise in hadronic scattering amplitudes is probably due to the fact that there are no real gluons in the theory. The mechanism responsible for cancellation of the pomeron also seems to be inhibiting possible non-partonic contributions to hard processes which are leading in N^{-1} [47]. Parton behavior might, then, be modified by the appearance of the pomeron.

Photonic degrees of freedom in four dimensions give rise to terms in the dimensional counting picture which are responsible for leading behavior in large angle scattering. These terms do not

appear in the 't Hooft model. Additionally, transverse photons might result in the presence of fixed poles [48] in the inelastic Compton amplitude in the soft scattering region and extra terms in the partonic description of the photon.

APPENDIX A: Simple Wave Function Identitities Due To Parity Invariance

In this appendix, we prove the relations of eqs.(III.B.12) and (III.B.13) using the Bethe-Salpeter formalism developed in Sec.(III.A.). As a first step, we find the complete Dirac structure of the meson wave function $\Phi^{(n)}_{\alpha\beta}(x)$ given by

$$\Phi^{(n)}_{\alpha\beta}(x;P) = \int dp_+ \Phi^{(n)}_{\alpha\beta}(P,p_+,p_- = xP_-) \tag{A.1}$$

in terms of the Bethe-Salpeter wave function of eq.(III.A.5). This structure can be found by observing that the vertex function, $\Gamma_{\alpha\beta}$, is proportional to $(\gamma_-)_{\alpha\beta}$. This can be seen directly from the structure of the T-matrix, eq.(III.A.19), or by noting from fig. (III.A.7) that $\Gamma_{\alpha\beta}$ is bracketted by γ_- matrices due to the quark-gluon vertices. The wave function $\Phi^{(n)}_{\alpha\beta}$ is related to the vertex by the addition of the external leg fermion propagators. Thus

$$\Phi^{(n)}_{\alpha\beta}(x;P) = f^{(n)}(x;P)\left\{\left[\gamma_+ p_- + m_a\right]\gamma_-\left[\gamma_+(p_- - P_-) + m_b\right]\right\}_{\alpha\beta}$$

$$= \phi^{a\bar{b}}_n(x)\left\{\frac{\gamma_+}{2} + \frac{m_a m_b \gamma_-}{4P_-^2 x(x-1)} + \frac{m_a(1-\gamma_5)}{2P_- x} + \frac{m_b(1+\gamma_5)}{2P_-(x-1)}\right\}_{\alpha\beta} \tag{A.2}$$

where $(1\pm\gamma_5)$ are defined in Sec.(II.A.2). The normalizing equality

$$\phi_n(x) = 4P_-^2 f^{(n)}(x,P)x(x-1) \tag{A.3}$$

is derived from eq.(III.A.13).

We next consider the effect of parity invariance on the integral of the wave function. Integrating both sides of eq.(III.A.17) without the γ_- projection with respect to x gives

$$\int_0^1 dx\phi^{(n)}_{\alpha\beta}(x) = \frac{4\pi^2}{P_-} < n| T(\bar{\psi}_\alpha(0)\psi_\beta(0))|0 > \tag{A.4}$$

The integration over x thus probes the wave function at the origin. We insert parity operators, $\mathscr{P}$, into eq.(A.4) using

$$\mathscr{P}\,\psi_\alpha(x_+,x_-) = (\gamma_0\psi)_\alpha(x_-,x_+) \tag{A.5}$$

and

$$\mathscr{P}\,|n;P_+,P_- > \; = (-1)^n|n;P_-,P_+ > \tag{A.6}$$

since the spectrum of the Hamiltonian is non-degenerate. Performing these operations gives

$$\int_0^1 dx(P_-\Phi^{(n)}_{\alpha\beta})(x;P_-,P_+) = (-1)^n\int_0^1 dx(P_-(\gamma_0\Phi^n\gamma_0)_{\alpha\beta})(x;P_+,P_-) \tag{A.7}$$

This gives two identities when eq.(A.2) is used for $\Phi^n_{\alpha\beta}$. Since $\gamma_0\gamma_+\gamma_0 = \gamma_-$ and $\gamma_0(1\pm\gamma_5)\gamma_0 = (1\mp\gamma_5)$ we get

$$M_n^2 \int_0^1 dx\phi_n(x) = (-1)^{n+1}m_a m_b \int_0^1 dx\,\frac{\phi_n(x)}{x(1-x)} \tag{A.8}$$

$$m_a \int_0^1 dx\,\frac{\phi_n(x)}{x} = (-1)^{n+1}m_b \int_0^1 dx\,\frac{\phi_n(x)}{(1-x)} \tag{A.9}$$

Equation (A.9) is eq.(III.B.12), and using eq.(A.9) in eq.(A.8) gives eq.(III.B.13).

We conclude by noting that eq.(III.B.13) can be derived directly from the 't Hooft eq.(III A.16) with the identity

$$\fint_0^1 dy \, \frac{1}{(y-x)^2} = \frac{1}{1-x} + \frac{1}{x} \tag{A.10}$$

APPENDIX B: Current Scattering in The 't Hooft Model.

The incorporation of the fermion currents $J^{(S)}, J^{(5)}$ and $J^{(V)}$ of eq.(II.C.4) into scattering amplitudes in the 't Hooft model can be implemented via the gauge variant quark current form factor depicted in fig.(B.1). Letting

$w_\Delta(p,q) = (p^2 - m^2)((p - q)^2 - m^2)\left[S(p)\right]\gamma_\Delta\left[S(p - q)\right]$ with $S(p)$ given in eq.(III.A.11) and Δ denoting one of the four gamma matrix indices, we get

$$w_S = p_-(p_- - q)\left(\frac{m^2 + q_-(x-1)\xi(p) + q_- x\xi(p-q)}{q_-^2 x(x-1)} + \frac{x\xi(p-q) - (x-1)\xi(p)}{q_- x(x-1)}\gamma_5 + \frac{m(2x-1)}{q_- x(x-1)}\gamma_+ + \frac{m\left[\xi(p) + \xi(p-q)\right]}{q_-^2 x(x-1)}\gamma_-\right)$$

$$w_5 = ip_-(p_- - q_-)\left(\frac{(x-1)\xi(p) - x\xi(p-q)}{q_- x(1-x)} + \frac{m^2 - q_-(x-1)\xi(p) - q_- x\xi(p-q)}{q_-^2 x(1-x)}\gamma_5 - \frac{m\gamma_+}{q_- x(x-1)} + \frac{m\left[\xi(p) - \xi(p-q)\right]\gamma_-}{q_-^2 x(x-1)}\right)$$

$$w_- = p_-(p_- - q_-)\left(\frac{m(2x-1)}{q_- x(x-1)} + \frac{m\gamma_5}{q_- x(x-1)} + \frac{m^2\gamma_-}{q_-^2 x(1-x)} + 2\gamma_+\right)$$

$$w_+ = p_-(p_- - q_-)\left(\frac{m\left[\xi(p) + \xi(p-q)\right]}{q_-^2 x(1-x)} + \frac{m\left[\xi(p-q) - \xi(p)\right]\gamma_5}{q_-^2 x(1-x)} + \frac{2\xi(p)\xi(p-q)\gamma_-}{q_-^2 x(1-x)} + \frac{m^2\gamma_+}{q_-^2 x(x-1)}\right) \qquad \text{(B.1)}$$

where $\xi(p) = \left[p_+ - \frac{g^2_N}{2\pi}\left(\frac{\mathrm{sgn}(p_-)}{\lambda} - \frac{1}{p_-}\right)\right]$. We have considered flavor conserving currents for simplicity.

These expressions show why the minus vector coupling is the simplest to deal with. It contains no ξ factor with divergent behavior as $\lambda \to 0$. The existence of the ξ factors in the other current couplings invalidates the λ power counting and, as a result, the rules of Sec.(III.C.). Thus, general current scattering amplitudes may not be calculated by the rules given. We see, however, from eq.(B.1), if the form factors are bracketted by γ_- matrices, all ξ dependence disappears. As a result, in any ring diagram where at least every other vertex is a γ_- vertex, the rules of the text apply with the insertion of the appropriate form factors f_Δ where

$$f_S(q,x) = mq_-\left[\frac{1}{x} - \frac{1}{1-x}\right] \; ; \quad f_5(q,x) = imq_-\left[\frac{1}{x} + \frac{1}{1-x}\right]$$

$$f_\mu(q,x) = 2q_-\left(g_{\mu+} - \frac{m^2}{2q_-^2 x(1-x)}\, g_{\mu-}\right) . \tag{B.2}$$

As a simple example, consider the direct current-meson coupling. From eq.(IV.A.1), we can see

$$\mathcal{J}^n_\Delta(q) = \frac{1}{2}\left[\frac{N}{\pi}\right]^{\frac{1}{2}} \int_0^1 dx\; f_\Delta(q,x)\phi_n^{a\bar{a}}(x) . \tag{B.3}$$

The property of the form factors, $f_S(x) = -f_S(1-x)$, $f_5(x) = f_5(1-x)$ and $f_\mu(x) = f_\mu(1-x)$, shows that the scalar current couples to even

parity mesons while the pseudoscalar and vector current couple to odd parity mesons.

APPENDIX C: Divergence Properties of Current Amplitudes.

Electromagnetic gauge invariance leads to the requirement that physical scattering matrix elements involving vector electromagnetic currents be conserved on all Lorentz indices

$$\partial_\mu \langle \alpha | T^*(\ldots J^\mu(x)\ldots) | \beta \rangle = 0 \qquad (C.1)$$

As is well known, the matrix element of time ordered products of operators does not in general satisfy this divergence condition due to the presence of non-covariant Schwinger terms [49]. Non-covariant terms must be added to the time ordered product matrix element to product the "T*" product matrix element, which is covariant and divergenceless [50].

It was shown in Appendix B that for diagrams where the computational rules of the text apply, an insertion of a vector current can be described by the quark vector form factor $f_\mu(q,y)$ of eq.(B.2). From this coupling we can derive a simple Ward identity

$$q^\mu f^a_\mu(q,y) = q^2 - \frac{m_a^2}{y} - \frac{m_a^2}{1-y} \qquad (C.2)$$

This form allows simplification of the divergence through the use of the 't Hooft eq.(III.A.16) and the wave function orthogonality eq.(III.B.2). A primary simplification, which serves as a good example of the kinds of manipulations involved, occurs in terms where the photon is meson dominated. These terms are of the form

$\int dwdy\ G(w,y;q^2)f^a_\mu(q,y)\chi(w)$, with χ being some given function. The divergence of this term is

$$q^\mu\int dwdy\ G(w,y;q^2)f_\mu(q,y)\chi(w) = \int dwdy\left(q^2 - \frac{m_a^2}{y} - \frac{m_a^2}{1-y}\right)G(w,y;q^2)\chi(w)$$

$$= \int dwdy\ \sum_k \left[(q^2 - M_k^2) + \left(M_k^2 - \frac{m_a^2}{y} - \frac{m_a^2}{1-y}\right)\right]\frac{\phi_k^{a\bar{a}}(w)\phi_k^{a\bar{a}}(y)}{q^2 - M_k^2 + i\varepsilon}\chi(w) \qquad (C.3)$$

$$= \int dw\chi(w) + e_a\int dwdy\ dz\ \frac{\phi_k^{a\bar{a}}(w)}{q^2 - M_k^2 + i\varepsilon}\left[\frac{\phi_k^{a\bar{a}}(y) - \phi_k^{a\bar{a}}(z)}{(y-z)^2}\right] = \int dw\chi(w)$$

We have used eq.(C.2) in the first step, the definition of the Green's function in the second step, orthogonality and the 't Hooft equation in the third step where the second term is zero due to the antisymmetry of the integrand under $y \leftrightarrow z$. Taking the divergence thus eliminates meson propagators in the photon channels, leaving terms which can cancel with those arising from the bare current coupling terms.

The direct vector current-meson coupling defined by eq.(B.3) satisfies

$$q^\mu \mathcal{J}_\mu^n\ (q) = (q^2 - M_n^2)\ \frac{1}{2}\sqrt{\frac{N}{\pi}}\ e_a \int_0^1 dx\phi_n^{a\bar{a}}(x) \qquad (C.4)$$

where eq.(III.B.13) has been used. We have thus shown the validity of the expression of eq.(IV.A.1) for the on-shell coupling.

The inelastic form factor, $\mathcal{F}_{\mu}^{nm} = \langle n|J_{\mu}|m\rangle$, is conserved in the 't Hooft model when the initial and final mesons are on mass shell. The divergence is given in general by

$$q^{\mu}\mathcal{F}^{nm}(x) = \left[(p_m^2 - M_m^2) - (p_n^2 - M_n^2)(1-x)\right] \cdot$$
$$\cdot \left[e_a \int dy \phi_m^{a\bar{b}}(y)\phi_n^{a\bar{b}}(y(1-x)+x) + (-1)^{n+m}(a \to \bar{b})\right] \tag{C.5}$$

for the $q^2 < 0$, Frame I, case. The variable x is defined through eq.(IV.B.6) using the off shell values for the masses.

The situation for the matrix elements of the time ordered product of two vector currents is complicated by the fact that in the $A_- = 0$ gauge, in view of the discussion of Appendix B, the plus-plus component of the tensor is not calculable by standard techniques. We will thus show that, for the matrix elements considered, there exists a Lorentz covariant tensor which is divergenceless on all indices whose minus-minus, minus-plus, and plus-minus components agree with those calculated in the model.

The vacuum polarization tensor when, defined in terms of $\mathcal{J}_{\mu}$ through the first equality in eq.(V.A.1) satisfies

$$q^{\mu}\Pi_{\mu-}(q^2) = \frac{1}{2}\left[\frac{N}{\pi}\right] e_a^2 \int_0^1 dx\, \phi_n(x) \int_0^1 dy\, \phi_n(y) = \frac{N}{2\pi}\, e_a^2 \tag{C.6}$$

where we have used eq.(III.B.2) and eq.(C.4). This divergence is

however spurious, since $\Pi_{\mu\nu}$ must be regularized. Regulating so as to insure current conservation gives the second equality of eq.(V.A.1).

The tensor $\mathcal{K}^{n}_{\mu\nu}$ discussed in Sec. (V.B) can be written in an off mass shell covariant form from the diagrams of fig.(V.B.1) in terms of $\mathcal{J}_{\mu}$ and f_{μ}. The divergence is given by

$$q^{\mu}_{I}\mathcal{K}^{(n)}_{\mu\nu}(x_1,x_2) = \frac{ie_a x_2}{2}\sqrt{\frac{N}{\pi}}\,(p^2 - M_n^2)(1 + (-1)^n)\int dw dy\Big[G(w,y;q_2^2)\cdot$$

$$\bullet\, f_{\nu}(q_2,w)\phi_n^{a\bar{a}}(yx_2)\Big] \qquad (C.7)$$

The on-shell cancellation is very delicate, depending crucially on the even parity of the decaying mesons.

Finally, we turn to the more complicated case of the Compton anplitude, $\mathcal{M}_{\mu\nu}$ of Sec.(VI.A.), with external mesons on shell. Evaluation of the divergence is simplest in Frame I with the aid of eqs.(C.5) and (C.7) for the off-shell divergences of the Compton subamplitudes. To this end we define a quantity $C^{nm}_{\mu\nu}$ by

$$C^{nm}_{\mu\nu}(p_n,x_1 = -q/p_{n-},x_2 = q'_{-}/p_{n-})$$

$$= \sum_k\Big\{\mathcal{F}^{nk}_{\mu}(p_n,x_1)\,\frac{i}{s - M_k^2 + i\varepsilon}\,\mathcal{F}^{km}_{\nu}\Big(p_n + q,\ \frac{x_2}{1-x_1}\Big)$$

$$+\mathcal{F}^{nk}_{\mu}(p_n,x_2)\,\frac{i}{u - M_k^2 + i\varepsilon}\,\mathcal{F}^{km}_{\nu}\Big(p_n - q',\ \frac{x_1}{1-x_2}\Big) \qquad (C.8)$$

$$+\, i\mathcal{F}_{n;km}(p_n,x)\,\frac{i}{t - M_k^2 + i\varepsilon}\,\mathcal{K}^{k,a}_{\mu\nu}(q' - q,\ x_1/x, x_2/x)$$ Cont.

Cont. from 104

$$+ i\mathcal{T}_{n;mk}(p_n, 1 - x) \frac{i}{t - M_k^2 + i\varepsilon} \mathcal{K}_{\mu\nu}^{k,\bar{b}}(q' - q, x_1/x, x_2/x) \Big\} \quad . \tag{C.8}$$

The minus-minus, plus-minus, and minus-plus components of $C_{\mu\nu}^{nm}$ coincide with the respective components of the Compton scattering tensor, $\mathcal{M}_{\mu\nu}^{nm}$ in the model. Calculating $q^\mu C_{\mu\nu}$, we find a complete cancellation among crossing related terms proportional to $e_a e_{\bar{b}}$ and among the terms proportional to e_a^2 and e_b^2 which have meson propagators in the outgoing current channel in the s, t, and u channel meson exchange diagrams. The cancellation among crossing related terms in the s and u meson exchange channels with bare coupling to the outgoing current is incomplete, however, giving

$$q^\mu C_{\mu\nu} = i\, e_a \frac{(1-x)}{x_2} \int_0^1 dw\, \phi_m^{a\bar{b}}(w) \phi_n^{a\bar{b}}(w(1-x) + x)$$

$$\left[f_\nu^a\left(q', -\frac{w(1-x) + x_1}{x_2}\right) - f_\nu^a\left(q', -\frac{w(1-x)}{x_2}\right)\right]$$

$$+ (a \leftrightarrow \bar{b}). \tag{C.9}$$

$C_{\mu\nu}$ thus has a non-zero divergence and thus cannot be the correct Compton amplitude. However, by eq.(B.2), $q^\mu C_{\mu-} = 0$ and we then have proved $q^\mu M_{\mu-} = 0$.

In two dimensions it can be shown that a covariant tensor $M_{\mu\nu}(q_1, q_2)$ which satisfies $q^\mu M_{\mu-} = 0$, $M_{\mu\nu}(-q_1^\lambda, q_2^\lambda) = M_{\nu\mu}(q_2^\lambda, -q_1^\lambda)$

and the parity condition of eq.(VI.A.1) is divergencesless and can be written most generally as in eq.(VI.A.2). The M_{++} component is then defined through eq.(VI.A.2) in terms of one of the other tensor components. It cannot be expressed as a sum of simple products of off mass shell form factors. We have thus shown that eq. (VI.A.2) unambiguously gives the correct Compton scattering amplitude.

REFERENCES

1. Thorough treatment of the ideas of asymptotic freedom is given by H. D. Politzer, Phys. Rep. 14C, 129 (1974) and by D. J. Gross and F. Wilczek, Phys. Rev. D8, 3633 (1973).
2. A review of Regge theory is given by P. D. B. Collins, Phys. Rep. 1C, 104, (1971). Dual resonance models are reviewed by S. Mandelstam, Phys. Rep. 13C, 259 (1974).
3. Parton model concepts are discussed for example by R. P. Feynman, Photon-Hadron Interactions, W. A. Benjamin, Reading, MA (1972).
4. G. 't Hooft, Nucl. Phys. B72, 461 (1947).
5. G. 't Hooft, Nucl. Phys. B75, 461 (1974).
6. C. G. Callan Jr., N. Coote, and D. J. Gross, Phys. Rev. D13, 1649 (1976).
7. R. C. Brower, W. L. Spence, and J. H. Weis, UCSC 78/122 (1978).
8. M. B. Einhorn, Phys. Rev. D14, 3451 (1976).
9. J. Kripfganz and M. G. Schmidt, Nucl. Phys. B125, 323 (1977).
10. R. C. Brower, J. Ellis, M. G. Schmidt, and J. H. Weis, Nucl. Phys. B128, 131 (1977).
11. M. Einhorn, S. Nussinov, and E. Rabinovici, Phys. Rev. D15, 2282 (1977).
12. S. J. Brodsky and G. R. Farrar, Phys. Rev. D11, 1309 (1975). Dimensional counting is also discussed by V. Mateev, R. Muredyan, and A. Tavkhelidze, Nuovo Cimento Lett. 7, 719 (1973).
13. N. L. Fleishon, Nucl. Phys. B151, 261 (1979).

14. R. L. Jaffe, Phys. Rev. D4, 1507 (1971).

15. The matrix A_μ can be written in terms of hermitian color fields A^a_μ as $A_\mu = -\frac{i}{2}\tau^a A^a_\mu$, where τ^a are the matrices of the fundamental representation of the Lie algebra of U(N).

16. T. D. Lee and N. H. Christ, Phys. Rev. D12, 1684 (1975).

17. S. S. Shei and H. S. Tsao, Nucl. Phys. B141, 445 (1978).
T. N. Tomares, HUTP-78/A054 (1978).

18. L. Fadeev and V. Popov, Phys. Lett. 25B, 23 (1969). The discussion here is based on the presentation of S. Coleman, Secret Symmetry: An Introduction to Symmetry Breakdown and Gauge Fields in Laws of Hadronic Matter, ed. A. Zichichi, Erice (1973).

19. S. J. Chang and S. K. Ma, Phys. Rev. 180, 1506 (1968).
J. B. Kogut and D. E. Soper, Phys. Rev. D1, 2901 (1969).

20. See, for example, S. L. Adler and R. F. Dashen, Current Algebras and Applications to Particle Physics, Chapter 4, W. A. Benjamin, NY, 1968.

21. See, for example, ref. 3 or S. D. Drell and T. M. Yan, Annals of Physics, 66, 578 (1971).

22. S. Weinberg, Phys. Rev. 150, 1313 (1966).

23. This is emphasized by J. Kogut and L. Susskind, Phys. Rep. 8C, 79 (1973).

24. Investigations of the 't Hooft model in the $A_1 = 0$ gauge quantized on a spacelike surface include Y. Frishman et al., Phys. Rev. D15, 2275 (1977), N. K. Pak and H. C. Tze, Phys. Rev. D14, 3472 (1976), and A. J. Hanson, et al., SLAC PUB 1816 (1976).

25. I. Bars and M. B. Green, Phys. Rev. D17, 537 (1978).

26. L. F. Li and J. F. Willemsen, Phys. Rev. D10, 4087 (1974).

27. Y. Frishman, Nucl. Phys. B148, 74 (1979) App. A.

28. See, for xample, S. Coleman, Renormalization and Symmetry: A Review For Non-Specialists in Properties of The Fundamental Interactions B, 605, ed. A. Zichichi, Erice (1971).

29. K. G. Wilson, Phys. Rev. 179, 1499 (1969).

30. Equation (II.C.2) does not give the leading terms of the light cone expansion which is determined by operators of the lowest twist.

31. The U(N) group is used to simplify the N dependence of the theory. In leading order in N, there is no difference between U(N) and SU(N).

32. G. Veneziano, Nucl. Phys. B117, 519 (1976).

33. E. E. Salpeter and H. A. Bethe, Phys. Rev. 84, 1232 (1951), S. Mandelstam, Proc. Roy. Soc. A, 233,248 (1955).

34. M. Durgut, Nucl. Phys. B116, 233 (1976), T. H. Hansson and K. Konishi, RL78-021 (1978).

35. B. R. Webber, Two Dimensional Quantum Chromodynamics, talk delivered at the Workshop on Multiparticle Dynamics, Hakong, Japan (1978).

36. Equation (III.B.10) was first derived by Einhorn, Ref. 8, by demanding consistency with predictions of asymptotic freedom and more directly in Ref. 7. using detailed W.K.B. properties of the wave function.

37. A. Casher, J. Kogut, and L. Susskind, Phys. Rev. D10, 732 (1974).

38. M. Creutz, S. D. Drell and E. A. Paschos, Phys. Rev. 178, 2300 (1969).

39. See J. Ellis and R. L. Jaffe, Scaling, Short Distances and the Light Cone, Chapter 10, SLAC PUB 1353 (1973).

40. The power fall off of the 't Hooft wave function is coincidentally exactly that used in counting rules based on renormalizable perturbation theory. As a result, the "large angle" 't Hooft model behavior is well described in many cases by the four dimensional counting rules.

41. The dimensional counting modifications discussed here all appear at the simpler level of large q^2 form factor behavior. See Ref. 8, Sect. IV.

42. J. D. Bjorken and E. A. Paschos, Phys. Rev. 185, 1975 (1969).

43. S. J. Brodsky and P. Roy, Phys. Rev. D3, 2914 (1971).

44. J. Iliopoulos and E. A. Paschos, Phys. Rev. D6, 1340 (1972).

45. The connection between confinement singularities and high energy behavior is discussed in R. C. Brower, W. L. Spence, and J. H. Weis, Phys. Rev. Lett. 40, 674 (1978).

46. R. C. Brower, private communication.

47. Such terms are discussed by M. B. Einhorn, Phys. Rev. D15, 3037 (1976).

48. Fixed poles associated with bare photon couplings appear, for example, in the model of S. J. Brodsky, F. E. Close, and J. F. Gunion, Phys. Rev. D5, 1384 (1972).

49. J. Schwinger, Phys. Rev. Lett. 3, 296 (1959).

50. See, for example J. D. Bjorken, Phys. Rev. 148,1467 (1966).

51. P. Federbush and A. Tromba, Phys. Rev. D15, 2913 (1977).

FIGURE CAPTIONS

Figure II.A.1. Two dimensional Minkowski space. The light cone variable axes lie along the light cone, rotated at 45° to the space-time axes. The spacelike, $t = 0$, surface approaches th $x_{-} = 0$ surface when boosted into an infinite momentum frame.

Figure II.B.1. The Feynman rules for light cone quantized $(QCD)_2$. The letter a is a flavor index while i and j are color indices. Figure (a) shows the color representation of the gluon as a quark-antiquark pair. Figure (d) is a correction to U(N) gauge theory to give SU(N). This vertex does not occur to leading order in N^{-1}.

Figure II.D.1. The effect of putting a fermion loop in a diagram with color singlet sources. The fermion loop in fig. (b) creates an extra factor g^2 without creating any new color loops and is thus N^{-1} down from fig. (a).

Figure II.D.2. The effect of putting a handle in a diagram with color singlet sources. The crossed gluon handle of fig. (b) twists together the loops of planar fig. (a), resulting in a N^{-2} suppression.

Figure II.D.3. A quark line diagram contributing to a two particle intermediate state in meson-meson scattering. The two intermediate particles are represented by the cross-hatched areas. The diagram contains a quark loop and is thus non-leading in N^{-1}.

Figure III.A.1. The 4 point color singlet quark-antiquark vacuum amplitude, iD. The Greek indices are Dirac indices. The dots on the external lines indicate that external propagators are included in the amplitude. Exchange of single bound state particles with wave function Φ contribute to the dominant, pole behavior of the amplitude.

Figure III.A.2. An example of a contribution to D in the 't Hooft model. The set of a planar graphs are characterized by uncrossed ladder exchanges between renormalized quark lines.

Figure III.A.3. The relation between the full fermion propagator, iS, denoted by the darkened circle, and the proper self energy, $i\Sigma$.

Figure III.A.4. The relation between the full fermion propagator and the proper self energy induced by the requirements of planarity in leading order in N^{-1}.

Figure III.A.5. The Bethe-Salpeter equation for the bound state wave function $\Phi^{a\bar{b}}$ consisting of a quark a and an antiquark $\bar{b}$. The Lorentz invariant variable x is the fraction of minus momentum of the meson carried by the quark. Note that, by definition, Φ includes external propagators.

Figure III.A.6. The ladder exchange integral equation for the quark-antiquark color singlet scattering amplitude,

iT. Note that iT is obtained from iD of fig. (III.A.1) by truncation of external legs. The solution to the integral equation is represented in the second equality as the sum of a single gluon exchange and pole contributions with strength Γ_k, shown in fig.(III.A.7).

Figure III.A.7. The graphical struture of the meson vertex function, Γ_k, as expressed in eq.(III.A.24). The gluon has an infrared singular and principal value parts.

Figure III.C.1. Examples of Step 1 for creating mesonic graphs. In fig. (a), we show the mesonic diagrams contributing to $i\mathcal{T}_{n;km}(p_n,x)$ describing the decay of meson n into meson k and m. In fig. (b), we show the diagrams contributing to $i\mathcal{A}_{jk;mn}(p_j,x_k,x_m,x_n)$ describing the scattering of mesons j and k into mesons m and n. The three diagrams shown are labelled $\mathcal{A}^{st}$, $\mathcal{A}^{us}$, $\mathcal{A}^{ut}$, denoting the quark-antiquark color singlet channels in each diagram. Possible particle flavor content assignments contributing to these graphs are shown. For the rest of this paper, all quark lines are dressed unless otherwise indicated; the shaded circles are dropped.

Figure III.C.2. Examples of Step 2 of inserting T matrices into the diagrams of fig. (III.C.1). In fig. (a), we show that there are no possible insertions in the three point amplitude. In fig. (b), we show the T matrix insertions in the s and t channels of $\mathcal{A}^{st}$.

Figure III.C.3. Examples of Step 3 of eliminating gluons across bound states and computing the graph index m.

Figure III.C.4. Examples of Step 4 of time ordering each loop consisting of f fermion lines into f - 1 time orderings. The direction of positive minus momentum flow is indicated. In fig. (a), we have time ordered the three point diagram of fig.(III.C.3(a) while in fig. (b) we have time ordered the first diagram of fig. (III.C.3 (b)) for $\mathcal{A}^{st}$, for the case that $p_{m-} > p_{k-}$. The loop integration regions determined by each time ordering are indicated.

Figure III.C.5. Examples of Step 5 and 6 for the time ordered diagrams of fig.(III.C.4). Gluons are inserted to route the quarks into the bound states and the graph index m computed. The diagrams of fig. (a) contribute to the three point function using the rules of Step 6 and also to the meson exchange contributions to the four point function shown in fig.(III.C.2) using Step 7. The diagrams of fig.(b) do not contribute to the four point function since $m = 1 > 0$.

Figure III.C.6. Diagrammatic representation of the three point function, $i\mathcal{T}_{n;km}(p_n,x)$, as derived in fig. (III.C.1(a) - 5(a)). Note that each diagram involves a gluon exchange.

Figure III.C.7. Diagrammatic representation of the four point function $i\mathcal{Q}_{jk;mn}(p_j;x_k,x_m,x_n)$. In figs. (a), (b) and (c), we show the (us), (st), and (ut) contributions in terms of meson dominated strings of three point functions and contact terms. The representation is valid for $1 > x_m,x_n > x_k$.

Figure IV.A.1. The direct coupling of the vector current to meson n, denoted $\mathcal{J}^n_\mu$ in the text.

Figure IV.B.1. The inelastic form factor, $\mathcal{F}_\mu$. The incident current carries a fraction x of the final state momentum. Both bare and meson dominated coupling diagrams contribute.

Figure V.A.1. The vacuum polarization $\Pi_{\mu\nu}(q)$ for the vector current. The amplitude has the meson dominated structure indicated.

Figure V. B.1. The meson → current + current amplitude $\mathcal{K}_{\mu\nu}$. Note that there are no contributions from the case where both currents interact via bare couplings.

Figure V.C.1. The current + current → meson amplitude $\mathcal{N}_{\mu\nu}$ in Frame I where the incident spacelike current has negative minus momentum component. This incident

current is drawn to the right as a remnant of the time ordering.

Figure VI.A.1. The structure of the Compton amplitude $[\mathcal{M}_{\mu\nu}]_{I}$ in Frame I. The diagrams are meson exchange tree diagrams. No contact terms appear. The diagrams correspond one-to-one to the terms of eq.(VI.A.3).

Figure VI.A.2. The structure of the Compton amplitude $[\mathcal{M}_{\mu\nu}]_{II}$ in frame II. The first diagram represents contributions from the meson dominated four point function. The other diagrams contain at least one bare coupling vertex. The diagrams correspond one-to-one to the terms of eq.(VI.A.4).

Figure VI.B.1. An irreducible quark scattering diagram contributing to Compton scattering in the dimensional counting picture. The dotted lines are far off mass shell and give integer power behavior.

Figure VI.C.1. Parton handbag diagrams. The dotted propagators are dressed. The dashed line indicates that the discontinuity is to be taken.

Figure VI.C.2. Parton model of photoproduction of large mass lepton pairs via parton-antiparton annihilation.

Figure VI.C.3. Contributions to the photoproduction of large mass lepton pairs in the 't Hooft model in (a) Frame I and (b) Frame II. The (ut) contributions allow a parton-antiparton annihilation interpretation.

Figure B.1. The coupling of the fermion current of type Δ to quarks.

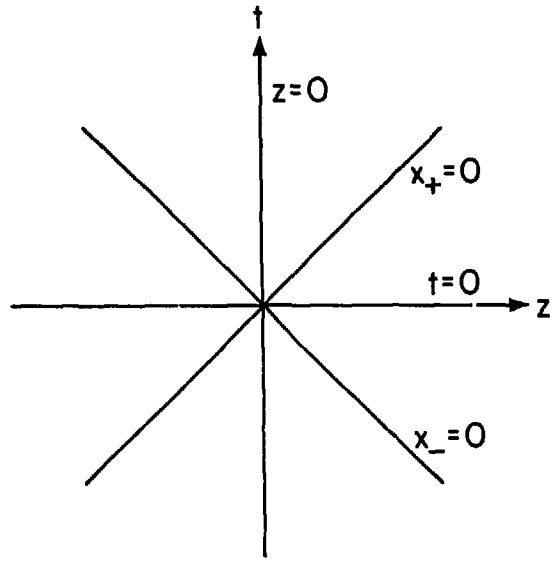

Figure II.A.1

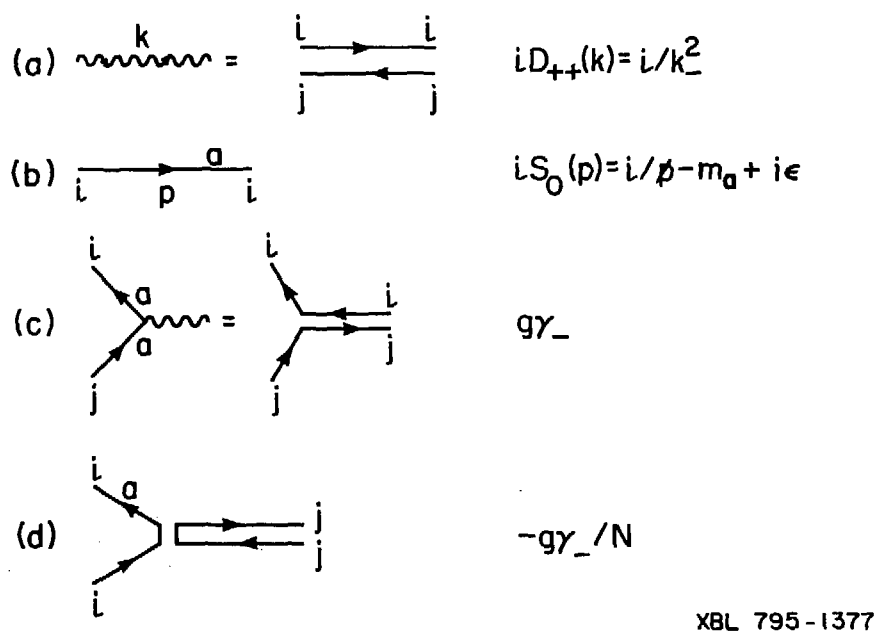

Figure II.B.1

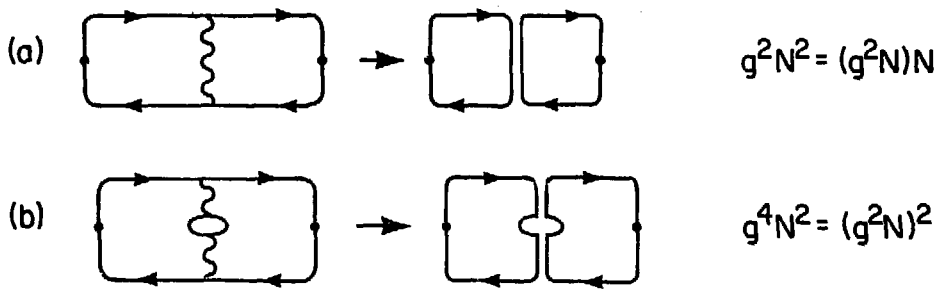

Figure II.D.1

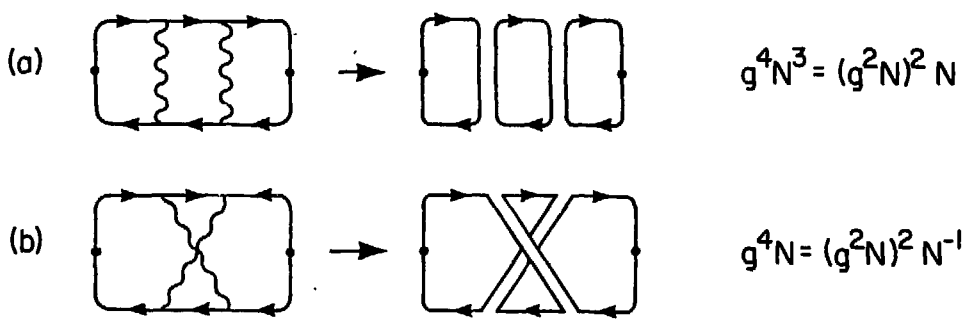

Figure II.D.2

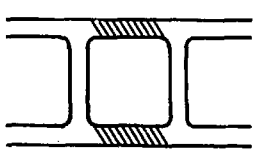

XBL 795-1378

Figure II.D.3

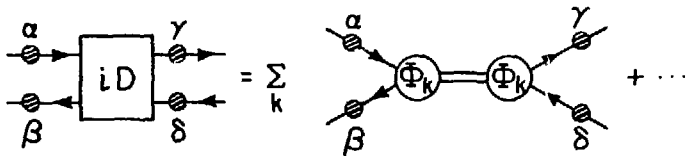

Figure III.A.1

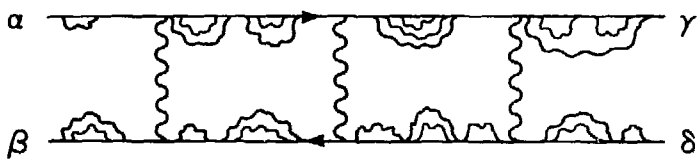

Figure III.A.2

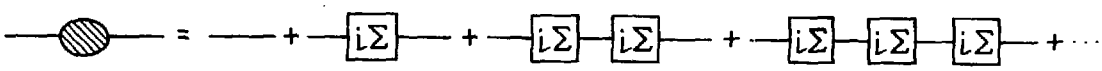

Figure III.A.3

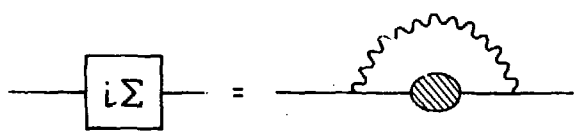

Figure III.A.4

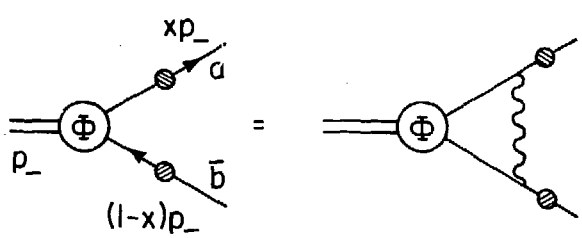

XBL 795-1379

Figure III.A.5

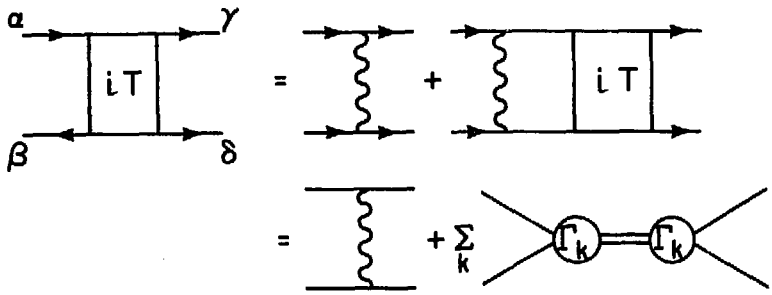

Figure III.A.6

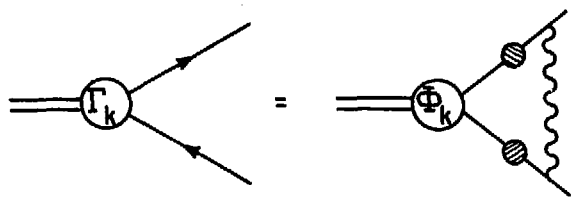

Figure III.A.7

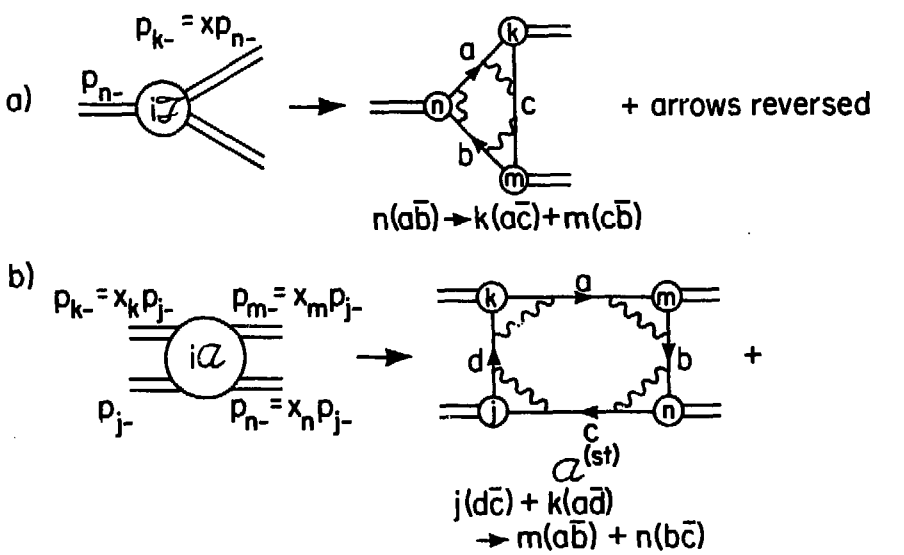

Figure III.C.1

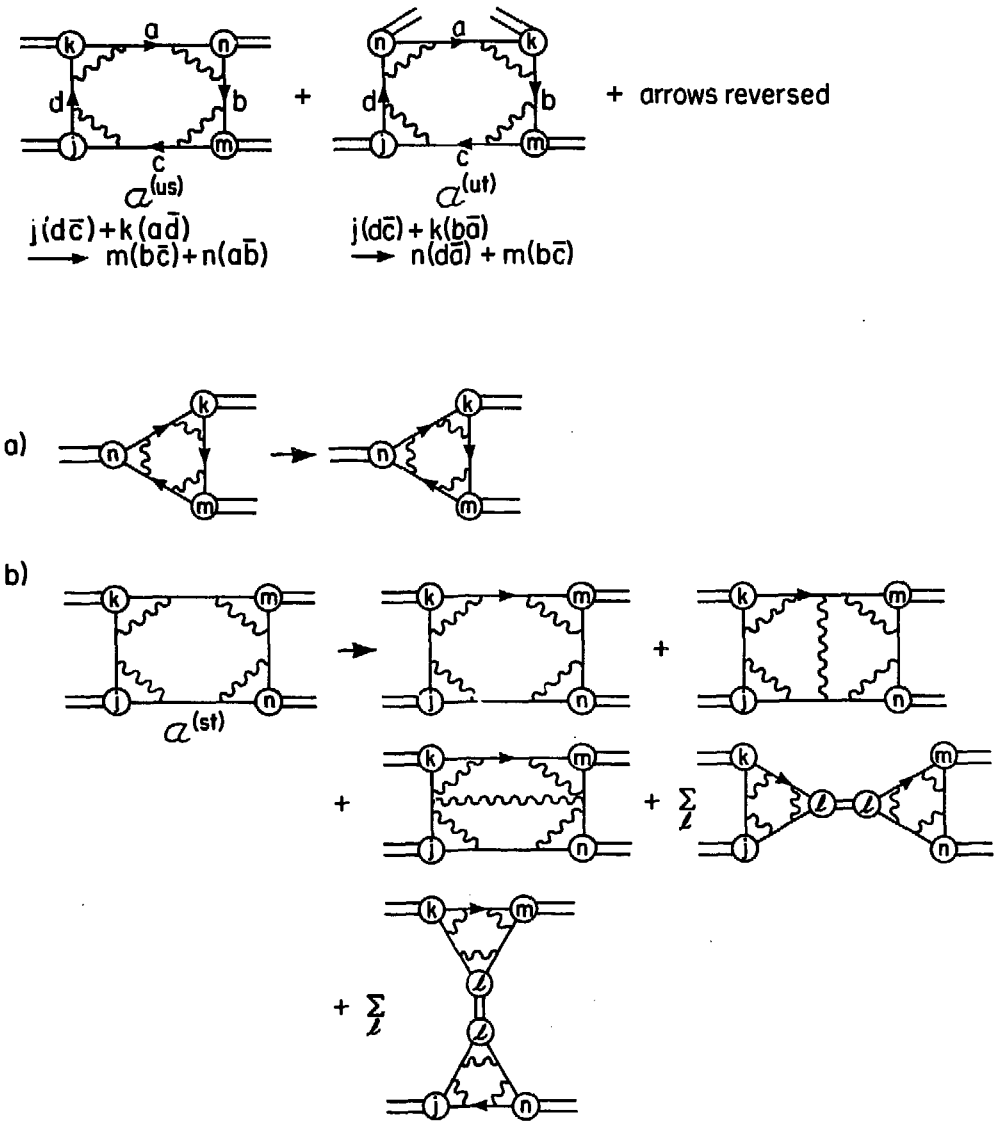

XBL 795-1381

Figure III.C.2

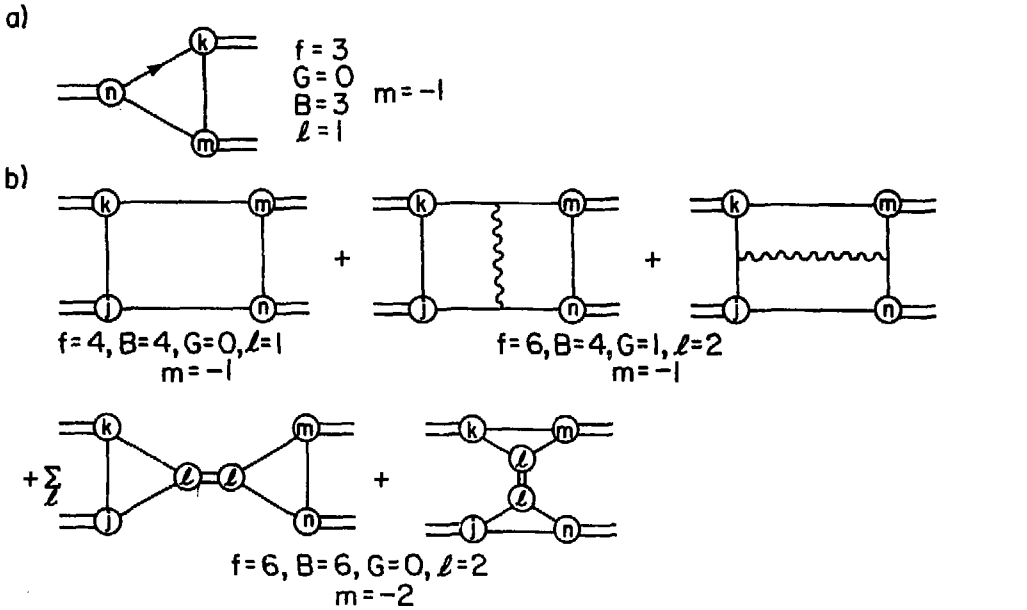

Figure III.C.3

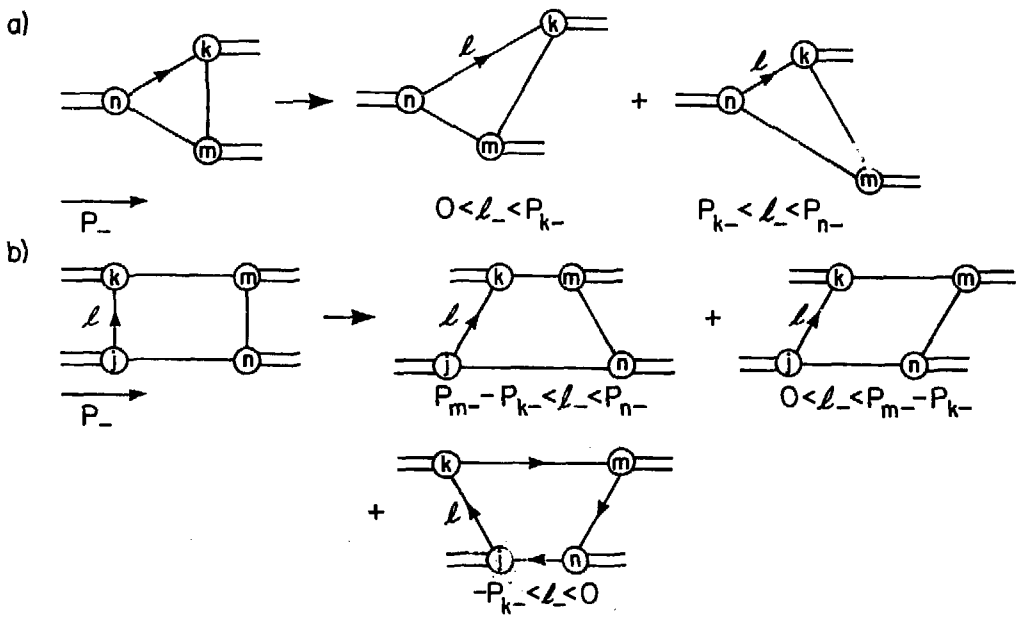

Figure III.C.4

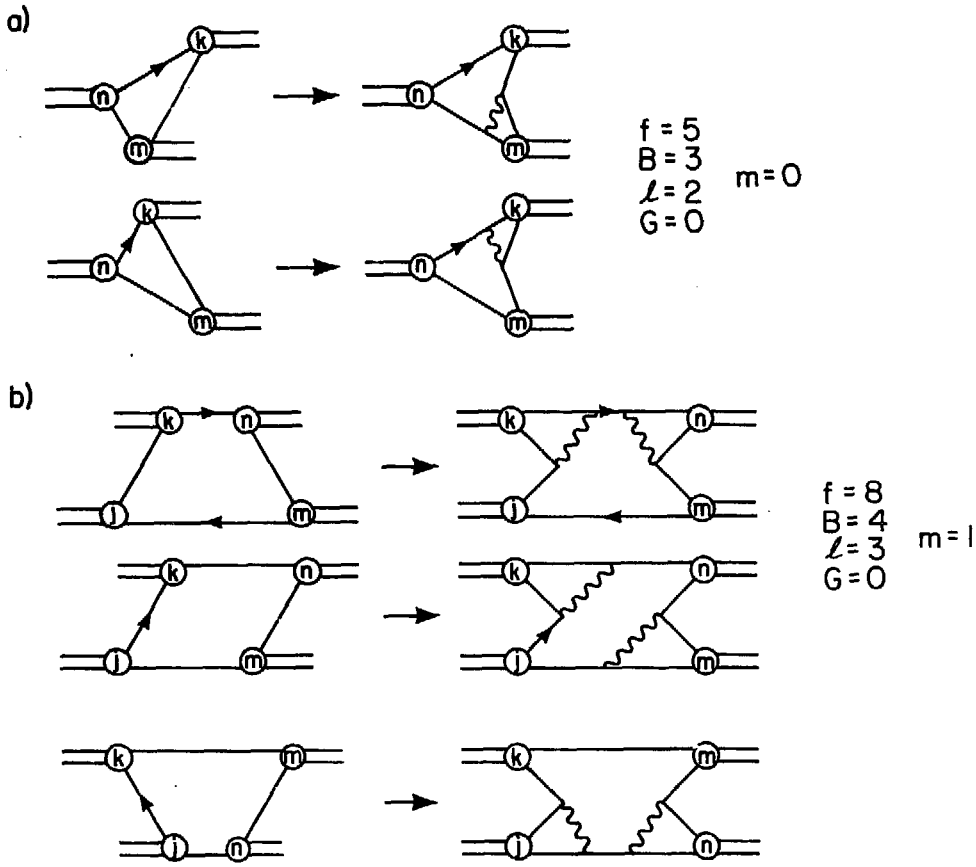

Figure III.C.5

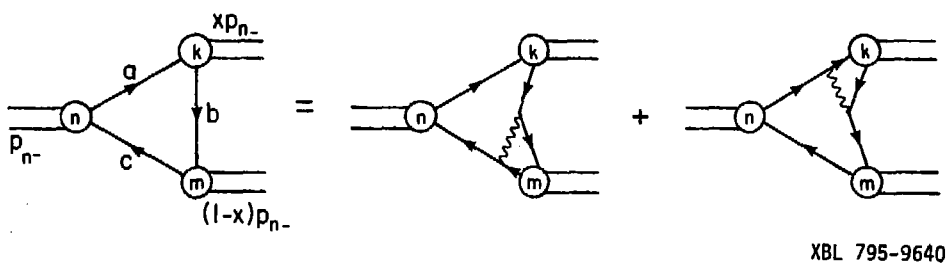

Figure III.C.6

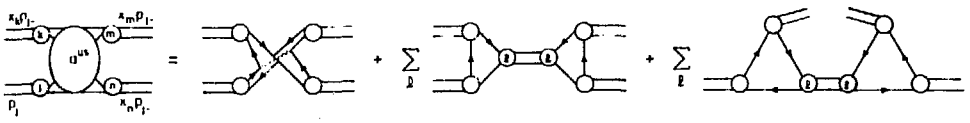

(a)

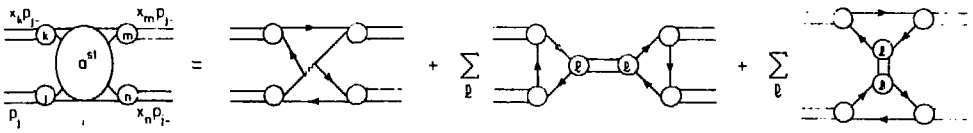

(b)

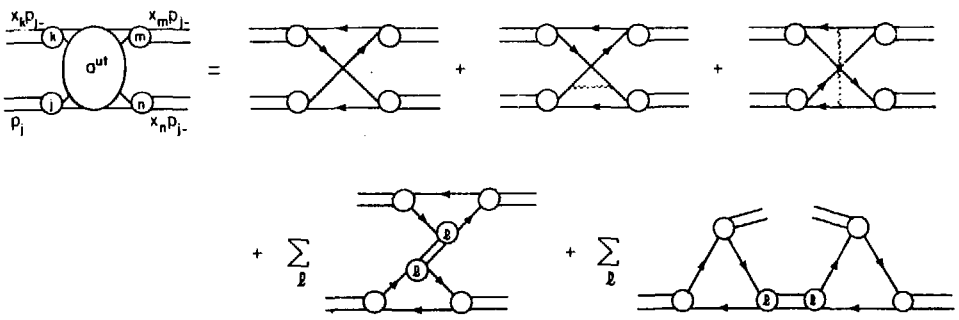

(c)

XBL 795-9639

Figure III.C.7

Figure IV.A.1

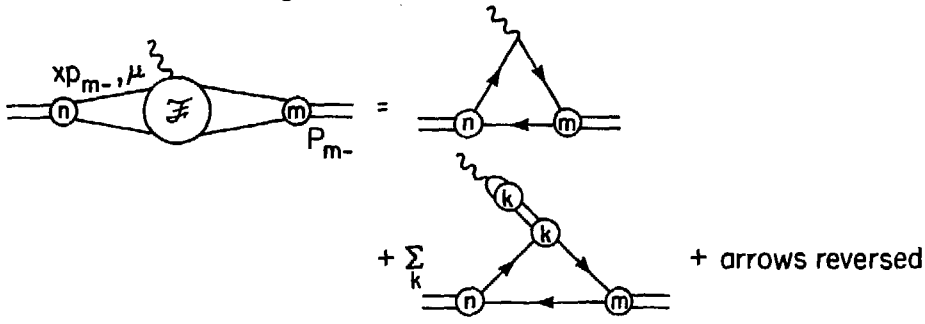

Figure IV.B.1

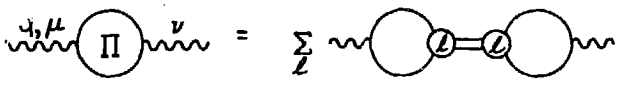

Figure V.A.1

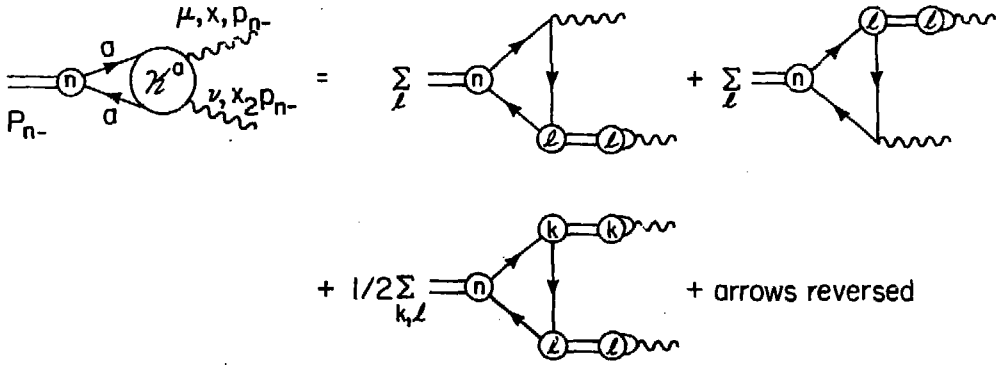

XBL 795-1384

Figure V.B.1

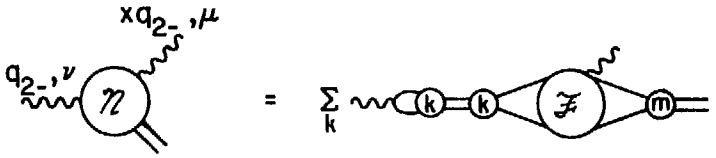

Figure V.C.1

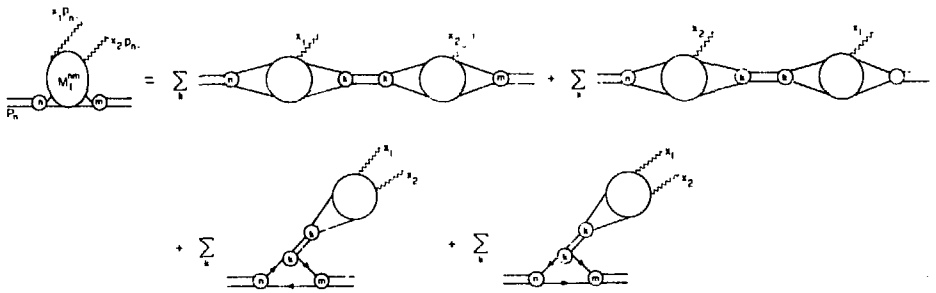

Figure VI.A.1

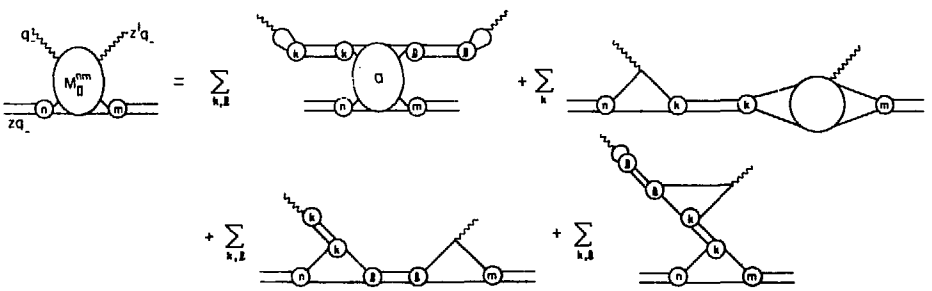

XBL 795-9641

Figure VI.A.2

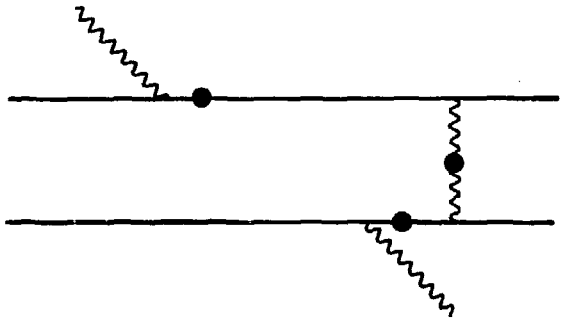

Figure VI.B.1

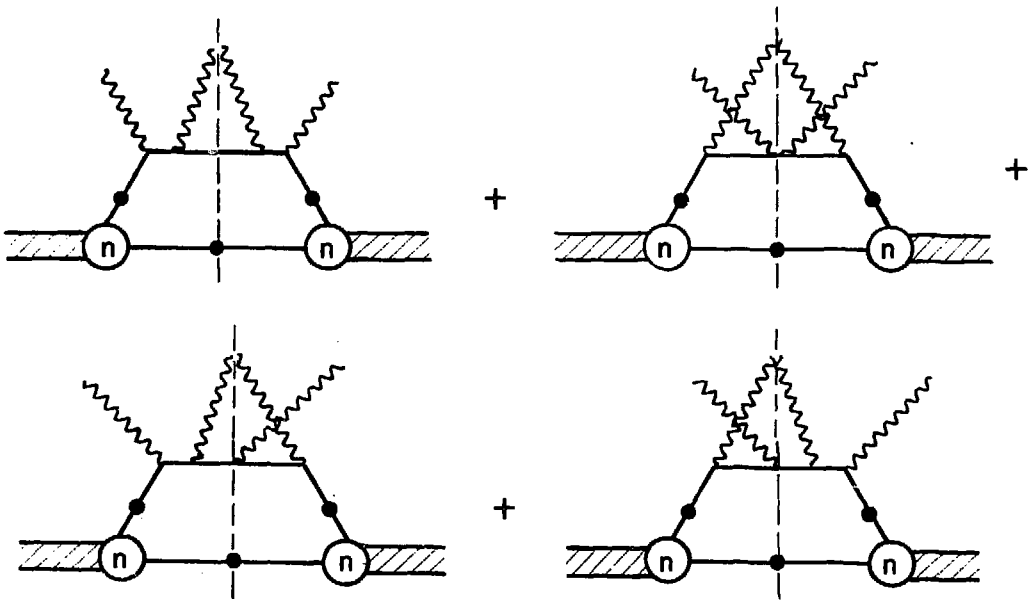

XBL 795-9642

Figure VI.C.1

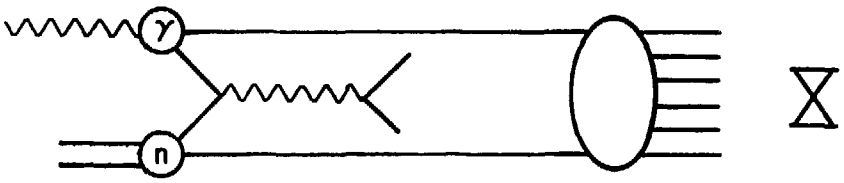

Figure VI.C.2

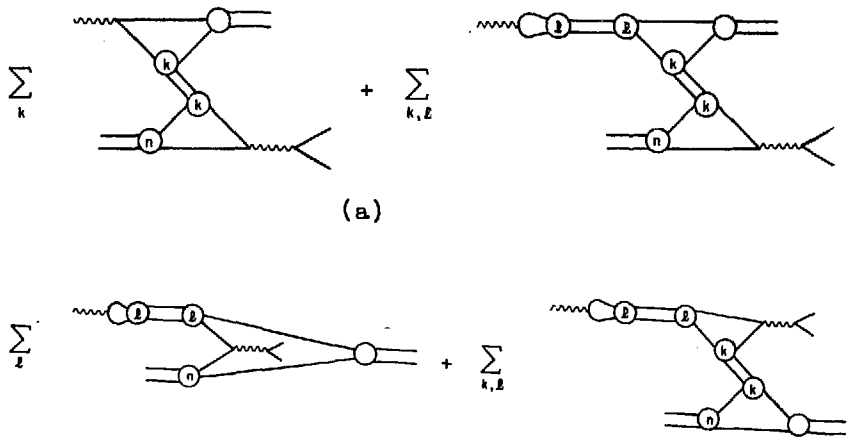

Figure VI.C.3

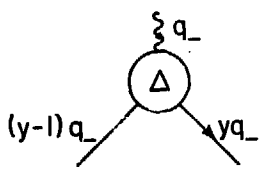

XBL 795-9638

Figure B.1

LIMIT	t	u	q^2	q'^2	M_m^2	x_1	x_2	z	z'
FORWARD HI ENERGY (Sect. VI.B.(1)) LARGE ANGLE (Sect. VI.B.(2))	$\frac{(M_n^2-M_\pi^2)(q'^2-q^2)}{s}$	$-s$	finite fixed	finite fixed	finite fixed	$-q^2/s$	q'^2/s	M_n^2/s	1
[illegible]-PROJECTION OF MASSIVE PAIRS "BOTHEN-PASCHOS LIMIT" (Sect. VI.C.(1))	$-2M_n\nu(x_1+x_2)$	$\frac{-s(1-x_2)}{1-x_1}\left(1-\frac{2M_n\nu(1-x_1)}{s}\right)$	$\frac{-x_1}{1-x_1}s$	$\frac{x_2 s}{1-x_1}\left(1-\frac{2M_n\nu(1-x_1)}{s}\right)$	$2M_n\nu(1-x_1-x_2)$	$0<x_1<1-x_2$ fixed	$0<x_2<1$ fixed	$M_n^2(1-x_1)/x_1$	$1-\frac{2M_n\nu}{s}(1-x_1)$
FULL PROJECTION OF MASSIVE PAIRS (Sect. VI.C.(2))	$y_1(y_2-1)s$	$y_2(y_1-1)s$	finite fixed	y_1y_2s	$(1-y_1)(1-y_2)s$	$-q^2/s$	y_1 $y_1y_2<y_1<1$ fixed	M_n^2/s	y_2 $y_1y_2<y_2<1$ fixed

TABLE I: LEADING BEHAVIOR AS $s \to \infty$ OF THE KINEMATIC VARIABLES IN THE LIMITS CONSIDERED